crystals

Review

Three-Dimensional Printing of Hydroxyapatite Composites for Biomedical Application

Yanting Han [1,†], Qianqian Wei [1,†], Pengbo Chang [2,†], Kehui Hu [3,4,*], Oseweuba Valentine Okoro [5], Amin Shavandi [5,*] and Lei Nie [1,*]

1 College of Life Sciences, Xinyang Normal University, Xinyang 464000, China; hanyt@xynu.edu.cn (Y.H.); weiqian2018@163.com (Q.W.)
2 Department of Materials Engineering, Zhengzhou Technical College, Zhengzhou 450121, China; cpb317@163.com
3 State Key Laboratory of Tribology, Tsinghua University, Beijing 100084, China
4 Department of Mechanical Engineering, Tsinghua University, Beijing 100084, China
5 BioMatter Unit—École Polytechnique de Bruxelles, Université Libre de Bruxelles, Avenue F.D. Roosevelt, 50-CP 165/61, 1050 Brussels, Belgium; oseweubaokoro@gmail.com
* Correspondence: hukehui@tsinghua.edu.cn (K.H.); amin.shavandi@ulb.be (A.S.); nielei@xynu.edu.cn (L.N.)
† These authors contributed equally to this work and should be considered co-first authors.

Abstract: Hydroxyapatite (HA) and HA-based nanocomposites have been recognized as ideal biomaterials in hard tissue engineering because of their compositional similarity to bioapatite. However, the traditional HA-based nanocomposites fabrication techniques still limit the utilization of HA in bone, cartilage, dental, applications, and other fields. In recent years, three-dimensional (3D) printing has been shown to provide a fast, precise, controllable, and scalable fabrication approach for the synthesis of HA-based scaffolds. This review therefore explores available 3D printing technologies for the preparation of porous HA-based nanocomposites. In the present review, different 3D printed HA-based scaffolds composited with natural polymers and/or synthetic polymers are discussed. Furthermore, the desired properties of HA-based composites via 3D printing such as porosity, mechanical properties, biodegradability, and antibacterial properties are extensively explored. Lastly, the applications and the next generation of HA-based nanocomposites for tissue engineering are discussed.

Keywords: hydroxyapatite; nanocomposites; 3D printing; polymer; hard tissue engineering

1. Introduction

Based on the integration of principles of cell biology, medical science, materials science, and biological engineering, tissue engineering (TE) aims to develop biological substitutes for the restoration or replacement of damaged and diseased tissue. TE has been applied in orthopedics, skin, cartilage, and neurons and organ reconstruction. A scaffold is essential for hard tissue regeneration. The scaffold needs to provide a suitable surface and space for the adhesion, proliferation, migration, and differentiation of cells. Hydroxyapatite ($Ca_{10}(PO_4)_6(OH)_2$, HA) is one of the essential inorganic components from bones and teeth. HA has been used as a bone-substitute material in hard TE due to its structural and functional similarity to human bones and teeth. HA are also widely applied in biomedical engineering due to their characteristic excellent biocompatibility, bioactivity, osteointegrity and osteoconductive properties and HA's similarity to the inorganic component of human beings [1,2]. Notably, 65% of human bone is composed of HA-like compounds [3]. Crucially however HA has poor mechanical properties, leading to the need for the development of suitable HA-composites that retain the aforementioned benefits of HA while having improved mechanical properties.

These HA-based composites (in combination with other biomaterials such as polymers or other inorganic materials) have been used to fabricate scaffolds with desired proper-

ties, including biocompatibility, interconnected porous morphology, adequate mechanical properties, biodegradability, and appropriate surface chemistry for cell attachment and proliferation. In addition to the 'biological' benefits of the use of such biomaterials, the use of these biomaterials will reduce the need for synthetics (fossil sourced materials) in the biomedical industry leading to overall improved environmental outcomes [4,5]. Biomaterials based on HA have therefore been under intense study for TE by several researchers in the last ten years (Figure 1).
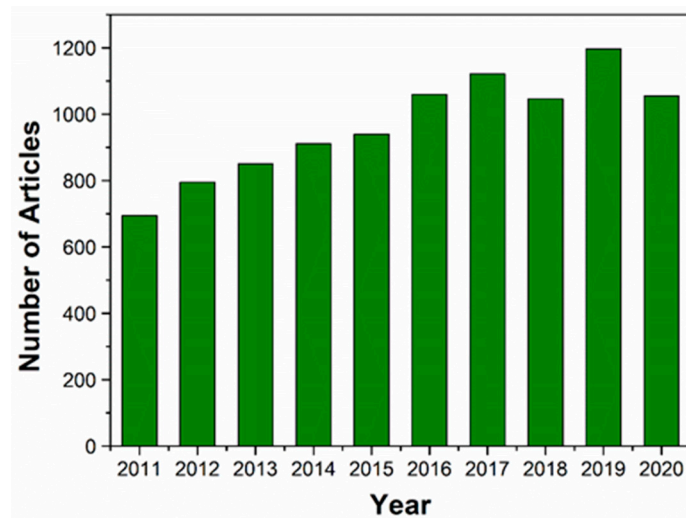
Figure 1. The number of articles published on HA and HA-based nanocomposites for TE in the last 10 years (January 2011 to December 2020). The data were obtained from Web of Science using the terms "hydroxyapatite" or "hydroxyapatite nanocomposites" and "TE".

According to the literature there are several methods that may be employed in the preparation of HA-based composites [6,7]. Some of these techniques include biomimetic mineralization [8], electrochemical deposition [9], lyophilization [10], electrospinning [11], self assembling [12], and chemical vapor deposition [13]. These techniques for HA-composite preparation are summarized and briefly described in Table 1.

Table 1. Some major methods employed in fabricating hydroxyapatite (HA) composites.

HA-Composites Fabrication Methods	Brief Description	Sources
Biomimetic mineralization	In this approach, the composite material is decorated in a solution of bioactive substances or simulated electrolyte body fluid solution (SBF). In such a solution, the increased concentration of calcium ions induces the nucleation of hydroxyapatite crystals on the selected composite material.	[14]
Electrochemical deposition	In this method, the hydroxyapatite composite is deposited onto the surface of a conductor using an electrolysis processes such that the solution contains the calcium ions and phosphate ions for (HA) and the relevant composite candidate (i.e., dissolved chitosan).	[15]
Lyphilisation	The composite materials (i.e., graphene and HA) are dispersed in an organic solvent after which the mixture is frozen. Sublimation of the frozen solution is subsequently achieved by reducing the pressure.	[16]

Table 1. *Cont.*

| HA-Composites Fabrication Methods	Brief Description	Sources
Electrospinning	This approach is employed when there is a need to develop fibrous scaffolds that can mimic the extracellular matrix of native tissue. Such fibers are prepared by electrospinning a precursor mixture containing ions (i.e., calcium ions in $Ca(NO_3)_2 \cdot 4H_2O$ and phosphate ions in $(C_2H_5O)_3PO$) and polymer additive, followed by thermal treatment.	[17,18]
Self-assembling	This is a self-aggregation process that involves the spontaneous aggregation to form the target composites. During the self-assembling process, the organic phase (i.e., collagen) is made to interact with the mineral phase (i.e., hydroxyapatite) via the use of suitable precursors (i.e., $Ca(OH)_2$ for Ca^{2+} and H_3PO_4 for PO_4^{3-}).	[12]
Chemical vapor deposition	In this method, the film is deposited on the surface of the substrate through chemical reaction from gas-phase or vapor-phase precursor (i.e., $Fe_2O_3/HA + H_2$ as carrier gas).	[13]
Hydrothermal	In this approach, a mixture composed of suitable precursors containing calcium ions (i.e., calcium nitrate tetrahydrate) and phosphate ions (diammonium hydrogen phosphate solutions) is used in dispersing the composite candidate material (i.e., graphene) at a high temperature condition (i.e., 180 °C).The hydrothermal method is also employed in the fabrication of three-dimensional reduced graphene oxide/hydroxyapatite (HA)/gelatin scaffolds.	[19,20].
Solvothermal Synthesis	HA nanoparticles are crystalized via a two-state solvothermal method at the high temperature of 180 °C. Calcium nitrate tetrahydrate and diammonium hydrogen phosphate are used as calcium and phosphate precursors, respectively.	[21]

Hull, a graduate of university of Colorado, USA displayed the first uses of additive manufacturing (AM) in 1984 [22,23]. AM technologies have been applied in many fields, including medical devices and TE [24,25]. Nowadays, 3D printing is considered as a promising technology to fabricate sophisticated biological products, including biological scaffolds, tissues, organs, and personalized medical devices, via printing biological materials, living cells, and signaling molecules. This review summarizes the available 3D printing techniques for the fabrication of HA-based nanocomposites. The different types of HA-based nanocomposites via 3D printing and their physicochemical and biological characteristics for tissue regeneration are subsequently discussed. Next, the desired properties and specific medical applications of HA-based nanocomposites are summarized. This review seeks to ascertain the primary properties of HA-based nanocomposites and emerging 3D printing techniques for the next generation of HA-based biomaterials for TE.

2. 3D Printing Technologies for HA-Based Nanocomposites

The procedure employed in 3D printing, based on the deposition of exact layers using biomaterials, occurs with or without encapsulating cells. The whole process mainly includes the preparatory phase, printing phase, and post-handling phase [26]. Computer graphics software (such as CAD/CAM) and the selection of biomaterials are employed in the preparatory phase. The post-handling process is involved in tissue maturation in a bioreactor, in vitro transplantation, or animal implantation. Inkjet-based 3D printing, stereolithography (SLA)-based 3D printing, extrusion-based 3D printing, and laser-based 3D printing are the four commonly used 3D printing strategies [27–29], and the 3D printing techniques used in the fabrication of HA-based nanocomposites are summarized in the following subsections.

2.1. Inkjet-Based 3D Printing

Inkjet-based 3D printing is also known as continuous inkjet and drop-on-demand inkjet printing. In this printing approach, a nozzle driven by thermal or acoustic forces is used to eject liquid droplets onto the substrate [26]. Different inkjet printers generate different droplets. The inkjet-based 3D printing has two different mechanisms, generically known as continuous inkjet printing (where a continuous stream of liquid drops is produced) and drop-on-demand inkjet printing (where individual drops are generated), as shown in Figure 2 [30]. In the drop-on-demand inkjet printing process, two methods are used to make the pressure pulse and promote droplet formation and ejection: the thermal and piezoelectric drop-on-demand inkjet printing methods. In the thermal drop-on-demand inkjet printing method, a small thin-film heater located in the fluid chamber is employed such that the imposition of a voltage gradient across the heater facilitates the heating of the fluid in direct contact with the heater. Sustained heating above the boiling temperature of the fluid will facilitate the formation of small vapor pockets or bubbles [31]. These bubbles collapse rapidly in the absence of the voltage gradient, since heat transfer from the heater to the fluid ceases. In the piezoelectric drop-on-demand inkjet printing method, a pressure pulse is generated via mechanical actuation using a piezoelectric transducer or electrostatic forces [32]. In both methods described above, the liquid phase is employed during the Inkjet-based 3D printing technique, while the solid is formed after liquid deposition. Due to the low viscosity (3.5–12 mPa·s) of the liquid utilized in inkjet-base printing, the delay of curing after the deposit of droplets, and the limited resolution in the vertical direction, this printing technique is employed in skin [33], bone [34], and cartilage [35] printings with high printing speed, high precision, and relatively low cost.
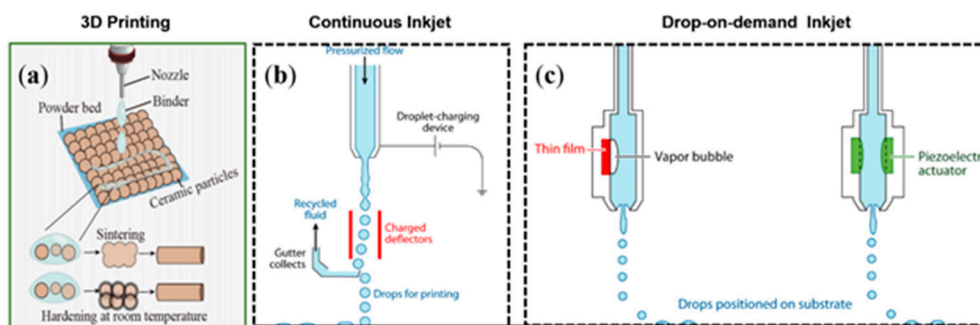
Figure 2. Schematic diagram showing the principles of 3D printing (**a**); and the operation of a continuous inkjet printer (**b**) and drop-on-demand inkjet printers (**c**) [32,36].

This inkjet-based 3D printing technique has been explored extensively in previous studies. For instance, Zhou et al. used an inkjet-based 3D printing technique to fabricate $CaSO_4/HA/\beta$-TCP (β-tricalcium phosphate) nanocomposites as tissue-engineered bone scaffolds. In the study, the HA/β-TCP powders were blended with $CaSO_4$-based powder, and a water-based binder was used to prepare bio-ink, after which solid and porous constructs were fabricated. Zhou et al. demonstrated that a positive correlation existed between the compressive strength of the printed scaffold and increasing $CaP/CaSO_4$ ratios. The ink of HA/$CaSO_4$ powders presented better physicochemical properties compared to the physicochemical properties of ink of β-TCP/$CaSO_4$ powders [37]. Strobel et al. [38] generated the porous biphasic calcium phosphate (BCP) scaffolds via indirect 3D printing of a powder composed of homogenized 35 wt.% HA, 35 wt.% β-TCP, and 30 wt.% of a modified potato starch powder. Due to starch consolidation, high porosity was achieved. In addition, osteogenic cells (primary osteoblasts) and growth factor (BMP-2) were seeded on printed constructs and cultivated in a flow bioreactor for a couple of weeks. According to the histological and molecular biological analyses, the combination of osteoblasts and BMP-2 synergistically enhanced bone formation of printed BCP scaffolds [35]. Similarly, Warnke et al. also printed BCP scaffolds by 3D printing, and the BCP scaffold was seeded

with human osteoblasts. The printed BCP scaffold displayed superior biocompatibility compared to the BCP scaffold by traditional fabrication methods [39].

2.2. Stereolithography (SLA)-Based 3D Printing

SLA, developed by Chuck Hull, who is widely regarded as the "father of 3D printing", is primarily used to manufacture polymeric structures [40]. SLA is a process where a photoreactive resin is selectively cured while a platform moves the scaffold after each new layer is formed [41]. In the SLA-based 3D printing technique, an ultraviolet (UV) laser beam is used to selectively harden the photopolymer resin, thus facilitating the construction of 3D models in a layer-wise fashion. Compared with inkjet-based printing, SLA-based 3D printing has many advantages, including high speed, high resolution, and reproducibility [41]. This technique employs a digital mirror array to control the light pattern, facilitating selectively crosslinking in the pre-polymer solution one layer at a time. SLA-based printing could ensure high cell viability since no external force is applied on cells during the printing process [42]. Usually, either UV light or near-UV blue light (405 nm) is employed in SLA-based 3D printing systems [43,44]. Apart from the high cell viability benefits of the SLA-based printing technique, possibilities exist to enhance the cell adhesion in the ink. This can be achieved using peroxidase, thus further advancing the ability of printing with living cells for enhanced cell compatibility [45,46].

Due to the aforementioned benefits of the SLA-based method, the use of the SLA-based 3D printing technique has been explored extensively. For instance, in the study by Barry et al. [47], HA-based oligocarbonate dimethacrylate (OCM-2) composite scaffolds were fabricated using UV light [47]. In comparison to UV or near-UV light, visible light may reduce the potential risk of carcinogenesis due to over-exposure of UV during printing, leading to the printed tissue scaffolds having higher cell viability. The printing system using visible light is shown in Figure 3. Woesz et al. [48] demonstrated the use of printing systems using visible light. They fabricated microporous HA scaffolds using the SLA approach with visible light; the scaffold had a strut size of 450 μm, with designed, fully interconnected macroporosity [48]. In another study undertaken by Chen et al. [49], SLA was employed in the preparation of a HA composite scaffold, with the biosafety of the resulting resin assessed. In this study, the investigation of the SLA prepared HA showed that the scaffold had toxic effects due to the utilization of a photosensitive resin. The study demonstrated that the photosensitive resin was completely pyrolyzed during the scaffold preparation process with the prepared HA having micro-holes which had good biosafety when assessed during pre-experiment of rabbit parietal implantation. While the use of the SLA technique in 3D printing has been employed, Le Guéhennec et al. [50] affirmed that the use of SLA in 3D printing of HA composites is limited by several factors. For instance, the entrapment of unreacted monomers and residuals and the use of phot-initiators and radicals may compromise the integrity of the bone matrix synthesis in addition to elevating the risk of cytotoxicity. Despite these challenges, the incorporation of HA via SLA has the overall effect of promoting bone regeneration due to the increase in osteoblast activity on HA surface [50].
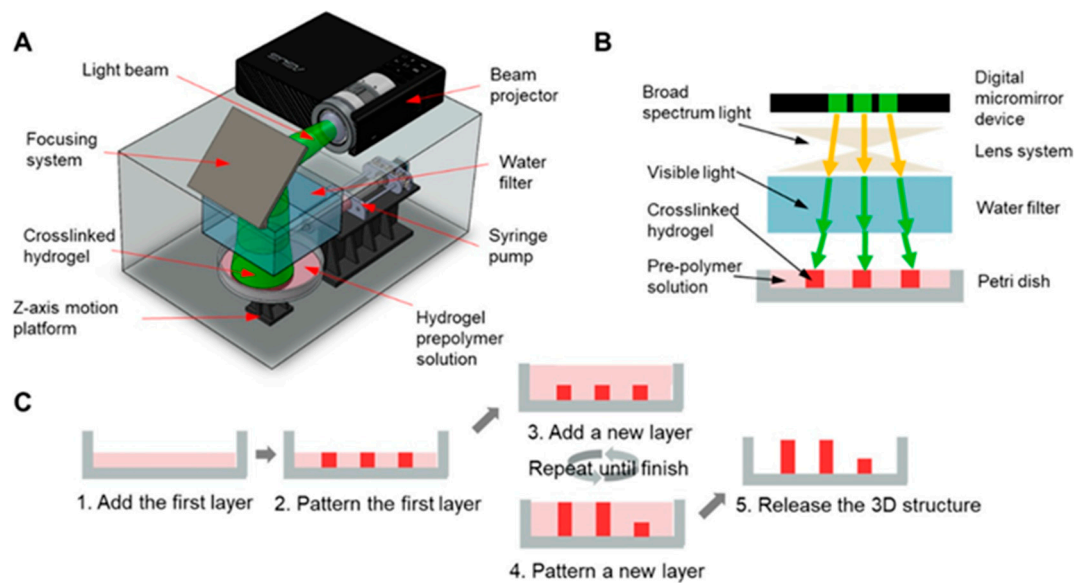
Figure 3. Schematic diagram of the visible-light-based SLA 3D printing system: (**A**) SLA printing system with various components; (**B**) working principles of single-layer printing; and (**C**) multiple layer printing process [51].

2.3. Extrusion-Based 3D Printing

The principle of extrusion-based 3D printing relies on extruding a viscous material using an extruder that is steered through a mechanical or electromagnetic actuator to create 3D objects [52,53]. According Derakhshanfar et al. [54], the extrusion-based 3D printing technique is characterized by different extrusion systems that can be cataloged as pneumatic pressure, piston, and screw driven systems, as shown in Figure 4. Extrusion-based 3D printing has many advantages, such as high cell seeding density, high printing speed, and scalability. This printing technique can also be used in printing continuous cylindrical filaments using different types of inks, after which the printed constructs may be crosslinked using ionic, photo, and thermal crosslinking mechanisms [55]. Extrusion-based processes mainly include direct ink writing (DIW, also called robocasting) and fused deposition modeling (FDM) in which the raw material is ejected via a nozzle [53]. The process of FDM is based on heating the material (polymer and polymer-ceramic composites) prior to squeezing it out of a nozzle, and by moving the nozzle, the material is deposited on a substrate, layer-by-layer [41]. The resulting printed constructs are subsequently heat-treated to eliminate the binder and densify the ceramic [56]. Similarly, Michna et al. [57] employed the extrusion-based 3D printing technique in fabricating HA scaffold using DIW. In their study, the desired characteristics of the printed HA scaffolds were achieved by customizing scaffold architecture and sintering conditions [57]. Sun et al. also utilized the DIW technique in applying silk fibroin ink, filled with HA nanoparticles, to print 3D scaffolds characterized by gradient pore spacings, ranging from 200 to 750 μm through the DIW technique [58]. On the other hand, the FDM approach was applied by Khodaei et al. [59], who fabricated a porous poly-lactic acid scaffold. The study showed that the elastic modulus and strength of porous polymer scaffolds could be similar to the surrounding tissue. Indeed, the polymers containing 29%, 49%, and 69% porosity had elastic coefficients of 502.7, 537.7, and 483.3 MPa, respectively [59].
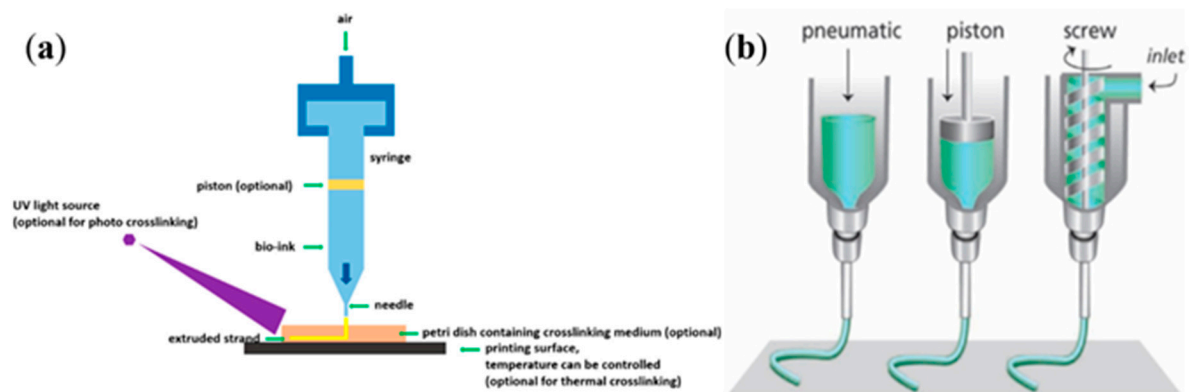
Figure 4. Schematic of extrusion-based 3D printing using various crosslinking mechanisms (**a**) [60]. This printing technique can be cataloged into three kinds: pneumatic-based, piston-based, and screw-driven-based 3D printing (**b**) [61].

2.4. Laser-Assisted 3D Printing

The working principle of laser-assisted 3D printing relies on a pulsed laser beam for deposition of bio-ink, including cells, onto a substrate to fabricate 3D objects. This printing device usually includes three elements: a pulsed laser source, a target coated with the material to be printed (the ribbon), and a receiving substrate (Figure 5) [62,63]. Keriquel et al. [64] reported the application of the laser-assisted 3D printing approach, in which they printed the nano-HA scaffold in the mouse calvaria defect model in vivo. Their decalcified sections and X-ray microtomography results demonstrate that laser-assisted 3D printing was sufficient to treat bone defects [64]. Selective laser sintering (SLS) printing was invented by Deckard and Beaman in 1986 at the University of Texas at Austin, USA. During SLS printing, a high-power laser beam is directed onto the powder bed to selectively and continuously irradiate the surface of powders to fuse them and ultimately create the 3D construct [65]. Xia et al. fabricated nano-HA/poly-ε-caprolactone (PCL), using the SLS technology, such that the porosity (78.54–70.31%) and mechanical strength (1.38–3.17 MPa) of printed scaffold could be regulated by variation of the printing parameters. The in vitro results indicate that the printed nano-HA/PCL scaffolds were more bioactive than the PCL scaffolds [66]. Compared to HA, BCP is usually challenging fabricate as a porous scaffold by SLS printing because of the short sintering time. The sintering ability of BCP ceramics can be significantly improved via compositing with polymers. Gao et al. [67] fabricated rectangular and porous BCP scaffold using SLS technique adding poly(L-lactic acid) (PLLA) (0–1 wt.%) into BCP nanoparticles powder, and the fracture toughness and micro-hardness of the sintered scaffolds could be adjusted by changing the PLLA content and laser power.

Having described the 3D printing techniques that may be employed in HA-based composites, with their utilization and benefits highlighted in the text, Table 2 comparatively summarizes the printing techniques discussed. Table 3 also summarizes the challenges of the major printing techniques discussed, with the parameters to optimize the printing technique also highlighted for completeness.
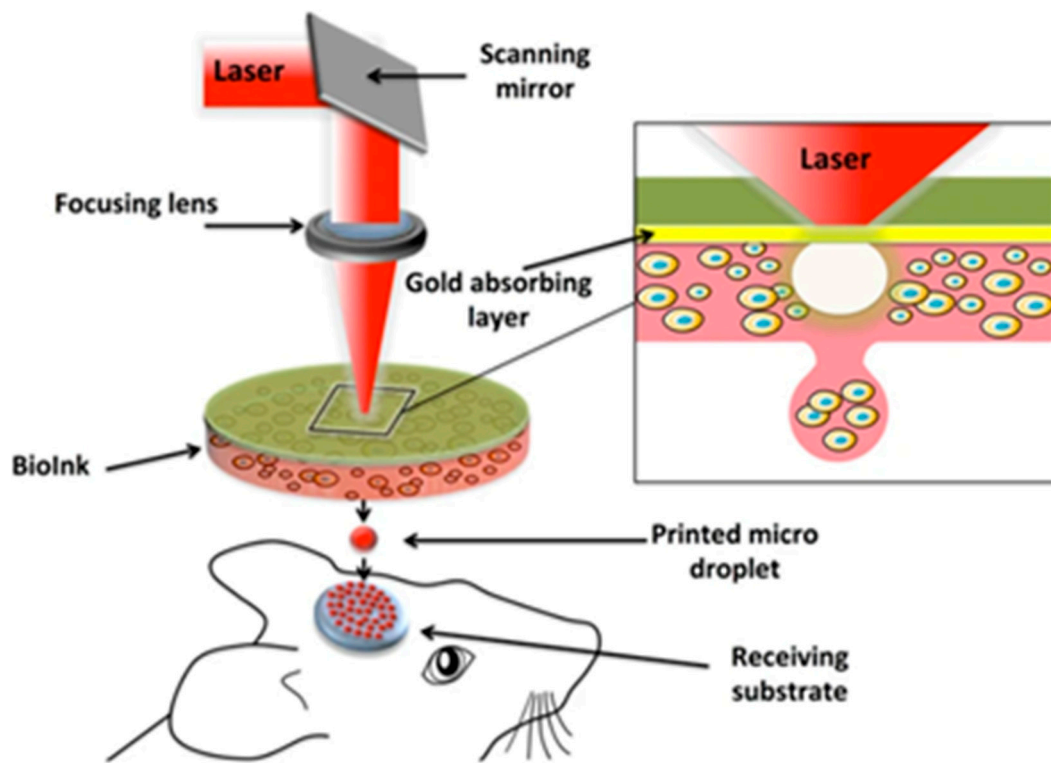
Figure 5. Diagram of laser-assisted printing approach. The laser-assisted printing system comprises of a pulsed laser beam, a focusing system, a ribbon, and a receiving substrate [63].

Table 2. Summary of the major printing techniques.

Materials	Cell Type	Outcome	Techniques	Sources
HA/β-TCP	Osteoblasts from femora and tibiae of male Lewis rats	Combination of this scaffold with primary osteoblasts and BMP-2 yielded significant amounts of newly formed bone in heterotopic locations and physiological gene expression patterns.	Inkjet-based 3D printing	[38]
HA	The preosteoblastic cell line MC3T3-E1, derived from mouse calvariae	The osteoblast-like cells were found to be present on the external and internal surface of the scaffold; they were embedded in collagenous extracellular matrix.	SLA-based 3D printing	[48]
Silk/HA	human bone marrow derived mesenchymal stem cells (hMSCs) and human mammary microvascular endothelial cells (hMMECs)	By combining HA, a good matrix for hMSCs osteogenesis, with silk to promote endothelial cell growth, migration was observed. The created scaffolds were capable of supporting both stem cell and endothelial cell functions to allow for new tissue formation and bone remodeling with vascular inputs within a single construct environment.	Extrusion-based 3D printing	[58]
HA	Human bone marrow stromal cells	Cells were tightly anchored to the surfaces of all scaffolds and had begun to spread	Laser-assisted 3D printing	[66]
HA/TCP	Rabbit Bone Marrow Stromal Cells (BMSCs)	the phosphoric acid scaffolds with a HA/β-TCP weight ratios of 60:40 may be the best candidate for bone TE applications.	Inkjet-based 3D printing	[68]

Table 2. *Cont.*

Materials	Cell Type	Outcome	Techniques	Sources
HA	Human osteoblast cells (HOBS)	The HOBS are attached to the surface of HA scaffolds and have high cellular activity.	SLA-based 3D printing	[47]
HA	The preosteoblastic cell line MC3T3-E1	The osteoblast-like cells were found to cover the whole external and internal surface of the scaffold, and they were embedded in collagenous extracellular matrix.	SLA-based 3D printing	[48]
HA	L929 cells and rabbit osteoblast cells	The rabbits had no adverse physiological reactions such as infection, and the wafer formed a strong bone connection with the defect, indicating that the final HAP samples have good biosafety in vivo.	SLA-based 3D printing	[49]
HA/TCP	Osteoblast-like MG-63 cells	The histological analysis did not indicate evidence of inflammation but highlighted close contacts between newly formed bone and the experimental biomaterials, revealing an excellent scaffold osseointegration.	SLA-based 3D printing	[50]
HA	The preosteoblastic cell line MC3T3-E1, derived from mouse calvariae	The osteoblast-like cells were found to be present on the external and internal surface of the scaffold; they were embedded in a collagenous extracellular matrix.	SLA-based 3D printing	[48]
Silk/HA	Human bone marrow derived mesenchymal stem cells (hMSCs) and human mammary microvascular endothelial cells (hMMECs)	By combining HA, a good matrix for hMSCs osteogenesis, with silk to promote endothelial cell growth, migration was observed. The created scaffolds could support both stem cell and endothelial cell functions to allow for new tissue formation and bone remodeling with vascular inputs within a single construct environment.	Extrusion-based 3D printing	[58]
CHA	Rabbit Bone Marrow Stromal Cells (BMSCs)	The printed CHA scaffolds had the advantages of promoting BMSCs proliferation and differentiation and promoting defect repair compared to the nonprinted CHA scaffolds	Extrusion-based 3D printing	[69]
Coll/HA	Vero cells	It was demonstrated that Coll/HA can be 3D printed, that the scaffold is conducive to cell proliferation, and that it is suitable for biomedical applications.	Extrusion-based 3D printing	[70]
HA/SF	Human bone marrow-derived mesenchymal stem cells (hBMSCs)	Cell attachment and penetration into scaffolds were supported by all the groups. Increased content of SF/HA led to better cell proliferation and enhanced ALP activity.	Extrusion-based 3D printing	[71]
HA/SA	Mouse bone mesenchymal stem cells (mBMSCs)	The sustainable drug release function of the porous scaffolds aided mouse bone mesenchymal stem cells (mBMSCs) being cultured on the porous scaffolds.	Extrusion-based 3D printing	[72]
HA/CH	MC3T3-E1 cells	The 3D 10% HAp/CH scaffolds etched with N2 plasma significantly improved cell proliferation. The 3D 20% HAp/CH scaffolds etched with O2 plasma showed the highest osteoblastic differentiation.	Extrusion-based 3D printing	[73]

Table 2. *Cont.*

Materials	Cell Type	Outcome	Techniques	Sources
PLA/HA	Human MG-63 osteoblast-like cell	PLA-HA scaffolds have proved to be an excellent composite material with enhanced surface activity due to the coating of HA nanoparticles.	Extrusion-based 3D printing	[74]
PCL/PLGA/ HA	Rat bone marrow stem cells (rBMSCs)	3D printable ink made of PCL/PLGA/HAp can be a highly useful material for 3D printing of bone tissue constructs.	Extrusion-based 3D printing	[75]
PMMA/ CNT/HA	L929 cells	Biocompatibility analysis indicates that introducing both HAp and CNT particles improves cell viability and growth.	Extrusion-based 3D printing	[76]
CH/PVA/HA	Mesenchymal stem cells (ATCC)	The scaffolds have high elastic modulus and good biocompatibility.	Extrusion-based 3D printing	[77]
PCL/GEL/ BC/HA	Human osteoblast cells (ATCC)	The PCL/GEL/BC/0.25%HA scaffold demonstrated good cell viability and cell adhesion.	Extrusion-based 3D printing	[78]
PLA/HA/Silk	MC3T3 osteoblast precursor cells	3D printed PLA, PLA/HA, and PLA/HA/Silk composite bone clips were successfully developed.	Extrusion-based 3D printing	[79]
PCL/HA/ TCP	Saos-2 cells	the fabricated hybrid scaffold had high porosity and excellent microstructural interconnectivity, and superior cell proliferation and alkaline phosphatase assay results for the hybrid scaffold.	Extrusion-based 3D printing	[80]
Sr/HA	MC3T3-E1 cells	Sr5-HA promoted cell proliferation, osteogenic differentiation, and cellular mineralization more efficiently compared with the other scaffolds.	Extrusion-based 3D printing	[81]
GEL/HA	Human umbilical cord blood-derived mesenchymal stem cells (hUCB-MSCs)	The scaffold supports the adhesion, growth, and proliferation of hUCB-MSCs and induces their chondrogenic differentiation in vitro.	Extrusion-based 3D printing	[82]

Table 3. Summary of the challenges of major printing techniques.

| Printing Technique	Parameters to Optimize Technique	Challenges
Inkjet-based 3D printing	Nozzle/extrusion temperature, printing speed, and layer thickness [83]. Specifically for materials such as ceramics, the solid loading and formulations of the ink also need to be considered [84]	The technique requires high temperatures which may preclude the incorporation of temperature sensitive bioactive molecules during the 3D printing process of HA based composites [85]. Additionally, when employed in printing of materials such as ceramics, the inks typically have low viscosity (i.e., low solid loading), to enable the use of the biomaterial. However, low viscosities lead to longer drying time and shrinkage. These challenges may also adversely affect the final accuracy of the printed scaffold [86]. Further concerns associated with the aggregation of solid particles due to convective macroscopic flow may lead to the printed structure having defects [86].

Table 3. *Cont.*

Printing Technique	Parameters to Optimize Technique	Challenges
SLA 3D printing	Typically, optimization of this techniques involves the consideration of the layer thickness, post curing time and orientation [87]. Due to issues associated with shrinkage, it is also crucial that formulations containing materials such as ceramics are optimized for proper viscosity while also avoiding issues of the solid segregation [86].	The technology can only use photopolymers with the utilization of a UV light further restricting the incorporation of living cells in the biomaterials [88]. Another challenge is the effect of light scattering due to the presence of ceramic particles in the suspensions since the scattering limits light penetrating. Furthermore, such scattering increases the curing width, leading to unfavorable effects on dimensional accuracy of the printing technique [89]. Furthermore, materials such as ceramics that absorb or refract photopolymerization wavelength are very difficult to process [86,90].
Digital Light Processing (DLP) 3 D printing	Factors to be considered to optimize the technique include the viscosity of the slurry, solid loading, and the specific operating mechanisms (i.e., top-down, bottom-up, method for recoating, etc.) [91].	According to the authors of [91], this technique is characterized by several challenges, with the major challenge when handling components such as ceramics related to the length/width ratio of the fabricated component. It was suggested that the risk of random fracturing in the fabricated component is enhanced when the length is ≥ 2 times the width. This challenge is presented when the bottom-up approach is employed. The alternative top-down approach may also present some limitations when employed in fabricating structures with large cross-sectional areas, with $3\,mm^2$ suggested as the preferred upper limit.
Extrusion-based 3D printing	To optimize the process, variables such as rod width (i.e., of the fused ceramic composite filament), layer thickness, building orientation, and the infill percentage must be considered [86,92].	Due to the high melting temperature of biomaterials such as ceramics, its use is not feasible with thermoplastic binders needed to formulate the composites such that the ceramic particles is ~60 vol% [86]. When printing materials, particularly ceramics are used, there is a major concern of there being an offset between the printed layers such that layer marks become distinctly visible (i.e., the staircase effect) [86]. Challenges related to surface roughness of the scaffold have also be highlighted [86]. Other challenges of this technique which also affects materials such as ceramics include the difficulty of biomolecules incorporation and low resolution [88].
Laser-assisted 3D printing	For this technique, it may be necessary to optimize the formulation, fabrication parameters (layer thickness, infill percentage, and extruder temperature [93]), position, and orientation for optimal printing processes [86]	When using materials such as ceramics, there are challenges of high shrinkage, high porosity, and the thermal-gradient-induced problem. Additionally, challenges such as low resolution, poor surface finish, and porous microstructures within the fabricated parts also persist when SLS is used [86]. It must also be stated that generic issues of high cost, difficulty in printing cells, and long processing times also negatively affect this technique [88].
FDM 3D printing	The optimization of this technique depends on several process parameters such as the rod width of the fused ceramic/polymer filament, layer thickness, building orientation, and raster angle [86]	This technique presents the challenge of the staircase effect when employed in printing ceramic composites ceramic parts. Significant concerns related to surface roughness also exist [86].

3. Hydroxyapatite (HA) and HA-Based Nanocomposites via 3D Printing

3.1. Hydroxyapatite

Hydroxyapatite (HA), ($Ca_{10}(PO_4)_6(OH)_2$), is characterized with a hexagonal crystallographic structure, as illustrated in Figure 6a. Figure 6a shows that a unit cell of HA contains Ca. PO_4 moieties are arranged such that four Ca atoms are surrounded by nine O atoms of the PO_4 moieties, while the other six Ca atoms are surrounded by the remaining six O atoms of the PO_4 moieties. Pure HA has the stoichiometric Ca/P ratio of 1.67, with lattice parameters of a-axis of 0.9422 nm and c-axis of 0.688 nm [94]. The chemical structure of HA is similar to the mineralized constituents of bone [53]. In addition, HA has excellent physicochemical properties, including osteoconductivity, bioactivity, re-sorbability, and slow decaying properties [95,96]. Furthermore, nanometer-sized HA can also increase intracellular uptake and reduce cell viability in vitro [97].
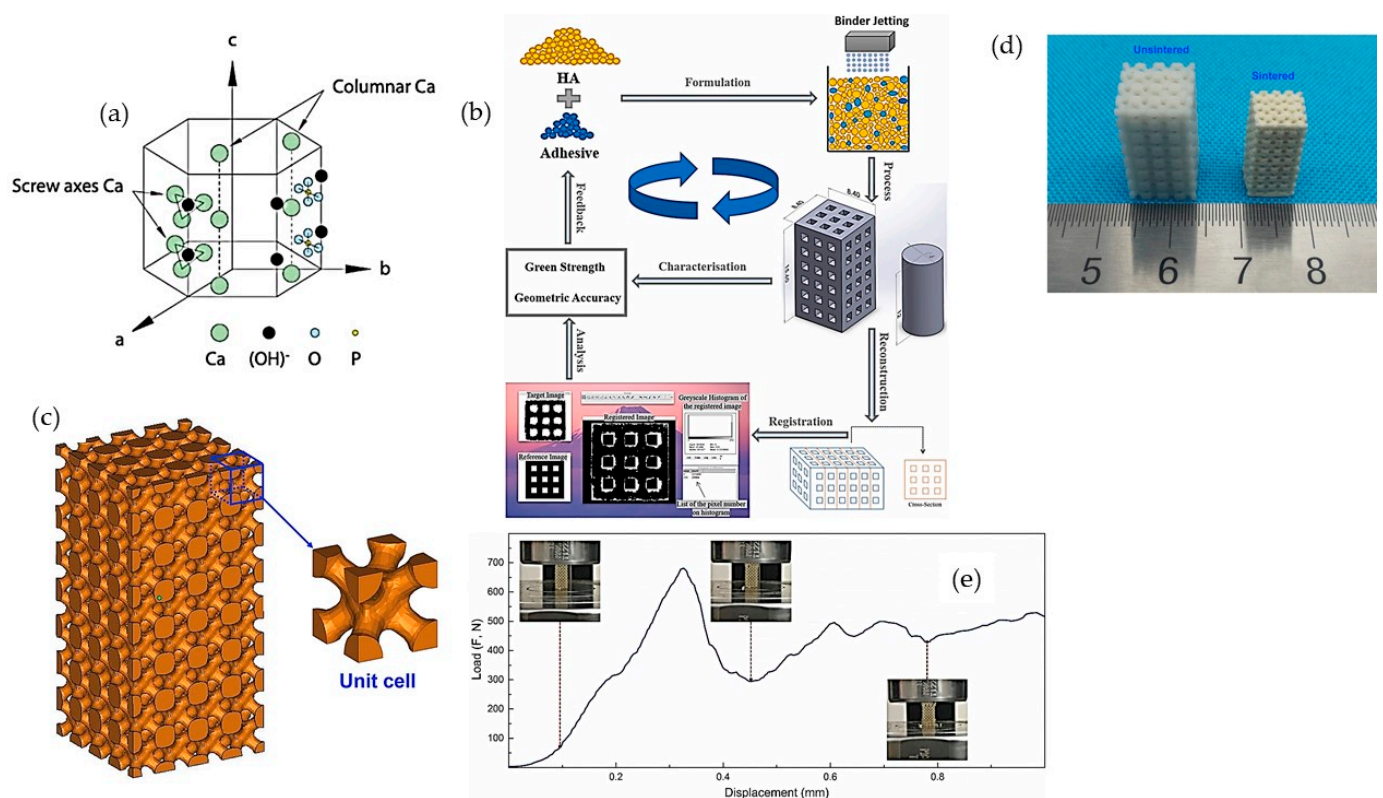

Figure 6. (**a**) Hexagonal crystallographic structure of the HA crystal [53]; (**b**) schematic diagram of fabrication of porous constructs via HA/adhesive powder mixtures [98]; (**c**) 3D models and objects of parts; (**d**) green body and as-sintered body; and (**e**) compression test of porous printed scaffolds [99].

Although HA is extensively being considered for hard tissue regeneration because of its presence in the native extracellular matrix (ECM) of bone tissue, extensive research has not been undertaken regarding pure-HA printed materials, due to the lack of bonding and flowability for the printing process [100]. Thus, various types of sacrificial materials and polymers are used as binders in the process of 3D printing to print neat HA constructs. To overcome the poor reactivity between HA powder with standard water-based ink, Zhou et al. [98] investigated different water-soluble adhesives to increase the 3D printability of HA powder, such as maltodextrin and polyvinyl alcohol (PVA) (Figure 6b). Zhou et al. showed that, by using a high molecular weight of PVA at 30 wt.% as adhesive, the printed formulation could achieve a geometrical accuracy of ~>85% and an excellent green compressive strength of 5.63 ± 0.27 MPa [98]. The curing, de-binding, and sintering parameters of the printing process influence the mechanical properties, porosity, and shrinkage of the sintered samples. Liu et al. [99] fabricated HA bone scaffold using the

DLP technique; the printed HA bone scaffolds displayed pore sizes of 300–600 μm, the porosity of around 49.8%, and compressive strength of 15.25 MPa, showing potential for bone repair applications (Figure 6c–e) [99]. Similarly, Seitz et al. [101] employed modified HA powder to print scaffolds; the polymer binder was removed after the consolidation of the printed ceramic green bodies at a temperature of 1250 °C in ambient air [101].

3.2. Hydroxyapatite (HA)/Polymer-Based Nanocomposites

The addition of a polymer to HA nanoparticles can enhance the printability of HA constructs [102–104]. Due to the suitability and compatibility to cellular environments, various polymers could be used to fabricate (no matter how complex) constructs in ambient or relatively mild chemical and environmental conditions [105]. Many synthetic and natural polymers can be used to reinforce HA scaffold via 3D printing for TE applications, as shown in Figure 7.
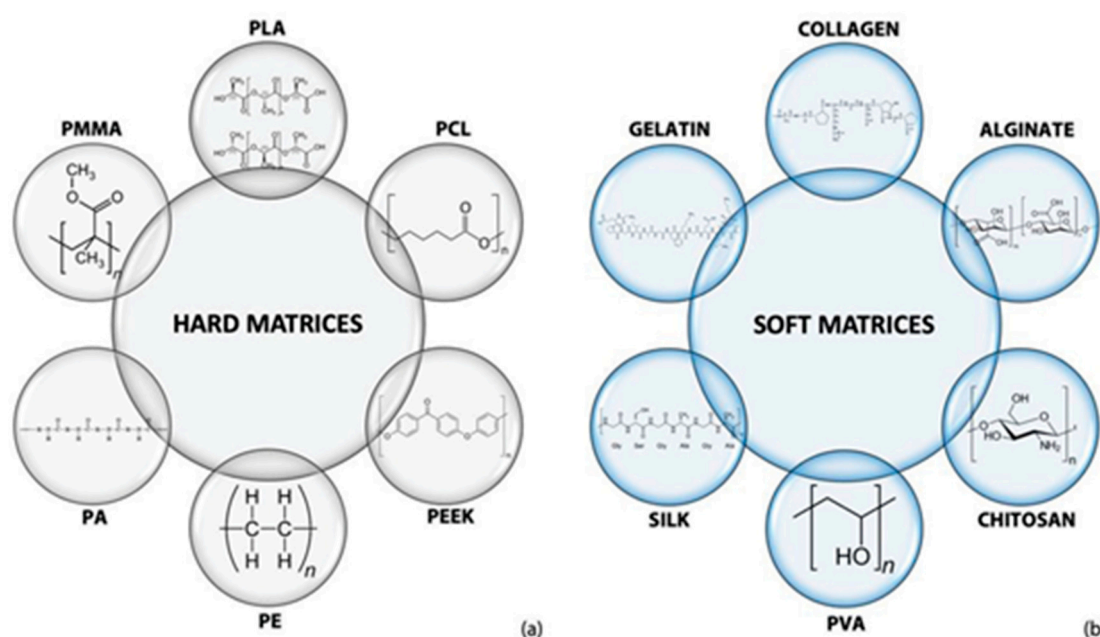

Figure 7. Polymers are used to composite with HA to build (**a**) hard and (**b**) soft matrices fabricated via 3D printing for TE [53]. Major nanocomposites which incorporate polymers to HA are discussed below.

3.2.1. HA/Collagen Nanocomposites

Many natural high-weight biomacromolecules can be used as bio-ink network precursors: collagen, fibrin, gelatin, silk, etc. [106,107]. The natural polymers, such as collagen and gelatin, contain amino-acid sequences (specifically, the adhesion ligand arginine-glycine-aspartic acid (RGD)) to which cells can readily attach [108]. Collagen refers to a family of fibrillary proteins with triple-helix structure of polyproline-II (PP-II) type. There are many types of collagen that differ in their ratios of helical to nonhelical domains, but all share a characteristic triple α-helix supramolecular structure that results from repeating glycine-X-Y sequences, where X and Y are typically proline and hydroxyproline, interspersed with alanine residues. Significantly, collagen type I represents 90% of the collagen present in the human body, mainly in skin, bones, tendons, and organs [105]. Collagen type I is the major structural component in the ECM and is widely used as a 3D hydrogel [109,110].

For instance, Lin et al. fabricated collagen/HA (collagen type I) using a low-temperature robocasting method, as shown in Figure 8 [69]. The printed scaffolds displayed excellent 3D structure. After the implantation in a rabbit femoral condyle defect model, in vivo results confirm that the printed scaffolds with interconnecting pores could facilitate cell penetration and mineralization and further enhance bone repair, compared with nonprinted scaffolds [69]. Ardelean et al. [70] employed a material composed of HA/collagen to print

using a 3D-Bioplotter Developer Series (Envision TEC) equipped with a 0.42-mm needle such that the distance between strands was maintained at 1 mm, while the pressure was set at 0.8 psi and the temperature and printing speed were specified as 4 °C and 40 mm/s, respectively. In vitro studies revealed that the printed HA/collagen constructs elicited similar cell viability and proliferation potentials with the negative control demonstrating their suitability for biomedical applications [70]. Montalbano et al. also used rod-like HA nanoparticles composited with type I collagen, together with an ammonium-based dispersing agent (Darvan 821-A) to obtain a homogeneous collagen/HA suspension, which was employed as bio-ink for extrusion 3D printing [111]. The obtained collagen/HA bio-ink showed that the shear thinning and sol-gel transition upon stimulus-physiological conditions and the mesh-like constructs could be printed [111].
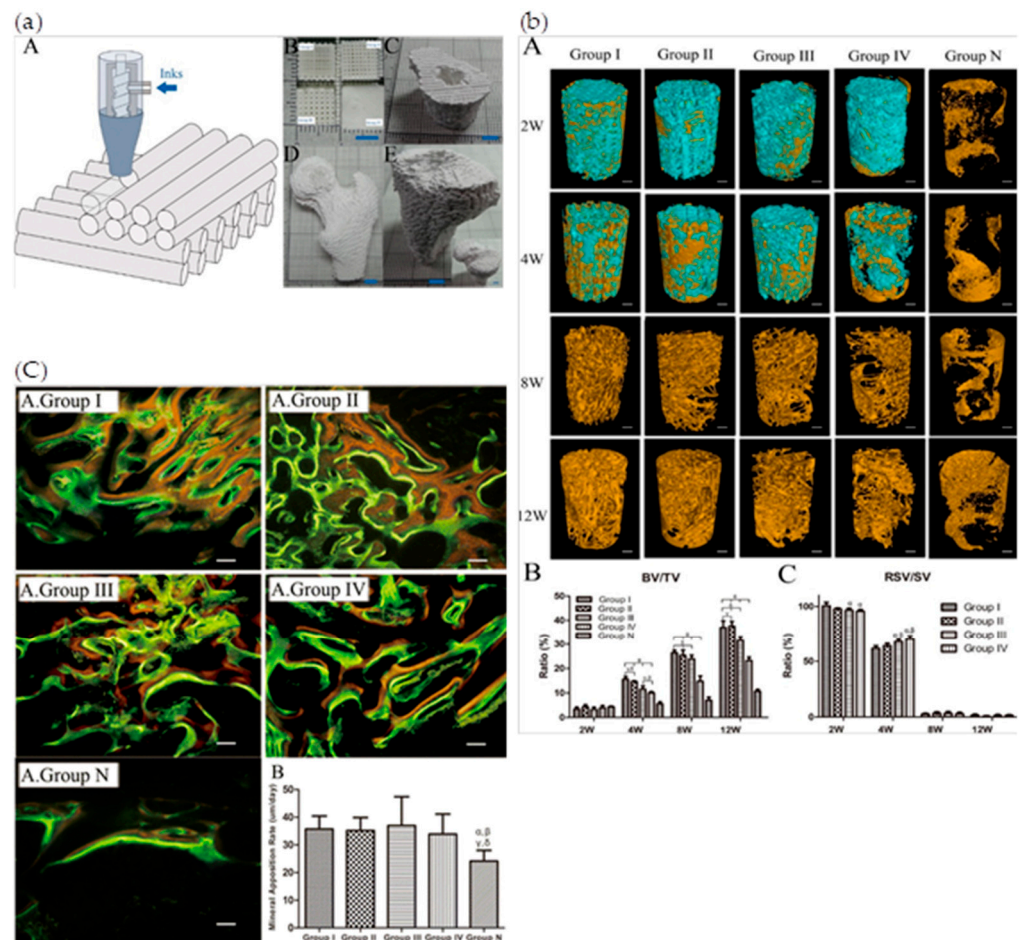

Figure 8. (**a**) The collagen/HA (collagen type I) scaffold with a grid-like microstructure was printed using robocasting approach at 4 °C. Scaffolds with different rod widths were obtained, including 300 μm (Group I), 600 μm (Group II), 900 μm (Group III), and nonprinted (Group IV). Scale bar: 5 mm. (**b**) Micro-CT 3D reconstruction results indicate the new bone formation at different weeks after in vivo implantation in the rabbit femoral condyle defect model. Scale bar: 1 mm. (**c**) The new bone formation was indicated using fluorochrome double-labeling for tetracycline (yellow) and calcein (green) at eight weeks. Scale bar: 100 μm [69].

3.2.2. Hydroxyapatite (HA)/Gelatin Nanocomposites

Gelatin is a water-soluble protein derived from the chemical, physical, or enzymatic hydrolysis of collagen type I, extensively used in the food industry. During the hydrolytic process of collagen, the triple-helix structure is broken, and the single-stranded macromolecules are achieved for gelatin. The molecular weight of gelatin ranges from 20 to 100 kDa depending on the product used, and the primary structure of gelatin is mainly

composed of over twenty different amino acids [112]. Compared to collagen, gelatin presents no cytotoxicity, good cell adhesion, faster biodegradability, easier preparation, and low cost, thus it can be considered as a sufficient candidate for printing [113]. Gelatin polymers with different molecular weights and isoelectric points can be obtained from various animal tissues, such as porcine, bovine, and fish. The combined use of gelatin and loaded HA presents an ideal microenvironment for cell adhesion, proliferation, and differentiation toward an osteogenic phenotype, due to the presence of intrinsically cell-adhesive motifs of gelatin [53]. The combined use of gelatin and HA was demonstrated in the study by Samadikuchaksaraei et al. [114] where HA/gelatin scaffold was fabricated using the layer solvent casting in combination with lamination techniques. The prepared HA/gelatin scaffold could support osteoblasts' adhesion and growth, and in vivo results confirm hat the scaffold could accelerate collagen content during the bone healing [114]. Chiu et al. [115] also obtained a HA/gelatin nanocomposite, modified using siloxane, such that the composite is easily formable as a scaffold. Similarly, Nosrati et al. [20] fabricated a HA/gelatin scaffold using a 3D printing method, with reduced graphene oxide (rGO) nanosheets used to reinforce the printed scaffoldThe addition of rGO/HA could result in smaller pores and higher 3D accuracy of scaffolds (Figure 9a) [20]. Comeau et al. [116] prepared a photo-cross-linkable methacrylated gelatin (GelMA)/HA bio-ink, such that the introduction of $CaCl_2$ or NaCl could be used in regulating the viscosity of GelMA/HA. The resulting GelMA/HA constructs could be printed by extrusion printing, and the dynamic modulus of the printed constructs could be regulated to that of articular cartilage by adjusting the content of HA (Figure 9b) [116]. While earlier discussion emphasized the enhanced support of osteoblasts' adhesion and growth (i.e., enhanced bioactivity) via the inclusion of gelatin, the introduction of gelatin may also inhibit crystallization of HA [117]. Notably, it is possible that the genlatin may also applied in drug release, due to its induction of degradation and deposition on apatite layer [117]. Further work in this regard is however required.
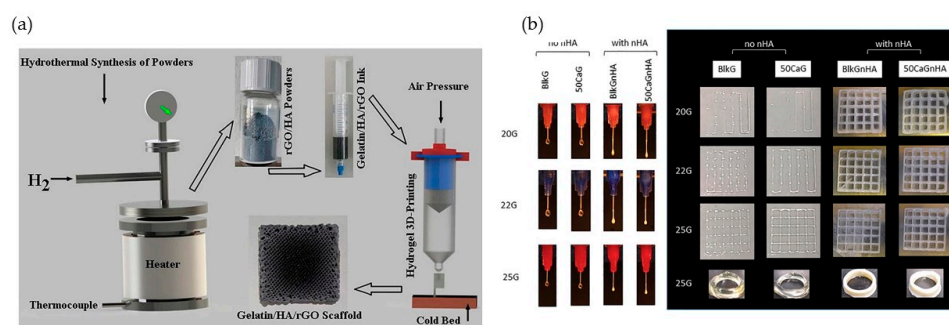

Figure 9. (**a**) Photo shows that the printability was improved while using methacrylated gelatin (GelMA) instead of gelatin, and the printability of GelMA/HA composite inks was qualitatively assessed [20]. (**b**) shows the different needle gauges were used to extrude the inks shown in the left images, and the right pictures show printed grids and tubes [116].

3.2.3. Hydroxyapatite (HA)/Silk Nanocomposites

It is well known that many arthropod species such as wasps, bees, and crickets produce silk proteins. As a protein fiber, silk fibroin (SF), derived from *Bombyx mori* cocoons, has historically been used as a natural polymer in the manufacture of surgical sutures. Due to its unique structure, which consists of hydrophobic β-sheet crystalline blocks staggered by hydrophilic amorphous acidic spacers, SF possesses outstanding mechanical properties and good biocompatibility both in vitro and in vivo [118,119]. SF has also established a good reputation for bone TE applications due to its many unique properties, including impressive biocompatibility, strong mechanical behavior, minimal/non-immunogenicity, tunable biodegradability, and ease of processability [120–123]. The concentration of SF solution needs to be increased to meet the rheology requirements of bio-ink using additional SF purification protocol, such as concentrating with a dialysis bag in polyethylene

glycol (PEG, molecular weight over 20,000 Da) solution, re-dissolving SF in organic solvents (such as formic acid), etc. [124,125]. Furthermore, the silk fibroin scaffolds displayed improved anticoagulant activity and the ability to support the adhesion and proliferation of endothelial and smooth muscle cells with high expression levels of phenotype-related marker genes and proteins, which is a potential use for vascular TE [126]. Liu et al. [127] confirmed that HA/SF composites could promote bone regeneration via signaling pathways associated with cells and biomaterial interaction. Huang et al. [71] also prepared a HA/SF suspension using in situ precipitation as bio-ink for 3D printing. The obtained 3D printed scaffolds showed good porosity of 70% with interconnected pores with diameter of ~400 μm and relatively high compressive strength of over 6 MPa [71]. The printed scaffolds also demonstrated good in vitro biomineralization activity in SBF while maintaining cell attachment and penetration [71]. Kaplan et al. fabricated 3D HA/silk micro periodic scaffolds as bone scaffolds by the direct-write assembly. The viscosity of HA/silk bio-ink was suitable for printing, with the 3D scaffolds characterized by gradient pore spacings ranging from 200 to 750 μm. After co-culturing with human bone marrow-derived mesenchymal stem cells (hMSCs) and human mammary microvascular endothelial cells (hMMECs), the patterned HA/silk filaments enhanced the osteogenesis and vasculogenesis in one system (Figure 10) [58].
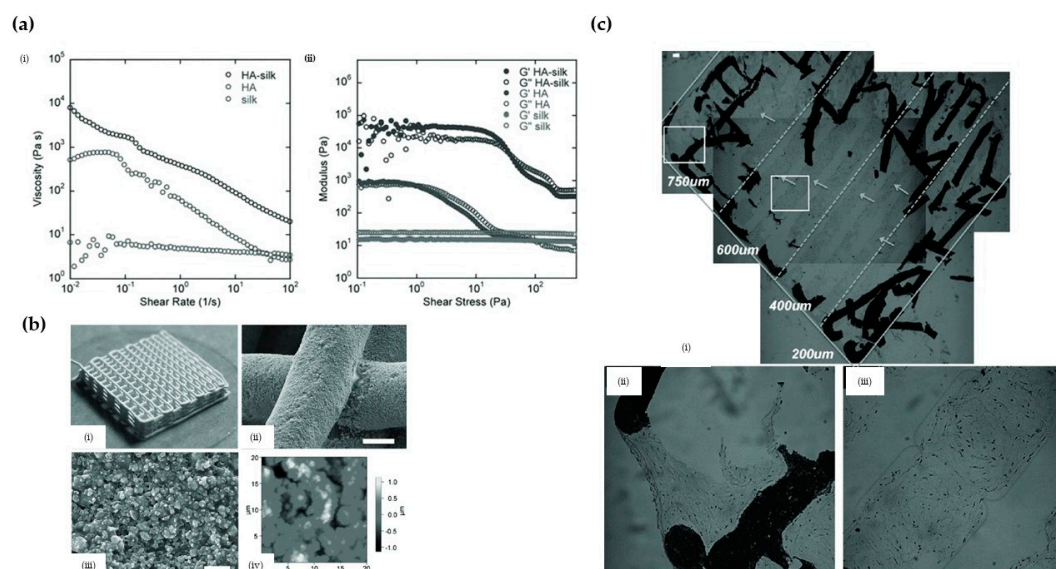

Figure 10. (**a**) The viscosity, elastic (G′), and viscous (G″) moduli of silk fibroin solution, HA suspension, and HA/silk bio-ink. (**b**) Optical image of printed 3D HA/silk scaffold by the direct-write assembly. The scaffold showed the gradient porosity structure confirmed by SEM and AFM investigations. (**c**) The osteogenesis of HA/silk scaffold cultured with hMSCs was evaluated by histological analysis, the gross morphology of cells on the printed scaffolds was observed. Scale bars: 100 μm [58].

3.2.4. Hydroxyapatite (HA)/Alginate Nanocomposites

Alginate is also a wide-used natural polymer for TE [128]. Alginates, as a family of polysaccharides, also called algin or alginic acid, are obtained from calcium, magnesium, and sodium alginate salts from the cell walls and intracellular spaces of brown algae [129]. The alginate structure is composed of a linear repetition of (1→4)-linked β-D-mannuronic acid (M) and α-L-guluronic acid (G) units, with $^4C_1$ ring conformation [53]. Alginate has a strong affinity for di- and trivalent cations and rapidly forms a gel in the presence of low concentrations of such ions (Mg^{2+} being an exception) at a range of pH values and temperatures [130]. Additionally, alginate is a negatively charged polysaccharide that is a suitable scaffold for cell growth [131]. Alginate can be modified by incorporating adhesion ligands (such as RGD) that promote cell attachment and functional groups (such as heparin) that can bind to and immobilize various growth factors. These modifications enable 3D

micropatterning of growth factors in the constructs [132]. However, poor cell adhesion and low osteogenesis ability have limited the capability of alginate for bone regeneration in vivo [133]. Several studies have also indicated that HA/alginate nanocomposites are suitable for TE, with enhanced bioactivity [134–136].

Some studies have been undertaken to demonstrate the functionality of such HA/alginate composites. In a study by Lin et al. [137], HA/alginate scaffold was fabricated and characterized by a well-interconnected porous structure. They showed that the mechanical and cell-attachment properties of HA/alginate scaffold were improved, compared to pure HA or alginate scaffolds. In vitro results display that the osteoblastic cell (rat osteosarcoma UMR106 cells) had a better attachment on HA/alginate composite scaffolds than the pure alginate scaffold [137]. The HA/alginate nanocomposite could be pre-crosslinked using D-Gluconic acid δ-lactone (GDL), and then the mechanical properties of printed HA/alginate scaffold were further improved. The porosity and pore structures of printed HA/alginate scaffold could be readily regulated by varying the printing conditions. During the printing process, the anti-inflammatory drug curcumin could be loaded on the printed scaffold to accomplish sustainable release of a drug. In addition, in vitro results displayed that mouse bone mesenchymal stem cells (mBMSCs) could have adhered to the porous HA/alginate scaffolds (Figure 11) [72].
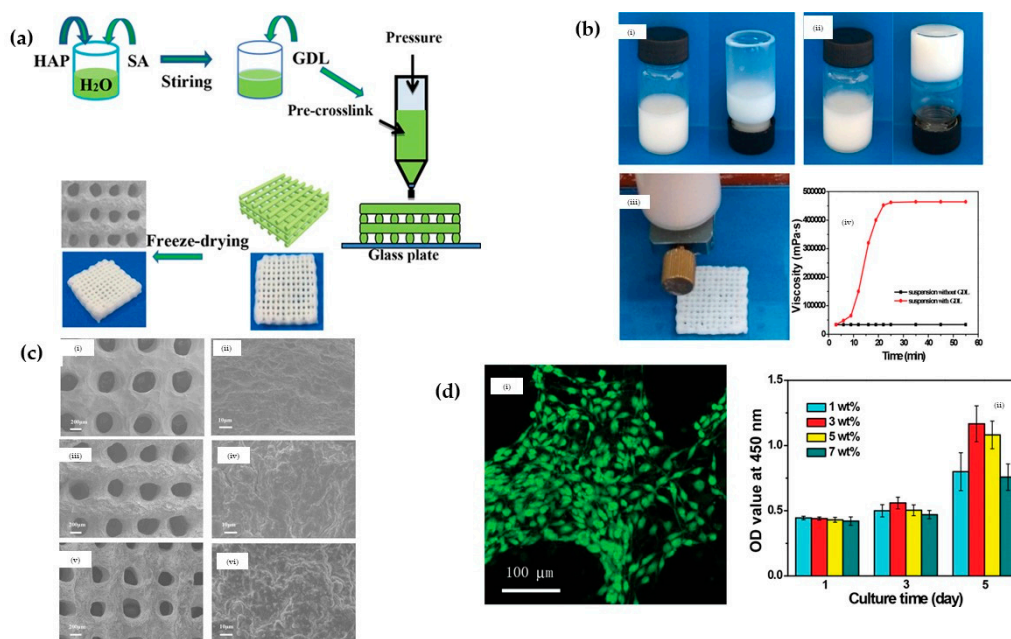

Figure 11. (**a**) Schematic illustration of the porous HA/alginate scaffolds fabricated by extrusion-based 3D printing, in which D-Gluconic acid δ-lactone (GDL) was used as pre-crosslinker. (**b**) Photographs of HA/alginate suspension and hydrogels formed using GDL. The viscosity of HA/alginate suspensions were tested over time using a certain shear rate. (**c**) SEM images of printed porous scaffold after soaking in calcium chloride solution for different times (0, 5, and 10 h). (**d**) The morphology and cell proliferation of BMSCs on printed scaffolds [72].

3.2.5. Hydroxyapatite (HA)/Cellulose Nanocomposites

It is well known that cellulose is the most widespread natural polymeric material in nature. Due to the high biocompatibility, specific binding sites for protein, and reasonable mechanical strength, cellulose is applied in TE [138]. The high density of reactive hydroxyl groups on cellulose fiber can also facilitate cell adhesive proteins such as fibronectin immobilizing on the surface of cellulose. Cellulose fiber is biocompatible for fabricating various scaffolds [139]. However, cellulose has certain limitations for bone engineering construction due to its low ability to induce osteogenesis. Turlybekuly et al. [140] fabricated HA/bacterial cellulose nanocomposites (Figure 12) by inkjet 3D printing, which could be applied in bone engineering. Favi et al. [141] prepared HA/bacterial cellulose scaffold with

well-defined honeycomb pore arrays using a laser patterning technique. The fabricated scaffold was shown to have a honeycomb pore array with diameter of 300 μm, which was suitable for bone TE applications. The incorporation of HA with cellulose can provide good mechanical strength to the nanocomposite scaffold, and the presence of cellulose in the scaffold can induce the orderly deposition of HA crystals the same as in natural bone. However, more work regarding the printability of HA/cellulose bio-ink for 3D printing needs to be undertaken.
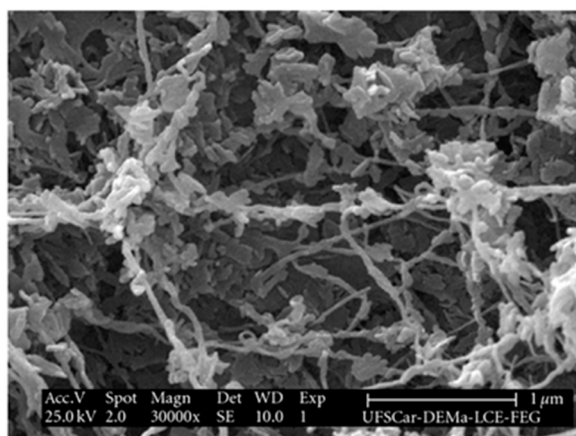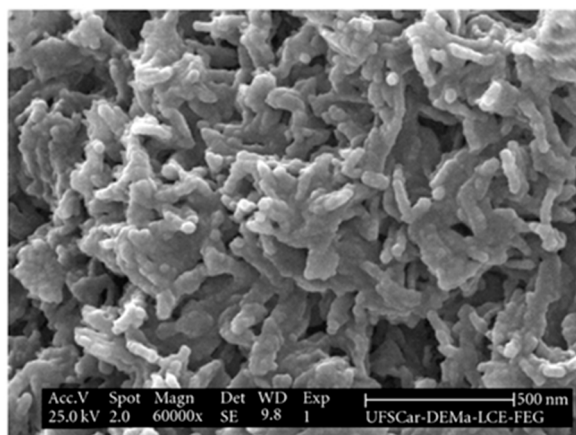

Figure 12. SEM images of the Bacterial cellulose-hydroxyapatite nanocomposites at: (**a**) 30,000×; and (**b**) 60,000×.

3.2.6. Hydroxyapatite (HA)/Chitosan Nanocomposites

Chitosan is a polysaccharide compound obtained by deacetylation of chitin, and chitosan displays good biocompatibility, degradability, solubility in dilute acids, and is nontoxic [142,143]. Chitosan is a linear copolymer of -(1–4) linked 2-acetamido-2-deoxy-D-glucopyranose and 2-amino-2-deoxy-D-glycopyranose [144]. Due to the presence of amino and hydroxyl groups, the chitosan molecule is similar to glycosaminoglycans, which are one of the components of ECM, and chitosan-based materials are widely used in bone, skin, and cartilage TE [145,146]. Since chitosan is a positively charged polysaccharide, it still requires chemical modification and/or mixing with other biomaterials to obtain optimal mechanical and physiological properties for TE [147,148]. There are several reports on HA reinforced chitosan scaffold fabricated using different methods, including 3D printing [73]. The 3D-printed HA/chitosan scaffolds showed a good attachment between layers, forming a regular and reproducible macroporous structure, fully interconnected, with pore size ranging from 200 to 400 μm. The high uniformity of the structure enhanced the mechanical

strength of printed HA/chitosan scaffold, thus improving its capacity to maintain its shape during the shrinkage phase of the dispensing medium [53]. HA/chitosan hybrids were also investigated by Dong et al. [149], who prepared a HA/chitosan hybrid as bio-ink via the addition of silica, and then the porous scaffold was fabricated by combining the sol-gel method and 3D plotting technique. The printed scaffolds possessed controllable and interconnected porous structures, and, compared with chitosan/silica scaffold, the mechanical strength of HA/chitosan greatly improved (compressive strengths of 10–13 MPa and elastic moduli of 21–27 MPa), which could meet the requirements of human trabecular bone (Figure 13a,b) [149]. Ang et al. [150] described a rapid prototyping robotic dispensing system to fabricate HA/chitosan composites. During the fabrication process, the solutions of HA/chitosan as bio-ink were extruded through a small Teflon-lined nozzle (internal diameter: 150 μm) (Figure 13c–e) [150]. Myung et al. fabricated HA/chitosan scaffolds containing 10% chitosan and 20% HA using an air extrusion-based plotter. The printed HA/chitosan scaffold showed good porosity and interconnected structure, increased hydrophilicity and bioactivity, and enhanced proliferation of pre-osteoblast cells on the surface [73]. Zhang et al. [151] discovered that the mechanical property of HA/chitosan composites could be regulated by adjusting the weight ratio of HA/chitosan, such that the maximum value of the compressive strength attains 120 MPa at the mass ratio of 70/30 of HA/chitosan. Owing to these excellent properties, the printed HA/chitosan nanocomposites scaffold has extensive potentials in bone TE and will contribute to the guided regeneration of new bone.
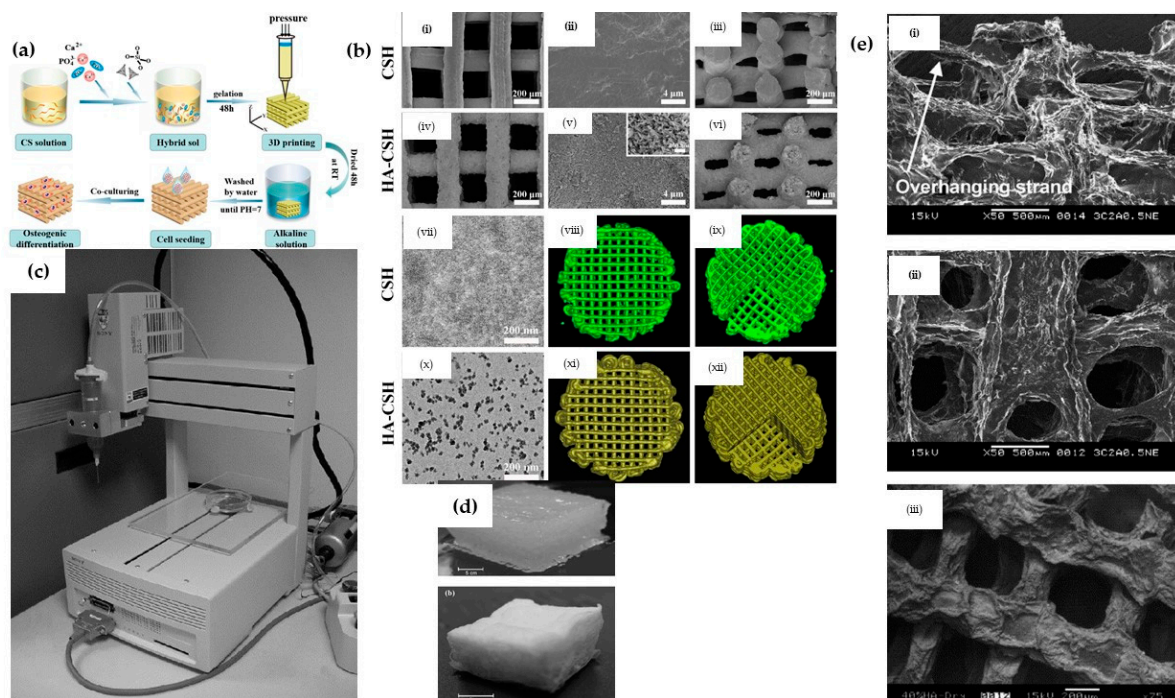
Figure 13. (**a**) Schematic illustration of HA/chitosan hybrid scaffold fabrication for bone TE; (**b**) pore size, morphology and connectivity of printed chitosan and HA/chitosan scaffolds [149]; (**c**) rapid prototyping robotic dispensing system for printing HA/chitosan scaffold; (**d**) the printed HA/chitosan scaffold before and after freeze-drying; and (**e**) SEM images of HA/chitosan scaffold [150].

3.2.7. Other Hydroxyapatite (HA)/Natural Polymer-Based Nanocomposites

Apart from collagen, gelatin, silk, alginate, cellulose, and chitosan, many other natural polymers such as hyaluronic acid (HA), hemicellulose, lignin, fibrin, agarose, decellularized extracellular matrix (dECM), etc., have been developed as bio-ink for 3D printing [152,153]. Wenz et al. [154] developed a bio-ink consisting of methacrylated hyaluronic acid (HAMA) and HA for bone printing (microextrusion printing). The primary human adipose-derived

stem cells could be encapsulated in HA/HAMA gels and had excellent cell viability after culturing for 28 days. The bio-ink with encapsulating cells showed excellent printability, and the printed grid structure's integrity remained intact over 28 days for cell culturing. The staining of bone matrix components such as collagen I, fibronectin, alkaline phosphatase, and osteopontin confirmed that the printed cell-laden HA/HAMA scaffolds were suitable biomaterials for bone regeneration [154]. Compared to a single natural polymer, multi-natural polymers composited with HA showed superior and improved properties for 3D printing. Crucially, given chitosan's primary attractive features of biocompatibility, flexibility adhesiveness, and anti-infectivity [155–158] and silk fibroin's (SF's) characteristics of mechanical strength, appreciable bio-affinity, and adequate oxygen permeability [159,160], compositing chitosan and SF with HA could significantly improve the microhardness, formability, and flexibility of HA-based nanocomposites [161,162]. This was demonstrated by Wang and Li [163], who confirmed that the compressive strength of HA/SF/chitosan nanocomposites was increased to 180 MPa, which was higher than pure HA, HA/SF, and HA/chitosan composites. Additionally, Peter et al. [164] also discovered that the prepared biological and mechanical properties of HA/chitosan/gelatin scaffolds were improved at the same time compared to that of HA/chitosan and HA/gelatin scaffolds [164]. Verma et al. [165] synthesized HA/chitosan/polygalacturonic nanocomposites, in which the strength was measured to be about 160 MPa. Abouzeid et al. [166] prepared T TEMPO-oxidized cellulose nanofibril/alginate hydrogel using extrusion-based 3D printing. Different forms of constructs were obtained, including half bone, the human ear, cubic, cylinder, and boat. The printed constructs maintained their shape and fidelity without the collapse of the filaments.

3.2.8. Hydroxyapatite (HA)/Poly (Lactic Acid) Based Nanocomposites

Poly(lactic acid) (PLA) is a nontoxic, bio-absorbable thermoplastic polymer produced by ring-open polymerization of lactide, and PLA can be acquired from the fermentation of sugar feedstock [167]. PLA has attractive biodegradable, good biocompatibility, and excellent mechanical properties because of its linear aliphatic structure [168–170]. Furthermore, the properties of PLA may be regulated by altering the ratio of its D- to L-isomers. For the above reasons, PLA was widely used as a matrix material in constructing biodegradable composites for bone repair [171,172], and bone-fixation devices used in orthopedics and oral surgery applications [173,174]. However, the application range of PLA is still limited because of the unpredictable hydrolysis and poor hydrophilicity [175]. Such problems could however be overcome by binding bioactive ceramics such as HA with PLA [176–180]. The HA/PLA composite was considered as a potential biomaterial for bone repair and replacement in the early years [181]. The degradation rate of PLA could be slowed by the dispersion of HA nanoparticles, while the mechanical property may also be improved by increasing the HA nanoparticles distribution [182,183]. The versatility of such HA/PLA composites was also discussed in the literature [184]. The porous HA/PLA scaffold could be printed using extrusion 3D printing for load-bearing bone tissue applications; the compression strength of printed constructs could be adjusted by employing finite element modeling and simulation, as shown in Figure 14a (adapted from [74]). According to the authors of [74], in vitro results show that cells had a better attachment and proliferation on printed HA/PLA scaffold than PLA scaffold [74]. Corcione et al. [185] fabricated HA microspheres/PLA scaffold using FDM (Figure 14b,c). The composite filaments were obtained first for 3D printing. Compared to printed PLA scaffold, HA/PLA scaffolds showed higher porosity and rougher surface. However, the mechanical performances of these HA/PLA scaffolds decreased [185]. Compared to PLA, poly-L-lactic acid (PLLA) displays a slower degradation, which is believed to result in a lower rate of inflammatory tissue reaction [174,186]. Due to the bioresorbable characteristic, HA/PLLA has bone-bonding potential for bone regeneration. During the new-bone formation, PLLA is resorbed via metabolization and excretion, and HA is assimilated in the body. Thus, the HA/PLLA construct has possible prospects for application in restricted-load areas [187,188]. For

instance, Verheven et al. [189] showed that the HA/PLLA composite at the mass ratio of 30/70 displayed the highest compressive and tensile strengths, stiffness, and Vickers hardness number. Further benefits of the HA/PLLA composite were demonstrated by Furukawa et al. [190], who confirmed that HA/PLLA using 30 wt.% HA presented an enhanced degradation rate compared to other design ratios.
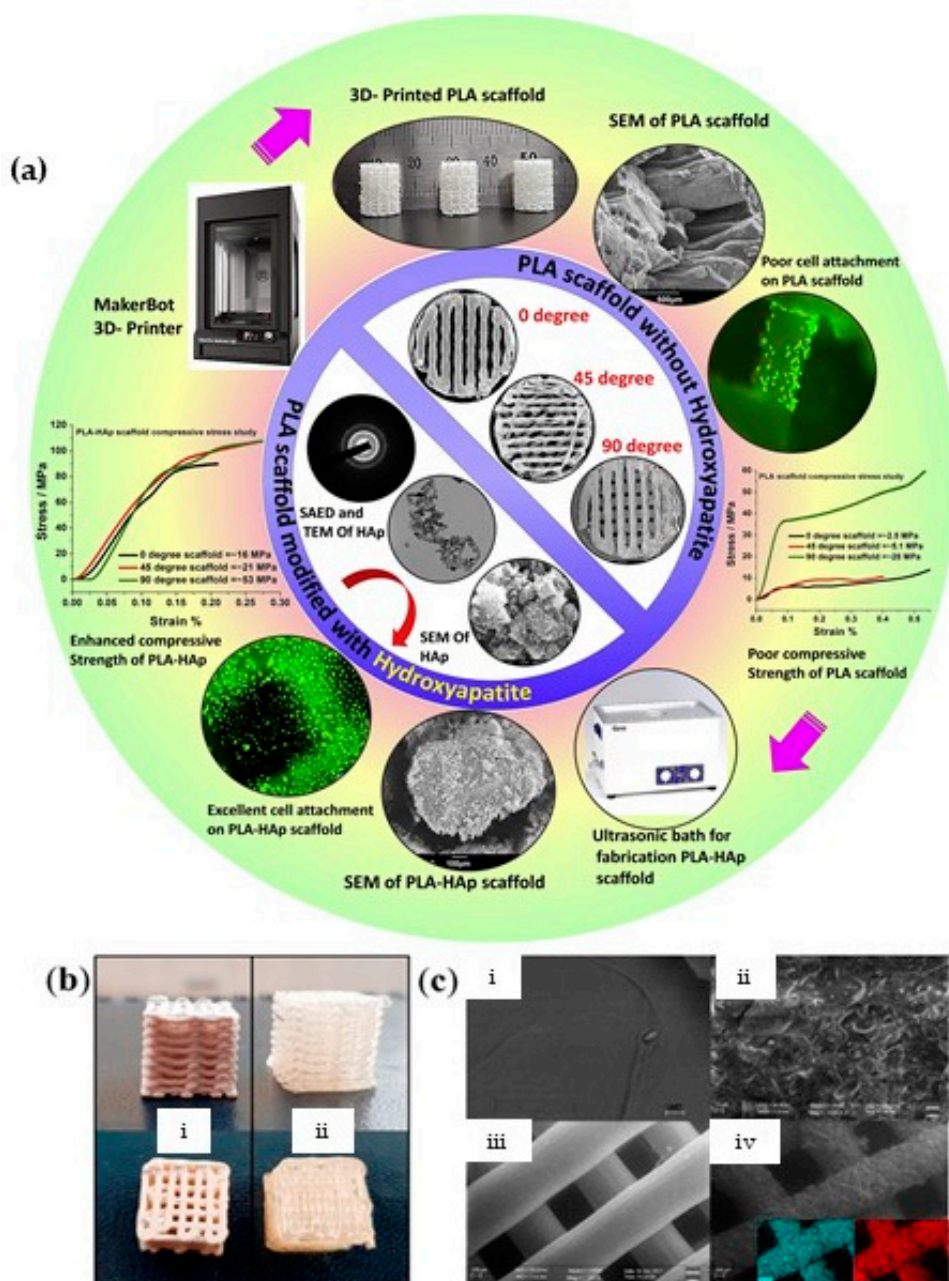
Figure 14. (**a**) Schematic representation of 3D printed PLA scaffold and HA/PLA scaffolds for bone TE application [74] (**b**) photos of 3D printed HA/PLA and HA scaffolds; and (**c**) SEM images of 3D printed PLA and HA/PLA scaffolds using FDM. The differences of surface and macrostructure for both scaffolds are displayed [185].

3.2.9. Hydroxyapatite (HA)/Poly-ε-Caprolactone Nanocomposites

Poly-ε-caprolactone (PCL) is commonly used as a synthetic biomaterial for bone tissue and periodontal applications due to its biocompatibility, suitability for various scaffold fabrication techniques, prolonged degradation rate, and mechanical stability. However,

PCL scaffolds can adversely affect bone regeneration because of the slow degradation rate of PCL, which remains intact for extended periods [191]. The aforementioned issue may be overcome by compositing with HA, such that the produced bone volume and the bone contour could be maintained over time after implantation. PCL and PCL-based scaffolds could be easily fabricated via 3D printing because of their good printability, and quick solidification after extrusion [75]. Hu et al. [192] fabricated HA/PCL scaffolds with hierarchical porous structures and tunable multi-functional performance via 3D printing. Xia et al. [66] also fabricated HA/PCL scaffolds using the SLS technique. The printed scaffolds had porosity ranging from 78.54% to 70.31%, and the corresponding compressive strength ranged from 1.38 to 3.17 MPa. SEM images showed that HA/PCL scaffolds displayed predesigned, well-ordered macropores, and interconnected micropores; the hMSCs could well attach and proliferate on printed scaffolds. The in vivo results confirm that the printed HA/PCL scaffolds not only enhanced the formation of new bone but also fulfilled all the basic requirements of bone TE scaffolds, which showed sizeable potential use in orthopedic and reconstructive surgery (Figure 15) [66].
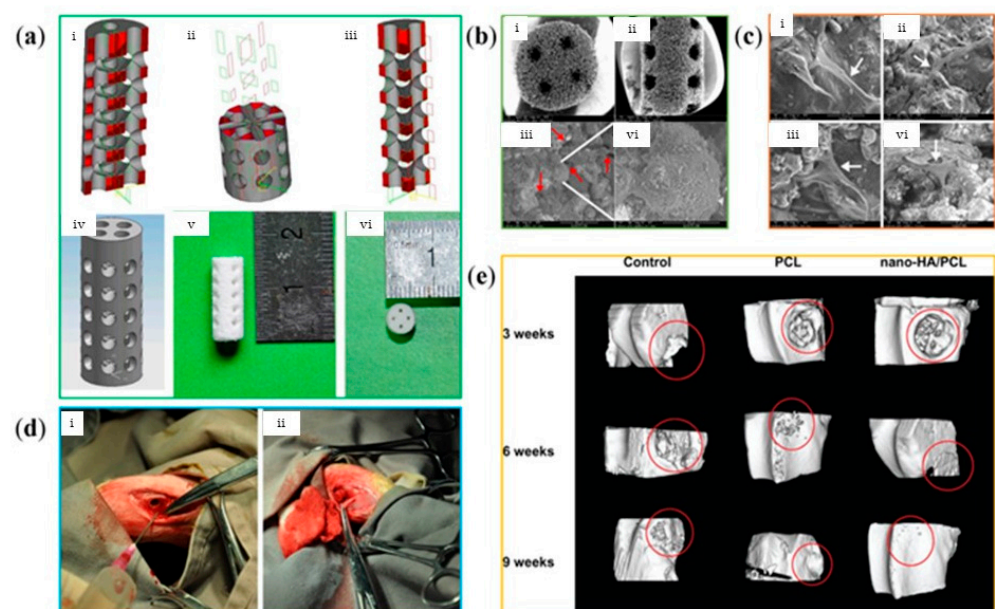
Figure 15. (**a**) The models of computer-aided design and printed HA/PCL scaffolds using SLS; (**b**) SEM images of printed HA/PLC scaffolds; (**c**) the morphology of hMSCs seeded on HA/PCL scaffolds; (**d**) the printed HA/PCL scaffolds were implanted in the femur defect of the rabbit; and (**e**) 3D reconstruction images of micro-computed tomography (micro-CT) confirmed the new bone was formed over weeks [66].

3.2.10. Hydroxyapatite (HA)/Polymethyl Methacrylate Nanocomposites

Polymethyl methacrylate (PMMA) is an FDA approved synthetic polymer widely employed in ophthalmic, orthopedic, and dental applications [193]. PMMA is also used as bone cement to fill the defects of any shape or size, thus it can be employed in the treatment of osseous tumors, trauma, disease, and birth defects in the skeletal system [193]. Petersmann et al. [194] printed PMMA scaffold with honeycomb structure using fused filament fabrication (FFF, one of the extrusion-based 3D printing techniques) for the cranial implant. The properties of the scaffold could be improved by topology optimization. However, there are several disadvantages for PMMA, such as brittleness and release of heat during polymerization, which can lead to necrosis at the bone cement interface. Thus, PMMA needs to be further modified to improve its formation and ameliorate stress shielding [195]. In another study by Tontowi et al. [195], PMMA powder was blended with methyl methacrylate (MMA) liquid to obtain PMMA pasta first, such that the PMMA pasta composited with HA

nanopowder could be used for 3D printing. The solidification time was increased with the increase of MMA content, but the tensile strength of HA/PMMA composites reduced due to the addition of HA [195]. Mahammod et al. [196] developed HA/PMMA using solvent casting particulate leaching technique; computational fluid dynamics (CFD) analysis concluded that HA/PMMA scaffold with 60 wt.% HA content tended to be the most promising choice for bone TE applications due to the best combination of porosity, permeability, and compressive strength [196]. The properties of HA/PMMA composites can be significantly improved using 3D printing in comparison with traditional techniques. Lal et al. [197] fabricated HA/PMMA scaffold using FDM technology for cranioplasty application, especially for large cranial defects, which provided a novel, economical, patient-specific fabrication method compared to traditional titanium and polyether ether ketone (PEEK) cranioplasty [197]. Since the mechanical properties of HA/PMMA nanocomposites are lower than those of PMMA, Esmi et al. composited HA/PMMA with carbon nanotubes (CNTs) as 3D-printing filaments. The nano-indentation results reveal that the modulus and hardness of HA/PMMA/CNTs were increased compared with those of HA/PMMA, while the biocompatibility test results confirm the obtained nanocomposites accelerated cell attachment, growth, and proliferation [76].

3.2.11. Hydroxyapatite (HA)/Polyvinyl Alcohol Nanocomposites

Polyvinyl alcohol (PVA) is a water-soluble thermoplastic that is usually used as a support material for 3D printing. PVA is commonly used in medical devices because of its good biocompatibility, high water solubility, and chemical resistance [198]. Mainly, PVA is widely applied in cartilage TE due to its similar tensile strength to human articular cartilage [199–201]. However, the non-degradability of PVA still limits its usage as an implantation scaffold in the body [202]. Notably, compositing PVA with calcium phosphate nanoparticles, such as HA, β-TCP, and BCP, showed promising application for the fabrication of scaffolds in bone TE [203–205]. Several research results confirm that the osteoconductive HA/PVA scaffold could be achieved for bone replacement [206]. PVA is sensitive to humidity, and softened PVA might cause air bubbles, thus reducing its functionality in printing processes. To our knowledge, few reports regarding HA/PVA scaffold fabrication via 3D printing exist in the literature. For instance, Chai et al. [207] fabricated HA/PVA scaffolds by powder-based 3D printing. The results show that the printed scaffold with 1.0 wt.% of PVA showed the best compressive strength. In addition, the printed HA/PVA processed excellent cytocompatibility; the comprehensive performances of HA/PVA scaffolds were better and much more suitable as bone scaffolds than those of HA/polyvinyl pyrrolidone (PVP) and HA/polyacryl amide (PAM) scaffolds fabricated by the same approach [207]. Chua et al. [203] also fabricated HA/PVA scaffolds using SLS technology, confirming that the printed scaffold has potential for joints and craniofacial applications. Another study [77] showed that the porous structure of HA/PVA scaffold, such as pore size, could be regulated by adjusting the content of HA in HA/PVA bio-ink before printing, as shown in Figure 16. In this study, Ergul et al. printed HA/PVA scaffold using the extrusion 3D printing technique. The results reveal that the HA/PVA [77] bio-ink with 15 wt.% of HA demonstrated significantly superior features for extrusion printing, with the elastic modulus of the printed scaffold being similar to that of natural bone.
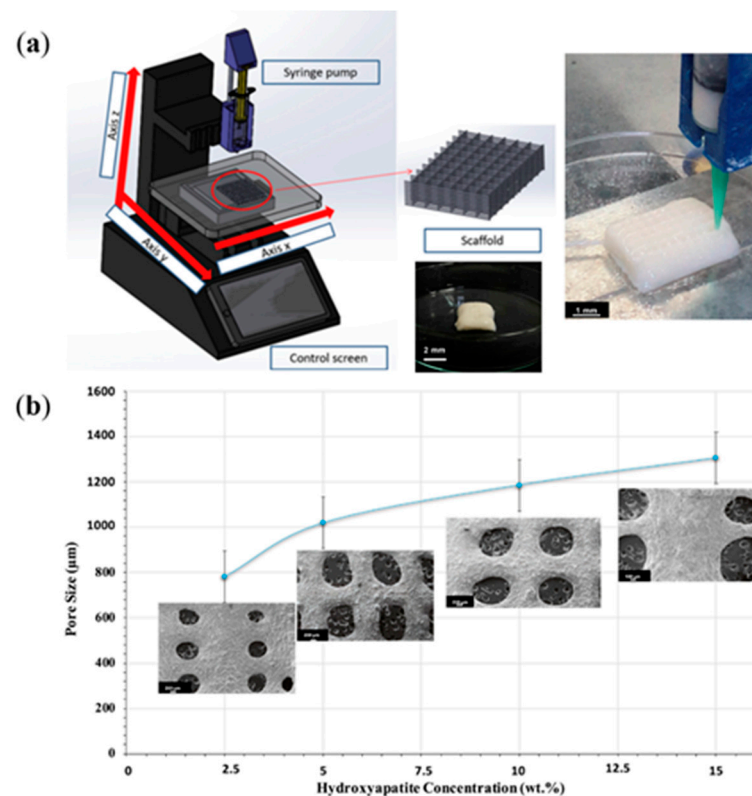
Figure 16. (**a**) 3D printing set up for fabrication of porous HA/PVA scaffold. (**b**) The pore size of printed scaffolds was regulated by adjusting the concentration of HA [77].

3.2.12. Hydroxyapatite (HA)/Poly(Propylene Fumarate) Nanocomposites

Poly(propylene fumarate) (PPF) is an unsaturated linear polyester that can be crosslinked through carbon double bonds along its backbone [208]. PLA, PCL, and PPF are considered as bioresorbable polymers that can degrade enzymatically or via hydrolysis in vivo. PPF may be degraded into nontoxic products of propylene glycol, poly(acrylic acid-co-fumaric acid), and fumaric acid [209]. PPF has been widely used in medical applications, including vascular stents, cartilage, blood vessel engineering, bone TE, etc. [210]. PPF may be printed into a variety of 3D shapes using extrusion-based printing and SLA3D printing [211,212]. Besides linear PPF oligomers, Fer et al. [213] developed PPF bio-ink for continuous DLP, with the printing speed improved. PPF is one of the promising candidate materials for load-bearing applications due to suitable mechanical properties [214,215]. However, the biomechanical and osteoconductive properties of PPF need to be further enhanced, e.g., through the addition of ceramic components to PPF [193]. Lee et al. [216] asserted that the osteoconductive ability of HA/PPF nanocomposites was increased compared with pure PPF. In addition, the hydrophilicity and serum protein adsorption on the surface of HA/PPF nanocomposites was shown to significantly increase, resulting in enhanced cell attachment, spreading, and proliferation over time [215]. Trachtenberg et al. [217] developed complex HA/PPF scaffolds using extrusion-based 3D printing for bone TE applications. The spatial deposition of HA in 3D nanocomposite scaffold may be controlled during the printing process. The printed scaffolds displayed well-defined layers with interconnected pores, which were considered as necessary for a successful bone implant (Figure 17a–c) [217]. Lee et al. [218] fabricated HA/PPF scaffolds by micro-SLA (MSTL) technology. During the preparation of the HA/PPF bio-ink, diethyl fumarate (DEF) was incorporated to reduce the viscosity, and the photo-initiator bis-acylphosphine oxide (BAPO) and 7 wt.% of HA were designed. The printed scaffolds displayed regular and connected pores, as shown in Figure 17d,e. Furthermore, in vitro results show that

MC3T3-E1 cells had a better cell adhesion and proliferation on printed HA/PPF than PPF scaffolds [218].
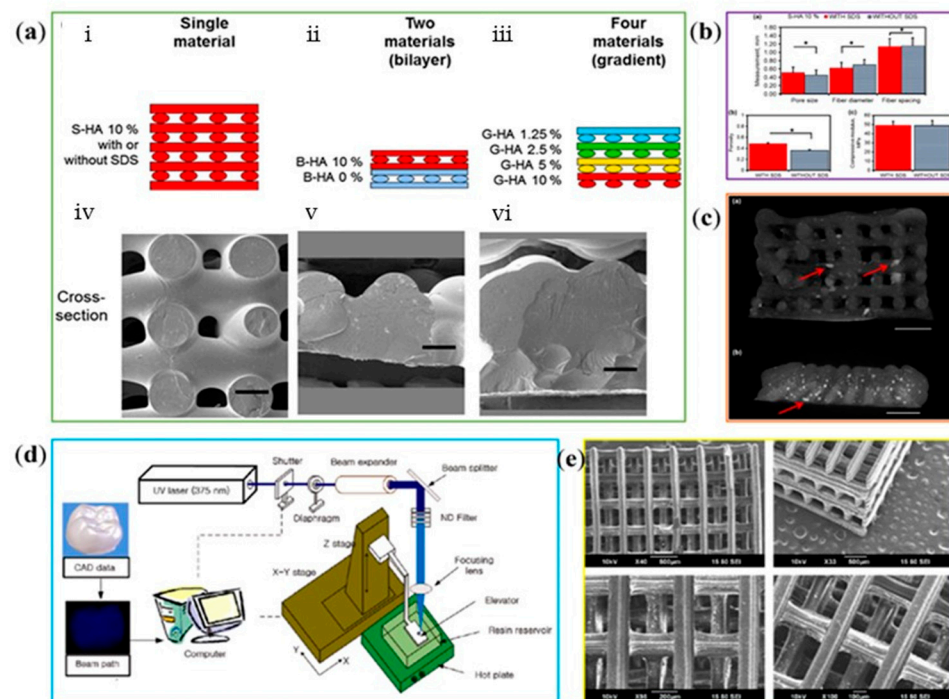
Figure 17. (**a**) The HA/PPF scaffolds consisted of well-defined layers with interconnected pores were printed using extrusion-based 3D printing. (**b**) The mean pore and fiber measurements, porosity, and compressive mechanical properties of printed HA/PPF scaffold were adjusted by adding sodium dodecyl sulfate (SDS). (**c**) Cross-sectional images of HA/PPF scaffold from a 3D reconstruction via micro-CT [217]. (**d**) HA/PPF could be printed using micro-SLA (MSTL). Before printing, diethyl fumarate (DEF) was used to reduce the viscosity. (**e**) SEM images of printed HA/PPF scaffolds [218].

3.2.13. Other Hydroxyapatite (HA)/Synthetic Polymer-Based Nanocomposites

In addition to the above mentioned synthetic polymers, several other synthetic polymers such as poly(ethylene glycol) (PEG), Pluronic, poly(acrylic acid) (PAA), and poly(glycolic acid) (PGA) have been used as composites with HA to print HA-based constructs for enhanced structural manipulability, flexibility, and versatile mechanical performances [100,219]. Comparatively, pure HA scaffolds present poorer mechanical properties compared to HA/synthetic polymer scaffolds [164]. It is however still challenging to achieve the targeted compressive strength and modulus for load-bearing applications in such HA/synthetic polymer scaffolds [216,220]. These challenges may be resolved via the utilization of the integration of multiple synthetic polymers in scaffolds. This is because such HA/multi-synthetic polymers scaffold systems show unexpected characteristics due to the synergistic effect of each synthetic polymer network. For example, Park et al. [220] produced HA/PLLA/PCL composites using surface etching, biomimetic coating, dip coating, and hot compression molding methods, demonstrating that the mechanical properties of the scaffolds, including flexural strain, flexural modulus, and compressive strength, could be regulated to match the mechanical properties of natural bone by manipulating the HA/PCL ratio and molding temperature. Charles et al. [221] also confirmed that the fracture toughness and fracture absorbed energy of HA/PLLA/PCL composites were favorably improved by using 5 wt.% of PCL, and the fracture properties decreased rapidly when the content of PCL was greater than 10 wt.%. More HA/multi-synthetic polymers nanocomposites that may be utilized as bio-ink will be developed in the near future; however, the properties of such nanocomposites and the manufacturing parameters need to be systematically studied in advance.

3.2.14. Hydroxyapatite (HA)/Natural Polymer/Synthetic Polymer-Based Nanocomposites

HA/natural polymer/synthetic polymer-based nanocomposites have been widely used for TE because the mechanical properties of the composite can be enhanced by synthetic polymers, and the various cellular activities can be enhanced by natural protein-based polymers, such that osteogenic differentiation is promoted. Ashraf et al. [222] fabricated porous HA/PVA/collagen (type I) using electrospinning techniques, which unidirectionally aligned HA nanoparticles to mimic the nanostructure of human bone tissue. They showed that the pore size and shape of prepared scaffolds could be adjusted, and the mechanical properties of scaffolds were improved compared to those of PVA/collagen scaffolds [222]. Considering the advantages of PLLA, such as good bio-absorbability, mechanical property, and biocompatibility, it could be composited with collagen to improve the low viscosity of collagen for 3D printing [223]. Several reports on HA/PLLA/collagen scaffolds with hierarchical microstructure reveal that not only is the structure of the scaffold similar to the natural bone, but HA/PLLA/collagen scaffolds also improve cell attachment and stimulate cell proliferation and differentiation, thus confirming that the HA/PLLA/collagen construct was suitable as orthopedic implant for bone TE [224–226]. In addition, there have been many studies on fabricating HA/PMMA/sericin nanocomposites, due to the excellent biocompatibility of sericin without allergenic activity and outstanding mechanical performance of PMMA [227–231]. For instance, Chirila et al. discovered that human corneal limbal epithelial cells could be re-attached and grown on sericin-based membranes [227]. Tontowi et al. prepared HA/PMMA/sericin nanocomposites as bone implants and showed that the mechanical strength was mainly decided by PMMA, while the diametral tensile strength of nanocomposites was dominantly affected by HA instead of sericin [232]. In a subsequent study, Tontowi et al. [233] confirmed that HA/PMMA/sericin nanocomposites could be used as bio-ink for extrusion-based 3D printing. The disadvantages of chitosan mainly include low bone-bonding bioactivity and mechanical strength and loosening of structural integrity under wet conditions. These disadvantages could be avoided in the chitosan/PLA composite, since the PLA serves to enhance the mechanical strength of the composite with excellent osteoconductivity and biodegradation for bone remodeling and growth [234–238]. Cai et al. [239] also prepared HA/PLA/chitosan nanocomposites as scaffold for traditional bone-defect repair. Niu et al. fabricated HA/PLLA/collagen nanocomposites with hierarchical microstructure; cell proliferation and differentiation on HA/PLLA/collagen scaffolds were improved compared to on HA/PLLA. However, the HA/PLLA/collagen scaffolds were shown to still lack osteoinductivity, which is considered a critical factor for bone regeneration [240]. Additionally, Niu et al. [241] fabricated HA/PLLA/collagen/chitosan scaffolds which displayed excellent osteoinductivity and suitable pore structure as inductive implant scaffold for bone regeneration [241].

Compared to cellulose, bacterial cellulose nanocrystal (BC) has better mechanical properties. In addition, BC has remarkable features, such as promoting cellular interactions and tissue development, bio-absorbable and nontoxicity. Cakmak et al. [78] fabricated porous HA/PCL/gelatin/BC constructs using the FDM approach. They showed that the pore structure of printed constructs may be regulated, such that cells could attach and proliferate on constructs [78]. Lu et al. [242] subsequently fabricated HA/PCL/silk fibroin constructs as artificial bone scaffolds using 3D printing. The printed scaffolds were implanted in the bone defect of New Zealand rabbits. The histological observation revealed that the new bone was apparently formed in 12 weeks, and the new bone volume was increased while double-transfected BMP-2/VEGF mesenchymal stem cells were loaded in printed scaffolds [242]. Kim et al. used a core–shell nozzle printing technique to fabricate HA-based nanocomposites, with PCL in the core region and HA/PVA/gelatin composites in the shell region. The printed scaffolds were also coated using collagen fibril to increase cell attachment and proliferation. Physicochemical and biological evaluations, such as mechanical, swelling, protein absorbing, cell proliferation, alkaline phosphatase (ALP)

activities, and calcium deposition, concluded that the printed scaffold showed significant potential for bone TE [243]. Yeon et al. [79] developed HA/PLA/silk nanocomposites as bone clip type internal fixation device using extrusion-based 3D printing. The results show that printed HA/PLA/silk constructs as bone clips had similar mechanical properties and superior biocompatibility compared to traditional bone clips. In addition, Yeon et al. showed that the HA/PLA/silk bone clip displayed excellent alignment of the bony segments across the femur fracture site, according to animal model results [79]. More types of HA/synthetic polymer/natural polymer-based nanocomposites will be developed using 3D printing in the future due to the printability of such bio-ink and the apparently improved properties of scaffolds.

3.3. Hydroxyapatite (HA)-Based Ceramics

3.3.1. Hydroxyapatite (HA)/β-Tricalcium Phosphate (BCP) Based Ceramics

β-tricalcium phosphate (β-TCP) is of low mechanical strength and degrades too quickly in a physiological environment. These properties may however be altered/improved via its combination with HA [38,50,68]. BCP has been used to fabricate bone graft materials for 30 years; BCP-based ceramics have proven efficacy in clinical indications [244,245]. Although many 3D printing approaches could be used to fabricate complex BCP-based ceramics, including inkjet printing, SLA, selective laser sintering, and DLP, the performance of BCP and BCP-based ceramics and their printable properties as bio-inks need to be further viewed [246]. Huang et al. [247] fabricated porous BCP ceramics using extrusion-based 3D printing with a motor-assisted micro-syringe (MAM) system; the morphology, pore size, and porosity of printed BCP scaffolds could be precisely controlled to optimize their mechanical properties [247]. Li et al. [244] obtained BCP scaffolds with a complex geometric structure using a slurry-based microscale mask image projection SLA. The BCP-based photocurable suspension with complex geometry was obtained first. After that, the curing performance and physical properties of BCP suspension were investigated to optimize the scaffold composite. The printed BCP scaffold presented excellent biocompatibility, as well as possessed sufficient mechanical strength compared to a long bone for surgery [244]. Wang et al. printed BCP scaffolds using inkjet 3D printing; 0.6 wt.% PVA solution and 0.25 wt.% Tween 80 were used as a binder to prepare BCP bio-ink. The printed BCP scaffold with HA/β-TCP mass ratio at 60:40 showed the best biocompatibility [68]. It is clear that the binder used will vary significantly depending on the researcher, printing technique, etc. Thus, in addition to the binder employed by Wang et al., some other examples of binders and the associated ceramic 3D printing techniques reported in the literature are highlighted in Table 4.

Table 4. Some binders employed in major 3D printing technologies.

3D Printing Technology	Binder	Some Notes	Source
DIW writing	Polymethylsilsesquioxane	This binder has been shown to be viable in the fabrication of ceramic matrix composite. In the study, polymethylsilsesquioxane and ceramics were used in the preparation of a preceramic polymer. Using this binder and 3D printing technology, complex ceramic matrix composite structures with porosity and compressive strength of ~75% and ~4 MPa were fabricated.	[248]

Table 4. *Cont.*

3D Printing Technology	Binder	Some Notes	Source
Inkjet-based 3D printing	Polymethylsilsesquioxane	This binder was employed in the 3D printing with β-TCP and a polysiloxane to manufacture bulk β-TCP with a silica coating. The mechanical strength of the final sintered porous structures was within the range of that of trabecular bones, in the order of 0.1–16 MPa.	[249]
Inkjet-based 3D printing	Colloidal silica	In this study, the focus was to demonstrate and assess the possibility of using the inkjet-based 3D printing technique and the colloidal silica binder in the fabrication of porous ceramic-based composite parts. Information regarding the mechanical strength of the composite was however not presented.	[250]
DLP 3D printing	Silicon resin	In this work, a DLP-based 3D printing technique was used in fabricating a ceramic composite while also employing silicon resin as the binder. The study showed that the compressive strength and elastic modulus values 3D-structured ceramic based lattice were 5.12 and 2.1 MPa, respectively.	[251]
Extrusion-based 3D printing	PVA	In this study, PVA was employed as a binder in the fabrication of structures of HA composites. The study showed that, at 7–14% of the polymer, HA composites are well extruded and presented a mechanical strength of ~4 MPa after hardening.	[252]
Selective laser sintering	Schelofix, Polymeric binder	In this study, water soluble Schelofix was employed as a binder in the fabrication of HA based composited for 3D printing of scaffolds. A structure with mechanical strength of 22 MPa via the printing technique was achieved.	[101]
Selective laser sintering	Polyvinyl alcohol	In this study, water-soluble PVA was employed as a binder, in the fabrication of ceramic based composites. The study showed that, by using the binder in conjunction with the selective laser sintering, the resulting structure has an average flexural strength of 363.5 MPa and a relative density of 98%.	[253]
SLA based 3D printing	Photopolymer binder such as (meth)acrylate monomer/oligomers	In the study [254] 1,6-hexanediol diacrylate was used as an acrylate-based monomer as the photopolymer binder with a ceramic content of 50 vol% to enable the fabrication of structures with high relative density of 99.95% and high flexural strength of 1008.5 MPa.	[255]

Zhang et al. printed a BCP scaffold using extrusion-based 3D printing approach. The physicochemical properties, porosity, and compressive strength of printed BCP scaffolds could be adjusted by changing HA/β-TCP ratio, and, especially, the degradation rate could be tailored to match the growth rate of new bone. The printed BCP was further used for

personalized beagle skull defect repair in vivo, and the histological results confirmed that the implanted scaffold was highly vascularized and well-combination with surrounding tissues [256]. Maria Touri et al. fabricated BCP scaffolds (HA/β-TCP ratio at 60:40) using a direct-write assembly (robocasting) approach. After that, the printed BCP scaffolds were further treated by coating an oxygen releasing agent consisting of calcium peroxide (CPO) encapsulated within a PCL matrix. The results demonstrate that the coated BCP scaffolds could improve osteoblast cells viability and proliferation as well as promote bone ingrowth under hypoxic conditions [257]. Luis Diaz-Gomez et al. used E-Shell® 300 with BCP powder (HA/β-TCP ratio at 50:50) to obtain a novel BCP bio-ink with reproducible printability and storability properties. This bio-ink had a consistent printability over two weeks. Then, the porous scaffolds were printed using an extrusion-based printing technique. The printed BCP scaffolds were further sintered at 1200 °C. The structure of BCP scaffolds, such as pore size, porosity, and isotropic dimensions, was not affected by sintering treatment (Figure 18). The mechanical properties of scaffolds were in the range of human trabecular bone, proving that the printed constructs could potentially load-bearing bond TE applications [258]. With the development of 3D printing techniques, more BCP-based bio-inks and scaffolds will be achieved in the future.
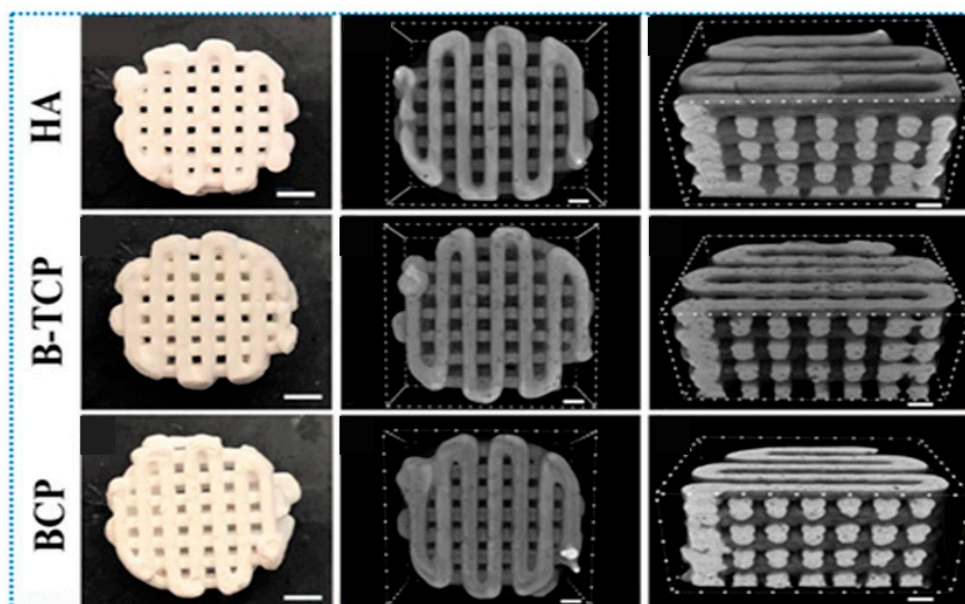
Figure 18. Optical images (left) and micro-CT images (middle and right) of HA, β-TCP, and BCP scaffolds printed by extrusion 3D printing [258].

3.3.2. Hydroxyapatite (HA)/Bioglass Based Ceramics

Bioglass, or bioactive glass, was invented by Hench from the University of Florida, in 1969. The first bioglass composition consisted of 46.1 mol% SiO_2, 24.4 mol% Na_2O, 26.9 mol% CaO, and 2.6 mol% P_2O_5 and was called 45S5 Bioglass [259,260]. The discovery of bioglass launched the field of bioactive inorganic materials, which can form a bond with bone tissues [261]. Bioglass has shown great potential in bone regeneration because of its osteoconductivity and osteo-productivity. Compared to HA, bioglass has a lower thermal conductive coefficient and better bioactivity. However, due to the high dissolution rate of bioglass in body fluids, bioglass scaffolds may degrade completely before the new bone forms [262,263]. Several reports state that HA/bioglass composites can be applied in bone regeneration due to their excellent bioactivity. Tan et al. [264] indicated that HA/bioglass could stimulate early osteogenesis and osteointegration at the interface in the biological environment. In addition, HA/bioglass constructs could improve the interfacial bonding to surrounding tissue without scar layer formation [265–269]. However, few reports on the 3D printing of HA/bioglass constructs are found in the literature.

For instance, Qi et al. [270] fabricated the calcium sulfate hydrate (CSH)/mesoporous bioactive glass (MBG) scaffolds using inkjet 3D printing approach (4th 3D Bioplotter™, EnvisionTEC GmbH, Germany). The printed scaffolds had a regular and uniform structure and excellent apatite mineralization ability, and in vivo results confirm that CSH/MBG scaffolds could greatly enhance new bone formation in calvarial defects [270]. Seyedmajidi et al. also obtained HA/bioactive glass as cell scaffolds for rat tibia reconstruction. The radiological, histopathological, and histomorphometric assessments indicated that the trabecular thickness and rate of new bone formation were increased [271,272].

3.3.3. HA-Based Composites of Titanium Ceramics

Besides calcium phosphate ceramics, titanium and its alloys, such as titanium dioxide (TiO_2) and titanium alloy (Ti-6Al-4V, Ti64), can be used to fabricate scaffolds for TE. This is because TiO_2 has good biocompatibility, chemical stability, good mechanical properties, and excellent strength-to-weight ratio. TiO_2 is also capable of enhancing the growth of bone and vascular tissues and osteoconductivity [273]. TiO_2 has therefore attracted much attention as a scaffold for tissue reconstruction, as demonstrated in some studies in the literature. For instance, Kim et al. fabricated HA/TiO_2 nanocomposites using HA doped TiO_2 particles and discovered that the strength and bioactivity of HA/TiO_2 nanocomposites were enhanced compared with TiO_2 constructs [274]. Additionally, Ti64, known for its excellent strength- to-weight ratio, is an $\alpha+\beta$ alloy that can be employed in fabricating porous scaffolds [275]. Such porous Ti64 scaffolds can be fabricated using the selective laser melting (SLM) method [276]. However, since Ti64 lacks some functionalities, such as blood compatibility and bone conductivity [277], the surface of Ti64 may be coated using HA to improve its physicochemical properties as demonstrated in the literature. For instance, Xia et al. [278] used a nanorod structured HA as a coating on the surface of Ti64 via atmospheric plasma spraying in combination with hydrothermal treatment, and subsequently showed that the constructed nano-structured surface could enhance cell responses and osseointegration. Additionally, Habibovic et al. [279] used a two-step biomimetic procedure (immersing into two types of SBF) to coat HA on Ti64 prostheses for reconstructing hip and knee joints. Recently, sol-gel coating, electrophoretic method, and magnetron sputtering coating techniques were developed to coat HA on porous Ti64 scaffold and thus enhance its bioactivity [280,281].

3.3.4. Other HA-Based Composites Containing Metals

In addition, some metals, such as iron (Fe) [282], copper (Cu) [283], zinc (Zn) [284], magnesium (Mg) [285], strontium (Sr) [286], silver (Ag) [287], gold (Au) [288], and selenium (Se) [289], have been used to prepare doped or co-doped HA. Sr is an essential trace element in bone (~0.01 wt.%). This is because these metals present a higher Young's modulus than bones, thus may provide stress shielding for the bone. These metals generally therefore provide beneficial mechanical properties of strength to HA. Some of these metals also possess unique properties. For instance, Sr is considered an important element that aids the decrease in bone resorption while also enhancing new bone formation. This is because of its important characteristic of promoting osteogenic differentiation of mesenchymal stem cells [290,291]. Sr-doped or -substituted HA can therefore induce osteogenesis, as demonstrated in several studies. For instance, Xu et al. demonstrated that the Sr/HA composite containing 5 wt.% of Sr led to optimal activity of osteogenic cells [292]. Yan et al. [293] also reported that Sr-HA using 20% of Sr displayed good osteoconductivity and could promote better bone growth for improved bone-implant integration. Li et al. later designed an Sr-doped HA/PPF scaffold, the in vitro cell results indicating that Sr-doped HA/PPF scaffold may better support cell adhesion, proliferation, and differentiation compared to HA/PPF scaffold [290]. Apart from the improved physicochemical properties, biological properties, mechanical properties, and antibacterial activities of constructs were improved using metal-doped HA, as reported by Ribeiro et al. [294]. According them,

Ag/Au/HA/silk fibroin exhibits significant inhibition ability against both Gram-positive and Gram-negative bacteria [294].

Finally, although methods such as SLS and selective laser melting technique constitute the most popular 3D printing for plastics and metal [86], these methods are considered insufficient for printing ceramics because of the enhanced risk of thermal induced stresses from thermal gradients in ceramics leading to distortions [86]. According to Chen et al. [86], other printing techniques, such as SLA and DLP, are considered most suitable for ceramic printing since feature resolution and surface finish can be controlled such that the mechanical properties of ceramic are not compromised. Considering these three major methods, a review of literature suggests that the SLA printing technique is the most common ceramic printing approach, as illustrated by the myriad studies on ceramic SLA undertaken in the literature [295–300]. The interest in ceramic SLA may be due to the high precision and quality that characterizes the SLA printing technique; ceramic SLA can facilitate the accurate fabrication of complex ceramic [301] composites. Furthermore, since ceramic SLA does not require a mold, the fabrication costs may be reduced. Notably, since ceramic SLA requires the polymerization of an ultraviolet-curable of ceramic particles in a photopolymer, the effectiveness of the technique will depend on ceramic materials not absorbing UV range necessary for the photosensitive organic matrix [302].

4. Desired Properties

The printed scaffolds via 3D printing for clinical applications require a series of characteristics, including porous interconnected network, mechanical properties, biocompatibility, bio-physicochemical properties, controllable degradation and adsorption rate, suitable surface chemistry and morphology, etc. (Figure 19) [303]. In this section, the desired properties of HA-based nanocomposites as scaffolds using 3D printing for TE are discussed.
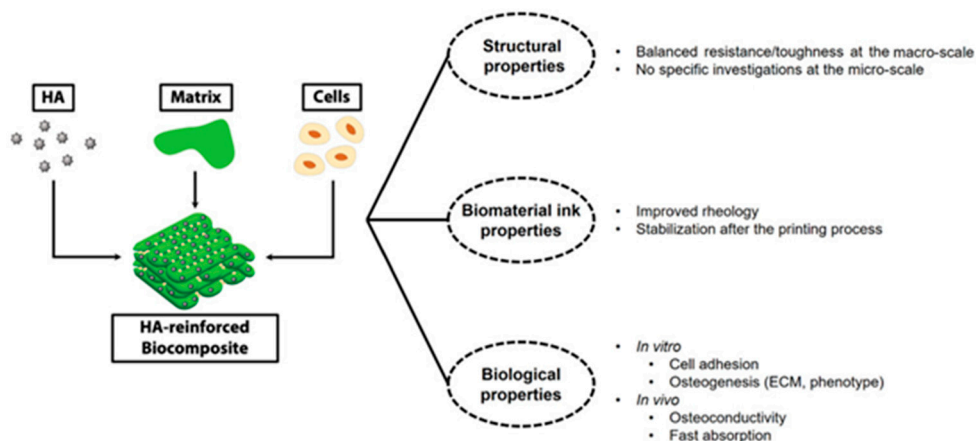

Figure 19. The desired properties of HA-based nanocomposites for TE applications [24,53].

4.1. Porosity

The porous architecture design for scaffold plays a significant role in tissue regeneration, and the controllable porosity is one of the main advantages in the 3D printing approach for the fabrication of scaffold [304,305]. A certain degree of porosity and interconnected porous structure for printed scaffold is needed, since the porous structure enhances the transport of nutrients, cells, drugs, genes, growth factors, protein, bioactive molecules, and waste matters and subsequently enhance the formation of new tissue [306–308]. Furthermore, a successful scaffold should balance porosity and mechanical function, with related properties such as degradation, biocompatibility, and osteogenesis of the scaffold also affected [304,309]. Lin et al. prepared HA/alginate scaffold with a well-interconnected porous structure using the traditional method; the scaffold had an average pore size of 150 μm and over 82% porosity [137]. The pore size of HA-based scaffolds may be increased and adjusted using the 3D printing approach. For instance, Huang et al. [71] fabricated

HA/silk fibroin nanocomposite using extrusion-based 3D printing. The scaffold had large interconnected pores of ~400 μm, with a high adjustable porosity [71]. Lee et al. [310] also fabricated HA/chitosan/gelatin scaffolds using a 3D printing approach, with the scaffold pore size increasing to 500 μm [310]. Sultan et al. [311] used extrusion-based printing to obtain sodium alginate/gelatin/cellulose scaffolds with a double crosslinked interpenetrating polymer network (IPN). The scaffolds displayed a gradient porosity, where the pore size ranged from 80 to 2123 μm, and the roughness of the pore wall was favorable for cell interaction [311]. Computational methods, such as finite element analysis, could be used to design the suitable porous structure of scaffold with minimizing stress shielding and improving the osseointegration and long-term stability [312,313].

4.2. Mechanical Properties

The mechanical properties are essential for scaffolds, especially applying new tissues in load-bearing sites. It is essential for clinical success that the mechanical properties of fabricated scaffolds be consistent with those of the natural environment of tissue, such as bone [304]. There should also be a balance between the porosity and mechanical strength of the scaffold. There are many available methods used for adjusting or improving the mechanical strength of 3D printed constructs, including modifying the chemical/structural composition, optimizing processing, liquid phase sintering, thermally induced densification, microwave sintering, monomer/polymer infiltration, and doping [85,314,315]. Generally, HA/synthetic polymer-based nanocomposites, as hard matrix-based constructs, have been preferred as load-bearing replacements due to the excellent mechanical properties of synthetic polymers, such as PCL, PLA, and PEEK. However, natural polymers, including gelatin, collagen, alginate, chitosan, silk, etc., and some synthetic polymers, such as PVA, have been used with HA to fabricate soft matrix-based nanocomposites, which can be selected for load-bearing applications only after further cross-linked treatment [53]. Besides, the size and distribution of HA nanoparticles in constructs affect the mechanical properties at the cell level [316,317]. Lee et al. [318] discovered that the pore orientations could influence the mechanical properties of porous calcium phosphate ceramic scaffolds. They fabricated three types of porous calcium phosphate scaffolds with different pore orientations ($0°/90°$, $0°/45°/90°/135°$, and $0°/30°/60°/90°/120°/150°$). The scaffold with a pore orientation of $0°/90°$ displayed the highest compressive strength and modulus because some scaffold frameworks were parallel to the loading direction [318]. Senatov et al. [319] obtained porous HA/PLA scaffolds with an average pore size of 700 μm using FFF. The printed scaffold had the shape memory effect because the dispersed HA nanoparticles acted as nucleation centers during the PLA molecular chain ordering. The HA nanoparticles could inhibit the growth of cracks during the compression–heating–compression cycles [319]. Chen et al. [320] printed HA scaffold with macroporosity (~600 μm) using the 3D printing approach and discovered that the compressive properties of scaffolds mainly depended on the composition and inter-layer angle. Thus, "balancing" porosity, mechanical properties of scaffolds, and the characteristics of biocompatibility, biodegradability, antibacterial properties, etc. need to be further considered.

4.3. Biocompatibility

HA-based nanocomposites play the main role in cell seeding, proliferation, and differentiation for TE applications. It is critical that the materials (polymer or inorganic part) chosen to composite with HA for 3D printing should be biocompatible. In addition, the products produced from HA-based nanocomposites should be non-toxic without adverse reaction and immune rejection from the host [321]. HA-based nanocomposites made from natural polymers such as collagen, gelatin, silk fibroin, etc. are biocompatible for supporting cell attachment. However, nanocomposites using synthetic polymer bonded with covalent or ionic bonds show less biocompatibility compared with those using natural polymers [322].

4.4. Biodegradability

The adjustable biodegradation rate for ideal HA-based nanocomposites in TE can support the role of the scaffold during the tissue repair process. The ceramics have limited biodegradability, and the polymers have adjustable degradation rates depending on the molecular design. The available biodegradable polymers used for the fabrication of HA-based nanocomposites include protein-type polymers, polysaccharide-type polymers, and polyester-type polymers [323]. Hydrolytic and enzymatic degradation are two main pathways for the biodegradation and clearance mechanisms of HA/polymer nanocomposites. The peptide bonds in protein-type polymers can be degraded in vivo by enzymes; the polysaccharide-type polymers can be degraded by lysosomes and amylases; and the synthetic polymers with ester, urea, and urethane linkages can be degraded by hydrolytic reaction [324,325]. The strategy of compositing nondegradable materials and biodegradable materials as the binary scaffold while exhibiting bioactivity and biodegradability is still difficult, and how to exert the biodegradability of such binary scaffold remains a challenge [326]. Feng et al. [327] fabricated polyetheretherketone (PEEK)/PLLA/β-TCP scaffolds via selective laser sintering, and many caverns were formed due to the degradation of PLLA, which enabled β-TCP contact with body fluid for further ion-exchange. Manavitehrani et al. [328] introduced a porous biodegradable scaffold based on poly(propylene carbonate) (PPC) with starch and bioglass particles; benign degradation byproducts were produced during the biodegradation process. Ma et al. [329] developed a biodegradable piperazine (PP)-based polyurethane-urea (P-PUU) scaffold using air-driven extrusion 3D printing technology; the compressive modulus and strength and both in vitro and in vivo biodegradation properties could be moderated by the contents of PP in P-UU scaffolds. Additionally, the porosity, pore size, and swelling ratio of the scaffold could influence its degradation rate: scaffolds with smaller pore size and higher porosity had a faster degradation rate due to a larger surface area [330]. Thus, many factors need to be considered when designing the scaffold with a suitable biodegradation rate, such as the chemical crosslinking technique, which may be used to adjust the dissolution of HA-based nanocomposites.

4.5. Other Properties

Besides the properties of scaffold mentioned, several important aspects must be taken into consideration, such as elasticity, surface parameters, molecular mobility, environmental responsiveness to pH and temperature, metabolism of degradation products, and chemical functionality [331]. Many properties have been investigated in recent years to ensure that the scaffold can repair tissue safely, such as customized mechanical properties, antibacterial activity, etc. However, the scaffold potential for specific applications has specific characteristics related to the biological aspect, structure, and chemical composition [332]. Additional properties of 3D printed HA scaffolds are summarized in Table 5.

Table 5. Some properties of 3 D printed HA scaffolds.

Materials	Pore Size	Porosity	Compressive Strength	Some Notes	Sources
HA/chitosan	200–400 μm	No access	No access	-	[53]
Silk/HA	200–750 μm	50–80%	-	-	[58]
HA	300–600 μm	49.8%	15.25 MPa	-	[99]
HA/SF	400 μm	70%	6 MPa	Good in vitro biomineralization activity	[71]
HA/silk	200–750 μm	50–80%	-	Enhanced the osteogenesis and vasculogenesis	[58]
HA/bacterial cellulose	300 μm	-	-	Induces the orderly deposition of HA crystals	[141]
HA/chitosan/SiO$_2$	200 μm	53.57 ± 0.35%	10–13 MPa	Exactly comparable to human trabecular bone	[333]
HA/PCL	600–800 μm	78.54–70.31%	1.38–3.17 MPa	Satisfies basic requirements of bone TE scaffolds	[66]
HA	350 μm	52.26%	16.77 ± 0.38 MPa	Can be readily integrated with the native bone	[334]
HA	500 μm	50%	-	Promotes cell proliferation	[48]
HA	500 μm	31–33.5%	-	formed a strong bone connection	[49]
HA	450–570 μm	-	22 MPa	-	[101]
CHA	400 μm	71.8–82.9%	20 MPa	-	[69]
HA/SF	400 μm	70%	6 MPa	Good in vitro biomineralization activity	[71]
PLA/HA	-	47–69%	16–53 MPa	-	[74]
PCL/PLGA/HA	500 μm	-	15.9–20.9 MPa	-	[75]
HA/TCP	800 μm	50%	2.6 MPa	-	[68]
HA/TCP	500 μm	70%	23 MPa	-	[257]
Sr/HA	300–500 μm	-	3.8–4.2 MPa	Good osteogenesis	[81]

5. Applications of HA-Based Nanocomposites

HA-based nanocomposites fabricated using 3D printing serve as 3D templates to provide support for cells to attach, proliferate, and maintain their differentiated function in tissue regeneration [335]. HA-based constructs have been used in several applications, including bone, cartilage, dental, skin, and drug delivery (Figure 20).

The application of these HA-based nanocomposites constructs in bone, cartilage, dental, skin, and drug delivery are discussed briefly below.
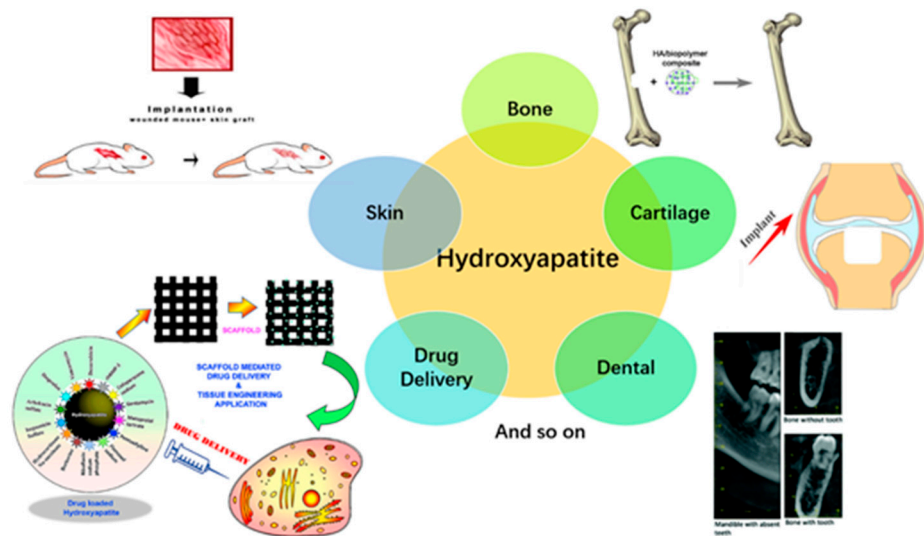
Figure 20. The applications of HA-based nanocomposites [336–340].

5.1. HA-Based Nanocomposites Constructs in Bone TE

The HA-based construct constitutes an excellent candidate as an orthopedic implant during prosthesis revision surgery since natural bone contains 70 wt.% of HA [341]. Compared to autografts and allografts, artificially-engineered bone scaffold with a complex hierarchical structure can avoid the risk of infection, disease transmission, and immune response [335]. The ideal scaffold as an engineered bond scaffold should meet various criteria, such as biocompatibility, osteoconduction, osteoinduction, mechanical properties, without compromising the interconnected porous structure [303,304,309]. The interconnected porous pure HA scaffold can be prepared using 3D gel-printing approach. Shao et al. [334] obtained the HA scaffold with a pore size of over 350 μm, a porosity of 52.26%, and maximum compressive strength and compressive modulus of the scaffold of 16.77 ± 0.38 and 492 ± 11 MPa, respectively [334]. The incorporation of the HA-based nanocomposites constructs in bone TE can be achieved via the development of hierarchical porous HA scaffold with micropores and macropores via combining 3D printing and microwave sintering [342]. These hierarchical HA scaffold can be readily integrated with the native bone. This approach was demonstrated by Song et al. [343], who reported the fabrication of hierarchical HA scaffold with interconnected pores by combining freeze-casting and extrusion-based 3D printing, such that the structure of human bone was mimicked from the microscopic (below 10 μm) to macroscopic (submillimeter to the millimeter) perspective.

5.2. HA-Based Nanocomposites Constructs in Cartilage TE

HA-based nanocomposites could also be employed in cartilage TE. Articular cartilage, covering the bone ends in diarthrodial joints, is viscoelastic connective tissue, which provides an efficient aqueous lubrication system with high load-bearing and low-friction properties [344]. Unfortunately, once a lesion or injury of articular cartilage occurs, it is difficult to heal due to its limited capacity to repair, and artificial cartilage is required in the clinic [345]. The 3D printing technique can be used to fabricate constructs with high structural complexity and flexibility, such as hydrogels, which exhibit the advantage of individualized precision customization, making the construct perfectly fit with the defective surface in the area of cartilage repair [346]. The application of HA-based nanocomposites constructs in cartilage TE has been demonstrated. For instance, Yuan et al. [338] prepared a composite hydrogel consisting of bovine serum albumin/sodium alginate and HA nanowires, and the in vivo results confirm that the hydrogel can promote the generation of new cartilage. Additionally, Hsieh et al. [347] printed biomimetic scaffolds consisting of HA/PCL and glycidyl–methacrylate–hyaluronic acid for healing osteochondral defects. The scaffolds were implanted in the knees of a miniature pig for a period of 12 months.

The hematoxylin and eosin staining and computer tomography (CT) results indicate that the cartilage was partially matured, and the hyaline cartilage was regenerated [347].

5.3. HA-Based Nanocomposites Constructs in Dental Applications

In the last few years, 3D printing for dental applications has notably increased, especially in the areas of oral and maxillofacial surgery, endodontics, orthodontics, prosthodontics, and periodontics. The possibility of individualized dental products drives 3D printing in this area [348]. Metal-, ceramic-, and polymer-based materials are common in the fabrication of dental prosthesis and crowns. Indeed, 3D printing is currently utilized to replace missing teeth [349]. The mechanical properties of constructs for prosthodontics application needs to be improved and issues with porosity avoided to ensure a denser and more compact structure. Such denser and more compact structure may be achieved via ink-jet printing rather than SLS or SLA printing [349]. Furthermore, the development of 3D printing, has promoted the development of regenerative endodontic procedures due to the improved precision and accuracy, while simultaneously ameliorating patient comfort [350]. It is reported that controlling infection is the key to the success of apical inducing angioplasty in the root canal. However, HA itself lacks bactericidal properties; HA-based nanocomposites with antibacterial properties can therefore inhibit the growth of microorganisms in the root canal [351].

5.4. HA-Based Nanocomposites Constructs in Drug Delivery Applications

HA has been used as a composite with biopolymer (e.g., alginate) matrices for a more precise and sustained drug release. For instance, Venkatasubbu et al. [352] loaded the drug ciprofloxacin onto a nano-HA composite with alginate. In their study, the drug was pre-adsorbed onto the ceramic particle before the formation of composite. They showed that the integration of HA-based nanocomposites prolonged the sustained release of ciprofloxacin compared to the ciprofloxacin-loaded HA only. HA/sodium alginate/chitosan (HA/SA/CS) composite microspheres were prepared using an emulsion crosslink technique while using calcium ions as a cross-linking agent [353]. According to Bi et al. [353], the drug loading and encapsulation efficiency of the HA composite was improved compared to when only HA nanoparticles were used. Nie et al. explored silver-doped HA/alginate and HA/β-TCP/alginate microparticles snd micro-clusters, which had excellent antibacterial properties. The obtained microparticles of the HA composite were shown to be useful as drug carriers for the controlled release of doxorubicin [354,355].

In summary, the significance of HA-composites cannot be overemphasized. Moreover, recent studies of 2021 have demonstrated their utilization in human studies. For instance, Kim and Kim [81] employed 3D strontium-substituted HA (Sr-HA) ceramic scaffolds to promote rapid cell proliferation, osteogenic differentiation, and cellular mineralization in human cells. They demonstrated the functionality of Sr-HA scaffold application as new bone graft substitutes in humans. Krzysztof et al. [356] assessed the manufacture of PEEK/HA composite via FFF to determine its suitability for orthopedic implants. They showed that the composite presented comparable mechanical properties to human femoral cortical bone. Huang et al. [82] also demonstrated the development of gelatin/HA hybrid materials which were applied in the fabrication of scaffold for human umbilical cord blood-derived mesenchymal stem cells. The scaffold could effectively support the growth and proliferation of stem cells as well as their adhesion while also inducing chondrogenic differentiation in vitro. Based on the reported success, it is anticipated that future work will further explore the utilization of HA-composites in humans. The next section provides some future expectations of HA composite applications in TE.

6. Next Generation of Hydroxyapatite (HA)-Based Nanocomposite Application in TE

The authors anticipate that improving the accuracy of printing and the functional complexities of printed nanoconstructs will enhance the application of HA-based nanocomposites in the biomedical industry. This is because the hierarchical complexity of nanocom-

posites may facilitate multi-material deposition, thus mimicking the heterogeneity of tissues and organs. Given the applicability of HA-based nanocomposites in drug delivery, the authors propose that future opportunities may exist for employing HA-based nanocomposites in the delivery of gene modifiers and targeted nutrients. Clearly, such applications will provide the opportunities for advanced and targeted cell and tissue modifications in the future. In addition, several factors such as printability, suitable mechanical strength, biodegradation, and biocompatible properties of HA-based composites will facilitate the use of 3D printing to fabricate on-demand, highly-personalized intricate designs at low costs in the future.

The physical, chemical, and biological properties of HA could be increased by incorporating metal ions into the structure of HA [357]. For instance, Popescu et al. synthesized lithium-doped HA, which showed remarkable biomineralization capacity in SBF, and stem cell proliferation on the surface of lithium-doped HA was improved [358]. Yazici et al. similarly prepared silver-doped HA (Ag-HA) with improved antibacterial properties, while the prepared Ag-HA was used for coating on magnesium-based alloys via the addition in SBF. The the morphology of HA formed was related to the Ag-HA content in SBF [359]. Nie et al. developed selenium-doped HA/β-TCP nanoparticles with in-situ incorporation of silver, which displayed excellent antibacterial properties [289]. They also exploited silver-doped HA/alginate or HA/β-TCP/alginate microparticles or micro-clusters with excellent antibacterial properties. The obtained microparticles or micro-clusters could be used as a drug carrier to control the release profiles of doxorubicin [354,355]. Recognizing that vascularization is of utmost importance for tissue regeneration, and functional vascularization of the biological scaffold is difficult to achieve using current 3D printing technologies, the extrusion-based printing discussed above can be used to obtain the necessary structural integrity of the final product. Crucially, however, the dense environment still limits the cellular network during the tissue regeneration process. Thus, a new strategy needs to be developed to address this process. Some researchers have tried to incorporate sacrificial materials into the scaffold during the fabrication. In addition, these sacrificial materials could provide initial mechanical support, and, once the constructs are fabricated, they could be removed [360]. The future development of HA-based nanocomposites using 3D printing is to overcome the aforementioned vascularization challenges. Furthermore, customized scaffolds using 3D printing technology must be further developed. Finally, the processing speed of 3D printing needs to be increased, while simultaneously avoiding mistakes and errors because the printing process is separated into various steps and not automated. It is predicted that the development of materials and 3D printing techniques will lead to HA-based nanocomposites for further clinical applications

7. Conclusions

In this paper, different 3D printing techniques for the fabrication of HA-based materials are reviewed in detail. This review systematically highlights the current state of HA-based nanocomposites. The desired characteristics and specific applications of HA-based nanocomposites are also discussed. The 3D printing techniques and HA-based materials discussed in this review are anticipated to improve strategies for the generation of functional tissues for replacement and repair in the biomedical industry. The 3D printing technology promotes a global revolution in the medical sciences, since many encouraging results have thus been achieved using HA-based nanocomposites in TE.

Institutional Review Board Statement: Not applicable.

Informed Consent Statement: Not applicable.

References

1. Gopi, D.; Kavitha, L.; Ramya, S.; Rajeswari, D. Chemical and green routes for the synthesis of multifunctional pure and substituted nanohydroxyapatite for biomedical applications. In *Engineering of Nanobiomaterials*; Grumezescu, A.M., Ed.; William Andrew Publishing: Norwich, NY, USA, 2016; Chapter 15; pp. 485–521. [CrossRef]
2. Lin, K.; Chang, J. 1—Structure and properties of hydroxyapatite for biomedical applications. In *Hydroxyapatite (Hap) for Biomedical Applications*; Mucalo, M., Ed.; Woodhead Publishing: Cambridge, UK, 2015; pp. 3–19. [CrossRef]
3. Fernando, S.; McEnery, M.; Guelcher, S.A. 16—Polyurethanes for bone TE. In *Advances in Polyurethane Biomaterials*; Cooper, S.L., Guan, J., Eds.; Woodhead Publishing: Cambridge, UK, 2016; pp. 481–501. [CrossRef]
4. Okoro, O.V.; Sun, Z.; Birch, J. Meat processing waste as a potential feedstock for biochemicals and biofuels—A review of possible conversion technologies. *J. Clean. Prod.* **2017**, *142*, 1583–1608. [CrossRef]
5. Okoro, O.V.; Shavandi, A. An assessment of the utilization of waste apple slurry in bio-succinic acid and bioenergy production. *Int. J. Environ. Sci. Technol.* **2021**. [CrossRef]
6. Shavandi, A.; Bekhit, A.E.-D.A.; Ali, M.A.; Sun, Z. Bio-mimetic composite scaffold from mussel shells, squid pen and crab chitosan for bone tissue engineering. *Int. J. Biol. Macromol.* **2015**, *80*, 445–454. [CrossRef] [PubMed]
7. Ratnayake, J.T.; Gould, M.L.; Shavandi, A.; Mucalo, M.; Dias, G.J. Development and characterization of a xenograft material from N ew Z ealand sourced bovine cancellous bone. *J. Biomed. Mater. Res. Part B Appl. Biomater.* **2017**, *105*, 1054–1062. [CrossRef] [PubMed]
8. Antebi, B.; Cheng, X.; Harris, J.N.; Gower, L.B.; Chen, X.-D.; Ling, J. Biomimetic Collagen–Hydroxyapatite Composite Fabricated via a Novel Perfusion-Flow Mineralization Technique. *Tissue Eng. Part C Methods* **2013**, *19*, 487–496. [CrossRef]
9. Zhang, J.M.; Lin, C.J.; Feng, Z.D.; Tian, Z.W. Hydroxyapatite/metal composite coatings prepared by multi-step electrodeposition method. *J. Mater. Sci. Lett.* **1998**, *17*, 1077–1079. [CrossRef]
10. Kim, H.-W.; Knowles, J.C.; Kim, H.-E. Hydroxyapatite and gelatin composite foams processed via novel freeze-drying and crosslinking for use as temporary hard tissue scaffolds. *J. Biomed. Mater. Res. Part A* **2005**, *72*, 136–145. [CrossRef]
11. Ito, Y.; Hasuda, H.; Kamitakahara, M.; Ohtsuki, C.; Tanihara, M.; Kang, I.-K.; Kwon, O.H. A composite of hydroxyapatite with electrospun biodegradable nanofibers as a tissue engineering material. *J. Biosci. Bioeng.* **2005**, *100*, 43–49. [CrossRef]
12. Ficai, A.; Andronescu, E.; Voicu, G.; Ghitulica, C.; Vasile, B.S.; Ficai, D.; Trandafir, V. Self-assembled collagen/hydroxyapatite composite materials. *Chem. Eng. J.* **2010**, *160*, 794–800. [CrossRef]
13. Li, H.; Zhao, N.; Liu, Y.; Liang, C.; Shi, C.; Du, X.; Li, J. Fabrication and properties of carbon nanotubes reinforced Fe/hydroxyapatite composites by in situ chemical vapor deposition. *Compos. Part A Appl. Sci. Manuf.* **2008**, *39*, 1128–1132. [CrossRef]
14. Nam, Y.S.; Yoon, J.J.; Park, T.G. A novel fabrication method of macroporous biodegradable polymer scaffolds using gas foaming salt as a porogen additive. *J. Biomed. Mater. Res.* **2000**, *53*, 1–7. [CrossRef]
15. Redepenning, J.; Venkataraman, G.; Chen, J.; Stafford, N. Electrochemical preparation of chitosan/hydroxyapatite composite coatings on titanium substrates. *J. Biomed. Mater. Res. Part A* **2003**, *66*, 411–416. [CrossRef] [PubMed]
16. Nair, M.; Nancy, D.; Krishnan, A.G.; Anjusree, G.S.; Vadukumpully, S.; Nair, S.V. Graphene oxide nanoflakes incorporated gelatin-hydroxyapatite scaffolds enhance osteogenic differentiation of human mesenchymal stem cells. *Nanotechnology* **2015**, *26*, 161001. [CrossRef] [PubMed]
17. Zhou, Y.; Yao, H.; Wang, J.; Wang, D.; Liu, Q.; Li, Z. Greener synthesis of electrospun collagen/hydroxyapatite composite fibers with an excellent microstructure for bone tissue engineering. *Int. J. Nanomed.* **2015**, *10*, 3203–3215. [CrossRef]
18. Wu, Y.; Hench, L.L.; Du, J.; Choy, K.-L.; Guo, J. Preparation of Hydroxyapatite Fibers by Electrospinning Technique. *J. Am. Ceram. Soc.* **2004**, *87*, 1988–1991. [CrossRef]
19. Nosrati, H.; Mamoory, R.S.; Le, D.Q.S.; Bünger, C.E.; Emameh, R.Z.; Dabir, F. Gas injection approach for synthesis of hydroxyapatite nanorods via hydrothermal method. *Mater. Charact.* **2020**, *159*, 110071. [CrossRef]
20. Nosrati, H.; Sarraf Mamoory, R.; Svend Le, D.Q.; Bünger, C.E. Fabrication of gelatin/hydroxyapatite/3D-graphene scaffolds by a hydrogel 3D-printing method. *Mater. Chem. Phys.* **2020**, *239*, 122305. [CrossRef]
21. Nosrati, H.; Sarraf-Mamoory, R.; Le, D.Q.S.; Perez, M.C.; Bünger, C.E. Evaluation of Argon-Gas-Injected Solvothermal Synthesis of Hydroxyapatite Crystals Followed by High-Frequency Induction Heat Sintering. *Cryst. Growth Des.* **2020**, *20*, 3182–3189. [CrossRef]
22. Ishengoma, F.R.; Mtaho, A.B. 3D printing: Developing countries perspectives. *arXiv* **2014**, arXiv:1410.5349. Available online: https://arxiv.org/abs/1410.5349 (accessed on 27 March 2021).
23. Hull, C. Co-Founder and Chief Technology Officer. *Ann H.J. Smead Aerosp. Eng. Sci.* 2021. Available online: https://www.colorado.edu/aerospace/charles-hull (accessed on 2 February 2021).

24. Li, Y.; Wang, J.; Yang, Y.; Shi, J.; Zhang, H.; Yao, X.; Chen, W.; Zhang, X. A rose bengal/graphene oxide/PVA hybrid hydrogel with enhanced mechanical properties and light-triggered antibacterial activity for wound treatment. *Mater. Sci. Eng. C* **2021**, *118*. [CrossRef]

25. Sears, N.A.; Seshadri, D.R.; Dhavalikar, P.S.; Cosgriff-Hernandez, E. A Review of Three-Dimensional Printing in Tissue Engineering. *Tissue Eng. Part B Rev.* **2016**, *22*, 298–310. [CrossRef]

26. Zhang, B.; Gao, L.; Ma, L.; Luo, Y.; Yang, H.; Cui, Z. 3D Bioprinting: A Novel Avenue for Manufacturing Tissues and Organs. *Engineering* **2019**, *5*, 777–794. [CrossRef]

27. Bishop, E.S.; Mostafa, S.; Pakvasa, M.; Luu, H.H.; Lee, M.J.; Wolf, J.M.; Ameer, G.A.; He, T.-C.; Reid, R.R. 3-D bioprinting technologies in TE and regenerative medicine: Current and future trends. *Genes Dis.* **2017**, *4*, 185–195. [CrossRef] [PubMed]

28. Sundaramurthi, D.; Rauf, S.; Hauser, C. 3D bioprinting technology for regenerative medicine applications. *Int. J. Bioprint.* **2016**, *2*. [CrossRef]

29. Zhu, W.; Ma, X.; Gou, M.; Mei, D.; Zhang, K.; Chen, S. 3D printing of functional biomaterials for tissue engineering. *Curr. Opin. Biotechnol.* **2016**, *40*, 103–112. [CrossRef]

30. Martin, G.D.; Hoath, S.D.; Hutchings, I.M. Inkjet printing—The physics of manipulating liquid jets and drops. *J. Phys. Conf.* **2008**, *105*, 012001. [CrossRef]

31. Li, J.; Rossignol, F.; Macdonald, J. Inkjet printing for biosensor fabrication: Combining chemistry and technology for advanced manufacturing. *Lab Chip* **2015**, *15*. [CrossRef] [PubMed]

32. Derby, B. Inkjet Printing of Functional and Structural Materials: Fluid Property Requirements, Feature Stability, and Resolution. *Annu. Rev. Mater. Res.* **2010**, *40*, 395–414. [CrossRef]

33. Skardal, A.; Mack, D.; Kapetanovic, E.; Atala, A.; Jackson, J.D.; Yoo, J.; Soker, S. Bioprinted amniotic fluid-derived stem cells accelerate healing of large skin wounds. *Stem Cells Transl. Med.* **2012**, *1*, 792–802. [CrossRef] [PubMed]

34. Wang, Y.E.; Li, X.P.; Li, C.C.; Yang, M.M.; Wei, Q.H. Binder droplet impact mechanism on a hydroxyapatite microsphere surface in 3D printing of bone scaffolds. *J. Mater. Sci.* **2015**, *50*, 5014–5023. [CrossRef]

35. Cui, X.; Breitenkamp, K.; Finn, M.G.; Lotz, M.; D'Lima, D.D. Direct human cartilage repair using three-dimensional bioprinting technology. *Tissue Eng. Part A* **2012**, *18*, 1304–1312. [CrossRef]

36. Lin, K.; Sheikh, R.; Romanazzo, S.; Roohani, I. 3D Printing of Bioceramic Scaffolds-Barriers to the Clinical Translation: From Promise to Reality, and Future Perspectives. *Materials* **2019**, *12*, 2660. [CrossRef]

37. Zhou, Z.X.; Buchanan, F.; Mitchell, C.; Dunne, N. Printability of calcium phosphate: Calcium sulfate powders for the application of tissue engineered bone scaffolds using the 3D printing technique. *Mater. Sci. Eng. C Mater. Biol. Appl.* **2014**, *38*, 1–10. [CrossRef]

38. Strobel, L.A.; Rath, S.N.; Maier, A.K.; Beier, J.P.; Arkudas, A.; Greil, P.; Horch, R.E.; Kneser, U. Induction of bone formation in biphasic calcium phosphate scaffolds by bone morphogenetic protein-2 and primary osteoblasts. *J. Tissue Eng. Regen. Med.* **2014**, *8*, 176–185. [CrossRef]

39. Warnke, P.H.; Seitz, H.; Warnke, F.; Becker, S.T.; Sivananthan, S.; Sherry, E.; Liu, Q.; Wiltfang, J.; Douglas, T. Ceramic scaffolds produced by computer-assisted 3D printing and sintering: Characterization and biocompatibility investigations. *J. Biomed. Mater. Res. B Appl. Biomater.* **2010**, *93*, 212–217. [CrossRef]

40. Hull, C.W. Apparatus for Production of Three-Dimensional Objects by SLA. U.S. Patent US4575330A, 11 March 1986.

41. Nikolova, M.P.; Chavali, M.S. Recent advances in biomaterials for 3D scaffolds: A review. *Bioact. Mater.* **2019**, *4*, 271–292. [CrossRef] [PubMed]

42. Mandrycky, C.; Wang, Z.J.; Kim, K.; Kim, D.H. 3D bioprinting for engineering complex tissues. *Biotechnol. Adv.* **2016**, *34*, 422–434. [CrossRef]

43. Gauvin, R.; Chen, Y.C.; Lee, J.W.; Soman, P.; Zorlutuna, P.; Nichol, J.W.; Bae, H.; Chen, S.C.; Khademhosseini, A. Microfabrication of complex porous tissue engineering scaffolds using 3D projection stereolithography. *Biomaterials* **2012**, *33*, 3824–3834. [CrossRef]

44. Lin, H.; Zhang, D.N.; Alexander, P.G.; Yang, G.; Tan, J.; Cheng, A.W.M.; Tuan, R.S. Application of visible light-based projection stereolithography for live cell-scaffold fabrication with designed architecture. *Biomaterials* **2013**, *34*, 331–339. [CrossRef]

45. Gantumur, E.; Nakahata, M.; Kojima, M.; Sakai, S. Extrusion-Based Bioprinting through Glucose-Mediated Enzymatic Hydrogelation. *Int. J. Bioprint.* **2020**, *6*, 250. [CrossRef]

46. Sakai, S.; Mochizuki, K.; Qu, Y.; Mail, M.; Nakahata, M.; Taya, M. Peroxidase-catalyzed microextrusion bioprinting of cell-laden hydrogel constructs in vaporized ppm-level hydrogen peroxide. *Biofabrication* **2018**, *10*, 045007. [CrossRef]

47. Barry, J.J.A.; Evseev, A.V.; Markov, M.A.; Upton, C.E.; Scotchford, C.A.; Popov, V.K.; Howdle, S.M. In vitro study of hydroxyapatite-based photocurable polymer composites prepared by laser stereolithography and supercritical fluid extraction. *Acta Biomater.* **2008**, *4*, 1603–1610. [CrossRef]

48. Woesz, A.; Rumpler, M.; Stampfl, J.; Varga, F.; Fratzl-Zelman, N.; Roschger, P.; Klaushofer, K.; Fratzl, P. Towards bone replacement materials from calcium phosphates via rapid prototyping and ceramic gelcasting. *Mater. Sci. Eng. C* **2005**, *25*, 181–186. [CrossRef]

49. Chen, Q.; Zou, B.; Lai, Q.; Wang, Y.; Xue, R.; Xing, H.; Fu, X.; Huang, C.; Yao, P. A study on biosafety of HAP ceramic prepared by SLA-3D printing technology directly. *J. Mech. Behav. Biomed. Mater.* **2019**, *98*, 327–335. [CrossRef] [PubMed]

50. Le Guéhennec, L.; Van Hede, D.; Plougonven, E.; Nolens, G.; Verlée, B.; De Pauw, M.C.; Lambert, F. In vitro and in vivo biocompatibility of calcium-phosphate scaffolds three-dimensional printed by stereolithography for bone regeneration. *J. Biomed. Mater. Res. Part A* **2020**, *108*, 412–425. [CrossRef]

51. Wang, Z.J.; Kumar, H.; Tian, Z.L.; Jin, X.; Holzman, J.F.; Menard, F.; Kim, K. Visible Light Photoinitiation of Cell-Adhesive Gelatin Methacryloyl Hydrogels for Stereolithography 3D Bioprinting. *ACS Appl. Mater. Interfaces* **2018**, *10*, 26859–26869. [CrossRef]

52. Pati, F.; Jang, J.; Lee, J.-W. Extrusion Bioprinting. In *Essentials of 3D Biofabrication and Translation*; Elsevier: Amsterdam, The Netherlands, 2015; pp. 123–152. [CrossRef]

53. Milazzo, M.; Contessi Negrini, N.; Scialla, S.; Marelli, B.; Farè, S.; Danti, S.; Buehler, M.J. Additive Manufacturing Approaches for Hydroxyapatite-Reinforced Composites. *Adv. Funct. Mater.* **2019**, *29*. [CrossRef]

54. Derakhshanfar, S.; Mbeleck, R.; Xu, K.; Zhang, X.; Zhong, W.; Xing, M. 3D bioprinting for biomedical devices and tissue engineering: A review of recent trends and advances. *Bioact. Mater.* **2018**, *3*, 144–156. [CrossRef]

55. Ozbolat, I.T.; Hospodiuk, M. Current advances and future perspectives in extrusion-based bioprinting. *Biomaterials* **2016**, *76*, 321–343. [CrossRef]

56. Khalyfa, A.; Vogt, S.; Weisser, J.; Grimm, G.; Rechtenbach, A.; Meyer, W.; Schnabelrauch, M. Development of a new calcium phosphate powder-binder system for the 3D printing of patient specific implants. *J. Mater. Sci. Mater. Med.* **2007**, *18*, 909–916. [CrossRef]

57. Michna, S.; Wu, W.; Lewis, J.A. Concentrated hydroxyapatite inks for direct-write assembly of 3-D periodic scaffolds. *Biomaterials* **2005**, *26*, 5632–5639. [CrossRef]

58. Sun, L.; Parker, S.T.; Syoji, D.; Wang, X.; Lewis, J.A.; Kaplan, D.L. Direct-write assembly of 3D silk/hydroxyapatite scaffolds for bone co-cultures. *Adv. Healthc. Mater.* **2012**, *1*, 729–735. [CrossRef]

59. Khodaei, M.; Amini, K.; Valanezhad, A. Fabrication and Characterization of Poly Lactic Acid Scaffolds by Fused Deposition Modeling for Bone Tissue Engineering. *J. Wuhan Univ. Technol. Mater. Sci. Ed.* **2020**, *35*, 248–251. [CrossRef]

60. You, F.; Eames, B.F.; Chen, X. Application of Extrusion-Based Hydrogel Bioprinting for Cartilage Tissue Engineering. *Int. J. Mol. Sci.* **2017**, *18*, 1597. [CrossRef]

61. Malda, J.; Visser, J.; Melchels, F.P.; Juengst, T.; Hennink, W.E.; Dhert, W.J.A.; Groll, J.; Hutmacher, D.W. 25th Anniversary Article: Engineering Hydrogels for Biofabrication. *Adv. Mater.* **2013**, *25*, 5011–5028. [CrossRef]

62. Rodriguez-Salvador, M.; Ruiz-Cantu, L. Revealing emerging science and technology research for dentistry applications of 3D bioprinting. *Int. J. Bioprint.* **2018**, *5*. [CrossRef]

63. Keriquel, V.; Oliveira, H.; Remy, M.; Ziane, S.; Delmond, S.; Rousseau, B.; Rey, S.; Catros, S.; Amedee, J.; Guillemot, F.; et al. In situ printing of mesenchymal stromal cells, by laser-assisted bioprinting, for in vivo bone regeneration applications. *Sci. Rep.* **2017**, *7*. [CrossRef]

64. Keriquel, V.; Guillemot, F.; Arnault, I.; Guillotin, B.; Miraux, S.; Amédée, J.L.; Fricain, J.C.; Catros, S. In vivo bioprinting for computer- and robotic-assisted medical intervention: Preliminary study in mice. *Biofabrication* **2010**, *2*, 014101. [CrossRef]

65. Shirazi, S.F.; Gharehkhani, S.; Mehrali, M.; Yarmand, H.; Metselaar, H.S.; Adib Kadri, N.; Osman, N.A. A review on powder-based additive manufacturing for tissue engineering: Selective laser sintering and inkjet 3D printing. *Sci. Technol. Adv. Mater.* **2015**, *16*, 033502. [CrossRef]

66. Xia, Y.; Zhou, P.; Cheng, X.; Xie, Y.; Liang, C.; Li, C.; Xu, S. Selective laser sintering fabrication of nano-hydroxyapatite/poly-ε-caprolactone scaffolds for bone TE applications. *Int. J. Nanomed.* **2013**, *8*, 4197.

67. Gao, C.; Yang, B.; Hu, H.; Liu, J.; Shuai, C.; Peng, S. Enhanced sintering ability of biphasic calcium phosphate by polymers used for bone scaffold fabrication. *Mater. Sci. Eng. C Mater. Biol. Appl.* **2013**, *33*, 3802–3810. [CrossRef]

68. Wang, Y.; Wang, K.; Li, X.; Wei, Q.; Chai, W.; Wang, S.; Che, Y.; Lu, T.; Zhang, B. 3D fabrication and characterization of phosphoric acid scaffold with a HA/β-TCP weight ratio of 60:40 for bone TE applications. *PLoS ONE* **2017**, *12*, e0174870. [CrossRef]

69. Lin, K.F.; He, S.; Song, Y.; Wang, C.M.; Gao, Y.; Li, J.Q.; Tang, P.; Wang, Z.; Bi, L.; Pei, G.X. Low-Temperature Additive Manufacturing of Biomimic Three-Dimensional Hydroxyapatite/Collagen Scaffolds for Bone Regeneration. *ACS Appl. Mater. Interfaces* **2016**, *8*, 6905–6916. [CrossRef]

70. Ardelean, I.L.; Gudovan, D.; Ficai, D.; Ficai, A.; Andronescu, E.; Albu-Kaya, M.G.; Neacsu, P.; Ion, R.N.; Cimpean, A.; Mitran, V. Collagen/hydroxyapatite bone grafts manufactured by homogeneous/heterogeneous 3D printing. *Mater. Lett.* **2018**, *231*, 179–182. [CrossRef]

71. Huang, T.; Fan, C.; Zhu, M.; Zhu, Y.; Zhang, W.; Li, L. 3D-printed scaffolds of biomineralized hydroxyapatite nanocomposite on silk fibroin for improving bone regeneration. *Appl. Surf. Sci.* **2019**, *467–468*, 345–353. [CrossRef]

72. Liu, S.; Hu, Y.; Zhang, J.; Bao, S.; Xian, L.; Dong, X.; Zheng, W.; Li, Y.; Gao, H.; Zhou, W. Bioactive and Biocompatible Macroporous Scaffolds with Tunable Performances Prepared Based on 3D Printing of the Pre-Crosslinked Sodium Alginate/Hydroxyapatite Hydrogel Ink. *Macromol. Mater. Eng.* **2019**, *304*, 1800698. [CrossRef]

73. Myung, S.-W.; Kim, B.-H. Oxygen and nitrogen plasma etching of three-dimensional hydroxyapatite/chitosan scaffolds fabricated by additive manufacturing. *Jpn. J. Appl. Phys.* **2015**, *55*, 01AB07. [CrossRef]

74. Mondal, S.; Nguyen, T.P.; Pham, V.H.; Hoang, G.; Manivasagan, P.; Kim, M.H.; Nam, S.Y.; Oh, J. Hydroxyapatite nano bioceramics optimized 3D printed poly lactic acid scaffold for bone TE application. *Ceram. Int.* **2020**, *46*, 3443–3455. [CrossRef]

75. Moncal, K.K.; Heo, D.N.; Godzik, K.P.; Sosnoski, D.M.; Mrowczynski, O.D.; Rizk, E.; Ozbolat, V.; Tucker, S.M.; Gerhard, E.M.; Dey, M.; et al. 3D printing of poly(ε-caprolactone)/poly(D,L-lactide-co-glycolide)/hydroxyapatite composite constructs for bone tissue engineering. *J. Mater. Res.* **2018**, *33*, 1972–1986. [CrossRef]

76. Esmi, A.; Jahani, Y.; Yousefi, A.A.; Zandi, M. PMMA-CNT-HAp nanocomposites optimized for 3D-printing applications. *Mater. Res. Express* **2019**, *6*, 085405. [CrossRef]

77. Ergul, N.M.; Unal, S.; Kartal, I.; Kalkandelen, C.; Ekren, N.; Kilic, O.; Chi-Chang, L.; Gunduz, O. 3D printing of chitosan/poly(vinyl alcohol) hydrogel containing synthesized hydroxyapatite scaffolds for hard-TE. *Polym. Test.* **2019**, *79*, 106006. [CrossRef]

78. Cakmak, A.M.; Unal, S.; Sahin, A.; Oktar, F.N.; Sengor, M.; Ekren, N.; Gunduz, O.; Kalaskar, D.M. 3D Printed Polycaprolactone/Gelatin/Bacterial Cellulose/Hydroxyapatite Composite Scaffold for Bone Tissue Engineering. *Polymers* **2020**, 12. [CrossRef]

79. Yeon, Y.K.; Park, H.S.; Lee, J.M.; Lee, J.S.; Lee, Y.J.; Sultan, M.T.; Seo, Y.B.; Lee, O.J.; Kim, S.H.; Park, C.H. New concept of 3D printed bone clip (polylactic acid/hydroxyapatite/silk composite) for internal fixation of bone fractures. *J. Biomater. Sci. Polym. Ed.* **2018**, *29*, 894–906. [CrossRef] [PubMed]

80. Jeong, H.J.; Gwak, S.J.; Seo, K.D.; Lee, S.; Yun, J.H.; Cho, Y.S.; Lee, S.J. Fabrication of Three-Dimensional Composite Scaffold for Simultaneous Alveolar Bone Regeneration in Dental Implant Installation. *Int. J. Mol. Sci.* **2020**, *21*, 1863. [CrossRef]

81. Kim, H.-W.; Kim, Y.-J. Fabrication of strontium-substituted hydroxyapatite scaffolds using 3D printing for enhanced bone regeneration. *J. Mater. Sci.* **2021**, *56*, 1673–1684. [CrossRef]

82. Huang, J.; Huang, Z.; Liang, Y.; Yuan, W.; Bian, L.; Duan, L.; Rong, Z.; Xiong, J.; Wang, D.; Xia, J. 3D printed gelatin/hydroxyapatite scaffolds for stem cell chondrogenic differentiation and articular cartilage repair. *Biomater. Sci.* **2021**. [CrossRef]

83. Godec, D.; Cano, S.; Holzer, C.; Gonzalez-Gutierrez, J.J.M. Optimization of the 3D Printing Parameters for Tensile Properties of Specimens Produced by Fused Filament Fabrication of 17-4PH Stainless Steel. *Materials* **2020**, *13*, 774. [CrossRef]

84. Chen, Z.; Ouyang, J.; Liang, W.; Yan, Z.C.; Stadler, F.; Lao, C. Development and characterizations of novel aqueous-based LSCF suspensions for inkjet printing. *Ceram. Int.* **2018**, *44*, 13381–13388. [CrossRef]

85. Inzana, J.A.; Olvera, D.; Fuller, S.M.; Kelly, J.P.; Graeve, O.A.; Schwarz, E.M.; Kates, S.L.; Awad, H.A. 3D printing of composite calcium phosphate and collagen scaffolds for bone regeneration. *Biomaterials* **2014**, *35*, 4026–4034. [CrossRef]

86. Chen, Z.; Li, Z.; Li, J.; Liu, C.; Lao, C.; Fu, Y.; Liu, C.; Li, Y.; Wang, P.; He, Y. 3D printing of ceramics: A review. *J. Eur. Ceram. Soc.* **2019**, *39*, 661–687. [CrossRef]

87. Chockalingam, K.; Jawahar, N.; Ramanathan, K.N.; Banerjee, P.S. Optimization of stereolithography process parameters for part strength using design of experiments. *Int. J. Adv. Manuf. Technol.* **2006**, *29*, 79–88. [CrossRef]

88. Jariwala, S.H.; Lewis, G.S.; Bushman, Z.J.; Adair, J.H.; Donahue, H.J. 3D Printing of Personalized Artificial Bone Scaffolds. *3D Print. Addit. Manuf.* **2015**, *2*, 56–64. [CrossRef]

89. Gentry, S.P.; Halloran, J.W. Depth and width of cured lines in photopolymerizable ceramic suspensions. *J. Eur. Ceram. Soc.* **2013**, *33*, 1981–1988. [CrossRef]

90. de Hazan, Y.; Penner, D. SiC and SiOC ceramic articles produced by stereolithography of acrylate modified polycarbosilane systems. *J. Eur. Ceram. Soc.* **2017**, *37*, 5205–5212. [CrossRef]

91. Santoliquido, O.; Colombo, P.; Ortona, A. Additive Manufacturing of ceramic components by Digital Light Processing: A comparison between the "bottom-up" and the "top-down" approaches. *J. Eur. Ceram. Soc.* **2019**, *39*, 2140–2148. [CrossRef]

92. El Magri, A.; El Mabrouk, K.; Vaudreuil, S.; Ebn Touhami, M. Experimental investigation and optimization of printing parameters of 3D printed polyphenylene sulfide through response surface methodology. *J. Appl. Polym. Sci.* **2021**, *138*, 49625. [CrossRef]

93. Moradi, M.; Moghadam, M.K.; Shamsborhan, M.; Bodaghi, M. The Synergic Effects of FDM 3D Printing Parameters on Mechanical Behaviors of Bronze Poly Lactic Acid Composites. *J. Compos. Sci.* **2020**, *4*, 17. [CrossRef]

94. LeGeros, R.Z. Properties of osteoconductive biomaterials: Calcium phosphates. *Clin. Orthop. Relat. Res.* **2002**, *395*, 81–98. [CrossRef]

95. Zhou, H.; Lee, J. Nanoscale hydroxyapatite particles for bone tissue engineering. *Acta Biomater* **2011**, *7*, 2769–2781. [CrossRef]

96. Damien, E.; Hing, K.; Saeed, S.; Revell, P.A. A preliminary study on the enhancement of the osteointegration of a novel synthetic hydroxyapatite scaffold in vivo. *J. Biomed. Mater. Res. Part A* **2003**, *66A*, 241–246. [CrossRef]

97. Liu, X. Cell responses to two kinds of nanohydroxyapatite with different sizes and crystallinities. *Int. J. Nanomed.* **2012**, *7*, 1239–1250. [CrossRef]

98. Zhou, Z.; Lennon, A.; Buchanan, F.; McCarthy, H.O.; Dunne, N. Binder jetting additive manufacturing of hydroxyapatite powders: Effects of adhesives on geometrical accuracy and green compressive strength. *Addit. Manuf.* **2020**, 101645. [CrossRef]

99. Liu, Z.B.; Liang, H.X.; Shi, T.S.; Xie, D.Q.; Chen, R.Y.; Han, X.; Shen, L.D.; Wang, C.J.; Tian, Z.J. Additive manufacturing of hydroxyapatite bone scaffolds via digital light processing and in vitro compatibility. *Ceram. Int.* **2019**, *45*, 11079–11086. [CrossRef]

100. Kumar, A.; Kargozar, S.; Baino, F.; Han, S.S. Additive Manufacturing Methods for Producing Hydroxyapatite and Hydroxyapatite-Based Composite Scaffolds: A Review. *Front. Mater.* **2019**, *6*, 313. [CrossRef]

101. Seitz, H.; Rieder, W.; Irsen, S.; Leukers, B.; Tille, C. Three-dimensional printing of porous ceramic scaffolds for bone tissue engineering. *J. Biomed. Mater. Res. B Appl. Biomater.* **2005**, *74*, 782–788. [CrossRef] [PubMed]

102. Balasubramanian, V.; Herranz-Blanco, B.; Almeida, P.V.; Hirvonen, J.; Santos, H.A. Multifaceted polymersome platforms: Spanning from self-assembly to drug delivery and protocells. *Prog. Polym. Sci.* **2016**, *60*, 51–85. [CrossRef]

103. Bordes, P.; Pollet, E.; Averous, L. Nano-biocomposites: Biodegradable polyester/nanoclay systems. *Prog. Polym. Sci.* **2009**, *34*, 125–155. [CrossRef]

104. Xu, W.; Wu, X.; Sun, W. Review on polymer/layered silicates nanocomposites. *J. Chin. Ceram. Soc.* **2016**. [CrossRef]

105. Bedell, M.L.; Navara, A.M.; Du, Y.; Zhang, S.; Mikos, A.G. Polymeric Systems for Bioprinting. *Chem. Rev.* **2020**. [CrossRef]

106. Desimone, E.; Schacht, K.; Jungst, T.; Groll, J.; Scheibel, T. Biofabrication of 3D constructs: Fabrication technologies and spider silk proteins as bioinks. *Pure Appl. Chem.* **2015**, *87*. [CrossRef]

107. Xu, J.; Zheng, S.; Hu, X.; Li, L.; Li, W.; Parungao, R.; Wang, Y.; Nie, Y.; Liu, T.; Song, K. Advances in the Research of Bioinks Based on Natural Collagen, Polysaccharide and Their Derivatives for Skin 3D Bioprinting. *Polymers* **2020**, *12*, 1237. [CrossRef]

108. Koons, G.L.; Diba, M.; Mikos, A.G. Materials design for bone-tissue engineering. *Nat. Rev. Mater.* **2020**. [CrossRef]

109. Mazzocchi, A.; Devarasetty, M.; Huntwork, R.; Soker, S.; Skardal, A. Optimization of collagen type I-hyaluronan hybrid bioink for 3D bioprinted liver microenvironments. *Biofabrication* **2018**. [CrossRef]

110. Shoulders, M.D.; Raines, R.T. Collagen structure and stability. *Annu. Rev. Biochem.* **2009**, *78*, 929–958. [CrossRef]

111. Montalbano, G.; Molino, G.; Fiorilli, S.; Vitale-Brovarone, C. Synthesis and incorporation of rod-like nano-hydroxyapatite into type I collagen matrix: A hybrid formulation for 3D printing of bone scaffolds. *J. Eur. Ceram. Soc.* **2020**, *40*, 3689–3697. [CrossRef]

112. Echave, M.C.; SBurgo, L.; LPedraz, J.; Orive, G. Gelatin as Biomaterial for Tissue Engineering. *Curr. Pharm. Des.* **2017**, *23*, 3567–3584. [CrossRef]

113. Valot, L.; Martinez, J.; Mehdi, A.; Subra, G. Chemical insights into bioinks for 3D printing. *Chem. Soc. Rev.* **2019**, *48*, 4049–4086. [CrossRef]

114. Samadikuchaksaraei, A.; Gholipourmalekabadi, M.; Erfani Ezadyar, E.; Azami, M.; Mozafari, M.; Johari, B.; Kargozar, S.; Jameie, S.B.; Korourian, A.; Seifalian, A.M. Fabrication and In vivo evaluation of an osteoblast-conditioned nano-hydroxyapatite/gelatin composite scaffold for bone tissue regeneration. *J. Biomed. Mater. Res. Part A* **2016**, *104*, 2001–2010. [CrossRef] [PubMed]

115. Chiu, C.K.; Ferreira, J.; Luo, T.J.M.; Geng, H.X.; Lin, F.C.; Ko, C.C. Direct scaffolding of biomimetic hydroxyapatite-gelatin nanocomposites using aminosilane cross-linker for bone regeneration. *J. Mater. Sci. Mater. Med.* **2012**, *23*, 2115–2126. [CrossRef] [PubMed]

116. Comeau, P.; Willett, T. Printability of Methacrylated Gelatin upon Inclusion of a Chloride Salt and Hydroxyapatite Nano-Particles. *Macromol. Mater. Eng.* **2019**, *304*. [CrossRef]

117. Özsağıroğlu, T.B.; Nasün-Saygılı, G. The Impact of Gelatin Weight Ratio on Hydroxyapatite-gelatin Composites and Their SBF Behaviour. *Macromol. Symp.* **2015**, *352*, 8–15. [CrossRef]

118. Gomes, S.; Leonor, I.B.; Mano, J.F.; Rui, L.R.; Kaplan, D.L. *Silk-Based Biomaterials*; Wiley-VCH Verlag GmbH & Co. KGaA: Weinheim, Germany, 2012.

119. Wang, L.; Fang, M.; Xia, Y.J.; Hou, J.X.; Nan, X.R.; Zhao, Z.; Wang, X.Y. Preparation and biological properties of silk fibroin/nano-hydroxyapatite/graphene oxide scaffolds with an oriented channel-like structure. *RSC Adv.* **2020**, *10*, 10118–10128. [CrossRef]

120. Perrone, G.S.; Leisk, G.G.; Lo, T.J.; Moreau, J.E.; Haas, D.S.; Papenburg, B.J.; Golden, E.B.; Partlow, B.P.; Fox, S.E.; Ibrahim, A.M.S. The use of silk-based devices for fracture fixation. *Nat. Commun.* **2014**, *5*, 3385. [CrossRef]

121. Mottaghitalab, F.; Hosseinkhani, H.; Shokrgozar, M.A.; Mao, C.; Yang, M.; Farokhi, M. Silk as a potential candidate for bone TE. *J. Control. Release* **2015**, *215*, 112–128. [CrossRef]

122. Kundu, B.; Rajkhowa, R.; Kundu, S.C.; Wang, X. Silk fibroin biomaterials for tissue regenerations. *Adv. Drug Deliv. Rev.* **2013**, *65*, 457–470. [CrossRef]

123. Shi, L.; Wang, F.; Zhu, W.; Xu, Z.; Fuchs, S.; Hilborn, J.; Zhu, L.; Ma, Q.; Wang, Y.; Weng, X.; et al. Self-Healing Silk Fibroin-Based Hydrogel for Bone Regeneration: Dynamic Metal-Ligand Self-Assembly Approach. *Adv. Funct. Mater.* **2017**, *27*. [CrossRef]

124. Zhu, Z.H.; Ohgo, K.; Asakura, T. Preparation and characterization of regenerated Bombyx mori silk fibroin fiber with high strength. *Express Polym. Lett.* **2008**, *2*, 885–889. [CrossRef]

125. Wang, Q.S.; Han, G.C.; Yan, S.Q.; Zhang, Q. 3D Printing of Silk Fibroin for Biomedical Applications. *Materials* **2019**, *12*, 504. [CrossRef] [PubMed]

126. Liu, H.; Li, X.; Zhou, G.; Fan, H.; Fan, Y. Electrospun sulfated silk fibroin nanofibrous scaffolds for vascular tissue engineering. *Biomaterials* **2011**, *32*, 3784–3793. [CrossRef] [PubMed]

127. Liu, H.; Xu, G.W.; Wang, Y.F.; Zhao, H.S.; Xiong, S.; Wu, Y.; Heng, B.C.; An, C.R.; Zhu, G.H.; Xie, D.H. Composite scaffolds of nano-hydroxyapatite and silk fibroin enhance mesenchymal stem cell-based bone regeneration via the interleukin 1 alpha autocrine/paracrine signaling loop. *Biomaterials* **2015**, *49*, 103–112. [CrossRef] [PubMed]

128. Goh, C.H.; Heng, P.W.S.; Chan, L.W. Alginates as a useful natural polymer for microencapsulation and therapeutic applications. *Carbohydr. Polym.* **2012**, *88*, 1–12. [CrossRef]

129. Axpe, E.; Oyen, M.L. Applications of Alginate-Based Bioinks in 3D Bioprinting. *Int. J. Mol. Sci.* **2016**, *17*, 1976. [CrossRef] [PubMed]

130. Schuster, E.; Eckardt, J.; Hermansson, A.M.; Larsson, A.; Loren, N.; Altskar, A.; Strom, A. Microstructural, mechanical and mass transport properties of isotropic and capillary alginate gels. *Soft Matter* **2014**, *10*, 357–366. [CrossRef]

131. Baysal, K.; Aroguz, A.Z.; Adiguzel, Z.; Baysal, B.M. Chitosan/alginate crosslinked hydrogels: Preparation, characterization and application for cell growth purposes. *Int. J. Biol. Macromol.* **2013**, *59*, 342–348. [CrossRef] [PubMed]

132. Luo, Z.; Zhang, S.; Pan, J.; Shi, R.; Liu, H.; Lyu, Y.; Han, X.; Li, Y.; Yang, Y.; Xu, Z.; et al. Time-responsive osteogenic niche of stem cells: A sequentially triggered, dual-peptide loaded, alginate hybrid system for promoting cell activity and osteo-differentiation. *Biomaterials* **2018**, *163*, 25–42. [CrossRef]

133. Luo, Z.; Yang, Y.; Deng, Y.; Sun, Y.; Yang, H.; Wei, S. Peptide-incorporated 3D porous alginate scaffolds with enhanced osteogenesis for bone tissue engineering. *Colloids Surf. B Biointerfaces* **2016**, *143*, 243–251. [CrossRef] [PubMed]

134. Turco, G.; Marsich, E.; Bellomo, F.; Semeraro, S.; Donati, I.; Brun, F.; Grandolfo, M.; Accardo, A.; Paoletti, S. Alginate/Hydroxyapatite biocomposite for bone ingrowth: A trabecular structure with high and isotropic connectivity. *Biomacromolecules* **2009**, *10*, 1575. [CrossRef]

135. Colovic, B.; Jokanovic, V.; Petrovic, M. Self assembly of biomimetic hydroxyapatite on the surface of different polymer thin films. *J. Ceram. Process. Res.* **2012**, *13*, 398–404.
136. Venkatesan, J.; Bhatnagar, I.; Manivasagan, P.; Kang, K.H.; Kim, S.K. Alginate composites for bone tissue engineering: A review. *Int. J. Biol. Macromol.* **2015**, *72*, 269–281. [CrossRef]
137. Lin, H.R.; Yeh, Y.J. Porous alginate/hydroxyapatite composite scaffolds for bone tissue engineering: Preparation, characterization, and in vitro studies. *J. Biomed. Mater. Res. B Appl. Biomater.* **2004**, *71b*, 52–65. [CrossRef] [PubMed]
138. Torgbo, S.; Sukyai, P. Bacterial cellulose-based scaffold materials for bone tissue engineering. *Appl. Mater. Today* **2018**, *11*, 34–49. [CrossRef]
139. Hickey, R.J.; Pelling, A.E. Cellulose Biomaterials for Tissue Engineering. *Front. Bioeng. Biotechnol.* **2019**, *7*. [CrossRef]
140. Turlybekuly, A.; Sagidugumar, A.; Otarov, Y.; Magazov, N.; Pogrebnjak, A.; Savitskaya, I.; Akatan, K.; Kistaubayeva, A.; Talipova, A. Bacterial Cellulose/Hydroxyapatite Printed Scaffolds for Bone Engineering. In *Nanomaterials in Biomedical Application and Biosensors, Proceedings of the 9th IEEE International Conference on Nanomaterials: Applications & Properties, Oddesa, Ukraine, 10–15 September 2019*; Springer: Singapore, 2020; pp. 1–7.
141. Favi, P.M.; Ospina, S.P.; Kachole, M.; Gao, M.; Atehortua, L.; Webster, T.J. Preparation and characterization of biodegradable nano hydroxyapatite–bacterial cellulose composites with well-defined honeycomb pore arrays for bone tissue engineering applications. *Cellulose* **2016**, *23*, 1263–1282. [CrossRef]
142. Chen, H.; Xing, X.; Tan, H.; Jia, Y.; Zhou, T.; Chen, Y.; Ling, Z.; Hu, X. Covalently antibacterial alginate-chitosan hydrogel dressing integrated gelatin microspheres containing tetracycline hydrochloride for wound healing. *Mater. Sci. Eng. C Mater. Biol. Appl.* **2017**, *70*, 287–295. [CrossRef] [PubMed]
143. Ivanova, E.P.; Bazaka, K.; Crawford, R.J. 2—Natural polymer biomaterials: Advanced applications. In *New Functional Biomaterials for Medicine and Healthcare*; Ivanova, E.P., Bazaka, K., Crawford, R.J., Eds.; Woodhead Publishing: Cambridge, UK, 2014; pp. 32–70.
144. Dash, M.; Chiellini, F.; Ottenbrite, R.M.; Chiellini, E. Chitosan—A versatile semi-synthetic polymer in biomedical applications. *Prog. Polym. Sci.* **2011**, *36*, 981–1014. [CrossRef]
145. Mescher, A. *Junqueira's Basic Histology: Text and Atlas*; McGraw-Hill Medical: New York, NY, USA, 2013.
146. Tigli, R.S.; Gumusderelioglu, M. Chondrogenesis on BMP-6 Loaded Chitosan Scaffolds in Stationary and Dynamic Cultures. *Biotechnol. Bioeng.* **2009**, *104*, 601–610. [CrossRef]
147. Tamimi, M.; Rajabi, S.; Pezeshki-Modaress, M. Cardiac ECM/chitosan/alginate ternary scaffolds for cardiac tissue engineering application. *Int. J. Biol. Macromol.* **2020**, *164*, 389–402. [CrossRef]
148. Domenech, M.; Polocorrales, L.; Ramirezvick, J.E.; Freytes, D.O. TE Strategies for Myocardial Regeneration: Acellular Versus Cellular Scaffolds? *Tissue Eng. Part B Rev.* **2016**, *22*, 438–458. [CrossRef]
149. Dong, Y.F.; Liang, J.N.; Cui, Y.H.; Xu, S.; Zhao, N.R. Fabrication of novel bioactive hydroxyapatite-chitosan-silica hybrid scaffolds: Combined the sol-gel method with 3D plotting technique. *Carbohydr. Polym.* **2018**, *197*, 183–193. [CrossRef]
150. Ang, T.H.; Sultana, F.S.A.; Hutmacher, D.W.; Wong, Y.S.; Fuh, J.Y.H.; Mo, X.M.; Loh, H.T.; Burdet, E.; Teoh, S.H. Fabrication of 3D chitosan-hydroxyapatite scaffolds using a robotic dispensing system. *Mater. Sci. Eng. C* **2002**, *20*, 35–42. [CrossRef]
151. Zhang, L.; Li, Y.; Yang, A.; Peng, X.; Wang, X.; Zhang, X. Preparation and in vitro investigation of chitosan/nano-hydroxyapatite composite used as bone substitute materials. *J. Mater. Mater. Med.* **2005**, *16*, 213–219.
152. Shavandi, A.; Hosseini, S.; Okoro, O.V.; Nie, L.; Babadi, F.E.; Melchels, F. 3D Bioprinting of Lignocellulosic Biomaterials. *Adv. Healthc. Mater.* **2020**. [CrossRef]
153. Liu, F.; Chen, Q.H.; Liu, C.; Ao, Q.; Tian, X.H.; Fan, J.; Tong, H.; Wang, X.H. Natural Polymers for Organ 3D Bioprinting. *Polymers* **2018**, *10*, 1278. [CrossRef]
154. Wenz, A.; Borchers, K.; Tovar, G.E.M.; Kluger, P.J. Bone matrix production in hydroxyapatite-modified hydrogels suitable for bone bioprinting. *Biofabrication* **2017**, *9*. [CrossRef]
155. Murugan, R.; Ramakrishna, S. Bioresorbable composite bone paste using polysaccharide based nano hydroxyapatite. *Biomaterials* **2004**, *25*, 3829–3835. [CrossRef]
156. Rusu, V.M.; Ng, C.-H.; Wilke, M.; Tiersch, B.; Fratzl, P.; Peter, M.G. Size-controlled hydroxyapatite nanoparticles as self-organized organic-inorganic composite materials. *Biomater. Guildf.* **2005**. [CrossRef]
157. Sailaja, G.S.; Velayudhan, S.; Sunny, M.C.; Sreenivasan, K.; Varma, H.K.; Ramesh, P. Hydroxyapatite filled chitosan-polyacrylic acid polyelectrolyte complexes. *J. Mater. Sci.* **2003**, *38*, 3653–3662. [CrossRef]
158. Yamaguchi, I.; Tokuchi, K.; Fukuzaki, H.; Koyama, Y.; Takakuda, K.; Monma, H.; Tanaka, J. Preparation and microstructure analysis of chitosan/hydroxyapatite nanocomposites. *J. Biomed. Mater. Res.* **2001**. [CrossRef]
159. Freddi, G.; Monti, P.; Nagura, M.; And, Y.G.; Tsukada, M. Structure and molecular conformation of tussah silk fibroin films: Effect of heat treatment. *J. Polym. Sci. Part B Polym. Phys.* **1997**, *35*, 841–847. [CrossRef]
160. Park, S.J.; Lee, K.Y.; Ha, W.S.; Park, S.Y. Structural changes and their effect on mechanical properties of silk fibroin/chitosan blends. *J. Appl. Polym. Sci.* **1999**, *74*, 2571–2575. [CrossRef]
161. Wang, L.; Nemoto, R.; Senna, M. Microstructure and Chemical States of Hydroxyapatite/silk Fibroin Nanocomposites Synthesized via A Wet-mechanochemical Route. *J. Nanoparticle Res.* **2002**, *4*, 535–540. [CrossRef]
162. Wang, L.; Nemoto, R.; Senna, M. Changes in microstructure and physico-chemical properties of hydroxyapatite–silk fibroin nanocomposite with varying silk fibroin content. *J. Eur. Ceram. Soc.* **2004**, *24*, 2707–2715. [CrossRef]

163. Wang, L.; Li, C. Preparation and physicochemical properties of a novel hydroxyapatite/chitosan–silk fibroin composite. *Carbohydr. Polym.* **2007**, *68*, 740–745. [CrossRef]

164. Peter, M.; Ganesh, N.; Selvamurugan, N.; Nair, S.V.; Furuike, T.; Tamura, H.; Jayakumar, R. Preparation and characterization of chitosan–gelatin/nanohydroxyapatite composite scaffolds for tissue engineering applications. *Carbohydr. Polym.* **2010**, *80*, 687–694. [CrossRef]

165. Verma, D.; Katti, K.S.; Katti, D.R.; Mohanty, B. Mechanical response and multilevel structure of biomimetic hydroxyapatite/polygalacturonic/chitosan nanocomposites. *Mater. Sci. Eng. C* **2008**, *28*, 399–405. [CrossRef]

166. Abouzeid, R.E.; Khiari, R.; Beneventi, D.; Dufresne, A. Biomimetic Mineralization of Three-Dimensional Printed Alginate/TEMPO-Oxidized Cellulose Nanofibril Scaffolds for Bone Tissue Engineering. *Biomacromolecules* **2018**, *19*, 4442–4452. [CrossRef]

167. Van den Eynde, M.; Van Puyvelde, P. 3D Printing of Poly(lactic acid). In *Industrial Applications of Poly(lactic acid)*; Di Lorenzo, M.L., Androsch, R., Eds.; Springer International Publishing: Cham, Switzerland, 2018; pp. 139–158.

168. Fini, M.; Giannini, S.; Giardino, R.; Giavaresi, G.; Rocca, M. Resorbable device for fracture fixation: In vivo degradation and mechanical behaviour. *Int. J. Artif. Organs* **1995**, *18*, 772–776. [CrossRef] [PubMed]

169. Taddei, P.; Monti, P.; Simoni, R. Vibrational and thermal study on the in vitro and in vivo degradation of a poly(lactic acid)-based bioabsorbable periodontal membrane. *J. Mater. Sci. Mater. Med.* **2002**, *13*, 469–475. [CrossRef]

170. Takayama, T.; Uchiumi, K.; Ito, H.; Kawai, T.; Todo, M. Particle size distribution effects on physical properties of injection molded HA/PLA composites. *Adv. Compos. Mater.* **2013**, *22*, 327–337. [CrossRef]

171. Nejati, E.; Mirzadeh, H.; Zandi, M. Synthesis and characterization of nano-hydroxyapatite rods/poly(l-lactide acid) composite scaffolds for bone tissue engineering. *Compos. Part A Appl. Sci. Manuf.* **2008**, *39*, 1589–1596. [CrossRef]

172. Zheng, X.; Zhou, S.; Li, X.; Weng, J. Shape memory properties of poly(D,L-lactide)/hydroxyapatite composites. *Biomaterials* **2006**, *27*, 4288–4295. [CrossRef] [PubMed]

173. Leenslag, J.W.; Pennings, A.J.; Bos, R.R.M.; Rozema, F.R.; Boering, G. Resorbable materials of poly(L-lactide). VI. Plates and screws for internal fracture fixation. *Biomaterials* **1987**, *8*, 70–73. [CrossRef]

174. Böstman, O.M. Absorbable implants for the fixation of fractures. *J. Bone Jt. Surg. Am.* **1991**, *73*, 148–153. [CrossRef]

175. Li, J.; Lu, X.L.; Zheng, Y.F. Effect of surface modified hydroxyapatite on the tensile property improvement of HA/PLA composite. *Appl. Surf. Sci.* **2008**, *255*, 494–497. [CrossRef]

176. Deng, X.; Hao, J.; Wang, C. Preparation and mechanical properties of nanocomposites of poly(D,L-lactide) with Ca-deficient hydroxyapatite nanocrystals. *Biomaterials* **2001**, *22*, 2867–2873. [CrossRef]

177. Shikinami, Y.; Matsusue, Y.; Nakamura, T. The complete process of bioresorption and bone replacement using devices made of forged composites of raw hydroxyapatite particles/poly l-lactide (F-u-HA/PLLA). *Biomaterials* **2005**, *26*, 5542–5551. [CrossRef] [PubMed]

178. Kikuchi, M.; Suetsugu, Y.; Tanaka, J.; Akao, M. Preparation and mechanical properties of calcium phosphate/copoly-L-lactide composites. *J. Mater. Sci. Mater. Med.* **1997**, *8*, 361–364. [CrossRef]

179. Yamaji, S.; Kobayashi, S. Effect of in vitro hydrolysis on the compressive behavior and strain rates dependence of tricalcium phosphate/poly(L-lactic acid) composites. *Adv. Compos. Mater.* **2013**, *22*, 1–11. [CrossRef]

180. Kobayashi, S.; Sakamoto, K. Bending and Compressive Properties of Crystallized TCP/PLLA Composites. *Adv. Compos. Mater.* **2009**, *18*, 287–295. [CrossRef]

181. Hong, Z.; Zhang, P.; He, C.; Qiu, X.; Liu, A.; Chen, L.; Chen, X.; Jing, X. Nano-composite of poly(L-lactide) and surface grafted hydroxyapatite: Mechanical properties and biocompatibility. *Biomaterials* **2005**, *26*, 6296–6304. [CrossRef]

182. Takayama, T.; Todo, M.; Takano, A. The effect of bimodal distribution on the mechanical properties of hydroxyapatite particle filled poly(L-lactide) composites. *J. Mech. Behav. Biomed. Mater.* **2009**, *2*, 105–112. [CrossRef] [PubMed]

183. Hong, Z.; Qiu, X.; Sun, J.; Deng, M.; Chen, X.; Jing, X. Grafting polymerization of L-lactide on the surface of hydroxyapatite nano-crystals. *Polymer* **2004**, *45*, 6699–6706. [CrossRef]

184. Naik, A.; Best, S.M.; Cameron, R.E. The influence of silanisation on the mechanical and degradation behaviour of PLGA/HA composites. *Mater. Sci. Eng. C* **2015**, *48*, 642–650. [CrossRef] [PubMed]

185. Corcione, C.E.; Gervaso, F.; Scalera, F.; Padmanabhan, S.K.; Madaghiele, M.; Montagna, F.; Sannino, A.; Licciulli, A.; Maffezzoli, A. Highly loaded hydroxyapatite microsphere/PLA porous scaffolds obtained by fused deposition modelling. *Ceram. Int.* **2019**, *45*, 2803–2810. [CrossRef]

186. Bostman, O.M. Osteoarthritis of the ankle after foreign-body reaction to absorbable pins and screws: A three- to nine-year follow-up study. *J. Bone Jt. Surg. Br.* **1998**, *80*, 333–338. [CrossRef]

187. Shikinami, Y.; Okuno, M. Bioresorbable devices made of forged composites of hydroxyapatite (HA) particles and poly-L-lactide (PLLA): Part I. Basic characteristics. *Biomaterials* **1999**, *20*, 859–877. [CrossRef]

188. Nie, L.; Suo, J.P.; Zou, P.; Feng, S.B. Preparation and Properties of Biphasic Calcium Phosphate Scaffolds Multiply Coated with HA/PLLA Nanocomposites for Bone Tissue Engineering Applications. *J. Nanomater.* **2012**, *2012*, 213549. [CrossRef]

189. Verheyen, C.C.P.M.; Wijn, J.R.D.; Blitterswijk, C.A.V.; Groot, K.D. Evaluation of hydroxylapatite/poly(L-lactide) composites: Mechanical behavior. *J. Biomed. Mater. Res.* **1992**, *26*, 1277–1296. [CrossRef]

190. Furukawa, T.; Matsusue, Y.; Yasunaga, T.; Shikinami, Y.; Okuno, M.; Nakamura, T. Biodegradation behavior of ultra-high-strength hydroxyapatite/poly(L-lactide) composite rods for internal fixation of bone fractures. *Biomaterials* **2000**, *21*, 889–898. [CrossRef]

191. Kwon, D.Y.; Kwon, J.S.; Park, S.H.; Park, J.H.; Jang, S.H.; Yin, X.Y.; Yun, J.H.; Kim, J.H.; Min, B.H.; Lee, J.H.; et al. A computer-designed scaffold for bone regeneration within cranial defect using human dental pulp stem cells. *Sci. Rep.* **2015**, *5*. [CrossRef]

192. Hu, Y.; Wang, J.; Li, X.; Hu, X.; Zhou, W.; Dong, X.; Wang, C.; Yang, Z.; Binks, B.P. Facile preparation of bioactive nanoparticle/poly(ε-caprolactone) hierarchical porous scaffolds via 3D printing of high internal phase Pickering emulsions. *J. Colloid Interface Sci.* **2019**, *545*, 104–115. [CrossRef] [PubMed]

193. Peter, S.J.; Miller, S.T.; Zhu, G.; Yasko, A.W.; Mikos, A.G. In vivo degradation of a poly(propylene fumarate)/β-tricalcium phosphate injectable composite scaffold. *J. Biomed. Mater. Res.* **1998**, *41*, 1–7. [CrossRef]

194. Petersmann, S.; Spoerk, M.; Huber, P.; Lang, M.; Pinter, G.; Arbeiter, F. Impact Optimization of 3D-Printed Poly(methyl methacrylate) for Cranial Implants. *Macromol. Mater. Eng.* **2019**, *304*, 1900263. [CrossRef]

195. Tontowi, A.E.; Kuswanto, D.; Sihaloho, R.I.; Sosiati, H. Composite of [HA/PMMA] for 3D-printer material application. *AIP Conf. Proc.* **2016**, *1755*, 150020.

196. Mahammod, B.P.; Barua, E.; Deb, P.; Deoghare, A.B.; Pandey, K.M. Investigation of Physico-mechanical Behavior, Permeability and Wall Shear Stress of Porous HA/PMMA Composite Bone Scaffold. *Arab. J. Sci. Eng.* **2020**, *45*, 5505–5515. [CrossRef]

197. Lal, B.; Ghosh, M.; Agarwal, B.; Gupta, D.; Roychoudhury, A. A novel economically viable solution for 3D printing-assisted cranioplast fabrication. *Br. J. Neurosurg.* **2020**, *34*, 280–283. [CrossRef]

198. Duran, C.; Subbian, V.; Giovanetti, M.T.; Simkins, J.R.; Beyette, F.R. Experimental desktop 3D printing using dual extrusion and water-soluble polyvinyl alcohol. *Rapid Prototyp. J.* **2015**, *21*, 528–534. [CrossRef]

199. Nie, L.; Zhang, G.H.; Hou, R.X.; Xu, H.P.; Li, Y.P.; Fu, J. Controllable promotion of chondrocyte adhesion and growth on PVA hydrogels by controlled release of TGF-beta 1 from porous PLGA microspheres. *Colloid Surf. B* **2015**, *125*, 51–57. [CrossRef] [PubMed]

200. Du, G.L.; Nie, L.; Gao, G.R.; Sun, Y.N.; Hou, R.X.; Zhang, H.; Chen, T.; Fu, J. Tough and Biocompatible Hydrogels Based on In Situ Interpenetrating Networks of Dithiol-Connected Graphene Oxide and Poly(vinyl alcohol). *ACS Appl. Mater. Interfaces* **2015**, *7*, 3003–3008. [CrossRef]

201. Hou, R.X.; Nie, L.; Du, G.L.; Xiong, X.P.; Fu, J. Natural polysaccharides promote chondrocyte adhesion and proliferation on magnetic nanoparticle/PVA composite hydrogels. *Colloid Surf. B* **2015**, *132*, 146–154. [CrossRef]

202. Velu, R.; Calais, T.; Jayakumar, A.; Raspall, F. A Comprehensive Review on Bio-Nanomaterials for Medical Implants and Feasibility Studies on Fabrication of Such Implants by Additive Manufacturing Technique. *Materials* **2019**, *13*, 92. [CrossRef] [PubMed]

203. Chua, C.K.; Leong, K.F.; Tan, K.H.; Wiria, F.E.; Cheah, C.M. Development of tissue scaffolds using selective laser sintering of polyvinyl alcohol/hydroxyapatite biocomposite for craniofacial and joint defects. *J. Mater. Sci. Mater. Med.* **2004**, *15*, 1113–1121. [CrossRef] [PubMed]

204. Nie, L.; Deng, Y.L.; Li, P.; Hou, R.X.; Shavandi, A.; Yang, S.F. Hydroxyethyl Chitosan-Reinforced Polyvinyl Alcohol/Biphasic Calcium Phosphate Hydrogels for Bone Regeneration. *ACS Omega* **2020**, *5*, 10948–10957. [CrossRef] [PubMed]

205. Nie, L.; Chen, D.; Suo, J.P.; Zou, P.; Feng, S.B.; Yang, Q.; Yang, S.H.; Ye, S.N. Physicochemical characterization and biocompatibility in vitro of biphasic calcium phosphate/polyvinyl alcohol scaffolds prepared by freeze-drying method for bone tissue engineering applications. *Colloid Surf. B* **2012**, *100*, 169–176. [CrossRef] [PubMed]

206. Nie, L.; Li, X.C.; Wang, Z.; Hu, K.H.; Cai, R.H.; Li, P.; Han, Y.T.; Sun, M.; Yuan, H.Y.; Suo, J.P.; et al. In vitro biomineralization on poly(vinyl alcohol)/biphasic calcium phosphate hydrogels. *Bioinspir. Biomim. Nanobiomater.* **2020**, *9*, 122–128. [CrossRef]

207. Chai, W.H.; Wei, Q.H.; Yang, M.M.; Ji, K.; Guo, Y.H.; Wei, S.M.; Wang, Y.N. The printability of three water based polymeric binders and their effects on the properties of 3D printed hydroxyapatite bone scaffold. *Ceram. Int.* **2020**, *46*, 6663–6671. [CrossRef]

208. Domb, A.J.; Manor, N.; Elmalak, O. Biodegradable bone cement compositions based on acrylate and epoxide terminated poly(propylene fumarate) oligomers and calcium salt compositions. *Biomaterials* **1996**, *17*, 411–417. [CrossRef]

209. He, S.; Timmer, M.D.; Yaszemski, M.J.; Yasko, A.W.; Engel, P.S.; Mikos, A.G. Synthesis of biodegradable poly(propylene fumarate) networks with poly(propylene fumarate)-diacylate macromers as crosslinking agents and characterization of their degradation products. *Polymer* **2001**, *42*, 1251–1260. [CrossRef]

210. Wilson, J.A.; Luong, D.; Kleinfehn, A.P.; Sallam, S.; Wesdemiotis, C.; Becker, M.L. Magnesium Catalyzed Polymerization of End Functionalized Poly(propylene maleate) and Poly(propylene fumarate) for 3D Printing of Bioactive Scaffolds. *J. Am. Chem. Soc.* **2018**, *140*, 277–284. [CrossRef]

211. Kim, K.; Dean, D.; Wallace, J.; Breithaupt, R.; Mikos, A.G.; Fisher, J.P. The influence of stereolithographic scaffold architecture and composition on osteogenic signal expression with rat bone marrow stromal cells. *Biomaterials* **2011**, *32*, 3750–3763. [CrossRef]

212. Luo, Y.Y.; Le Fer, G.; Dean, D.; Becker, M.L. 3D Printing of Poly(propylene fumarate) Oligomers: Evaluation of Resin Viscosity, Printing Characteristics and Mechanical Properties. *Biomacromolecules* **2019**, *20*, 1699–1708. [CrossRef]

213. Le Fer, G.; Luo, Y.Y.; Becker, M.L. Poly(propylene fumarate) stars, using architecture to reduce the viscosity of 3D printable resins. *Polym. Chem.* **2019**, *10*, 4655–4664. [CrossRef]

214. Lee, K.W.; Wang, S.; Lu, L.; Jabbari, E.; Currier, B.L.; Yaszemski, M.J. Fabrication and Characterization of Poly(Propylene Fumarate) Scaffolds with Controlled Pore Structures Using 3-Dimensional Printing and Injection Molding. *Tissue Eng.* **2006**, *12*, 2801. [CrossRef]

215. Lee, K.W.; Wang, S.; Yaszemski, M.J.; Lu, L. Physical properties and cellular responses to crosslinkable poly(propylene fumarate)/hydroxyapatite nanocomposites. *Biomaterials* **2008**, *29*, 2839–2848. [CrossRef]

216. Lee, K.W.; Wang, S.; Dadsetan, M.; Yaszemski, M.J.; Lu, L. Enhanced cell ingrowth and proliferation through three-dimensional nanocomposite scaffolds with controlled pore structures. *Biomacromolecules* **2010**, *11*, 682. [CrossRef]
217. Trachtenberg, J.E.; Placone, J.K.; Smith, B.T.; Fisher, J.P.; Mikos, A.G. Extrusion-based 3D printing of poly(propylene fumarate) scaffolds with hydroxyapatite gradients. *J. Biomater. Sci. Polym. E* **2017**, *28*, 532–554. [CrossRef] [PubMed]
218. Lee, J.W.; Ahn, G.; Kim, D.S.; Cho, D.W. Development of nano- and microscale composite 3D scaffolds using PPF/DEF-HA and micro-stereolithography. *Microelectron. Eng.* **2009**, *86*, 1465–1467. [CrossRef]
219. Alizadeh-Osgouei, M.; Li, Y.; Wen, C. A comprehensive review of biodegradable synthetic polymer-ceramic composites and their manufacture for biomedical applications. *Bioact. Mater.* **2019**, *4*, 22–36. [CrossRef]
220. Charles, L.F.; Shaw, M.T.; Wei, J.R.O. Fabrication and mechanical properties of PLLA/PCL/HA composites via a biomimetic, dip coating, and hot compression procedure. *J. Mater. Sci. Mater. Med.* **2010**, *21*, 1845–1854. [CrossRef]
221. Park, S.D.; Todo, M.; Arakawa, K.; Tsuji, H.; Takenoshita, Y. Fracture properties of bioabsorbable HA/PLLA/PCL composite material. *Proc. SPIE Int. Soc. Opt. Eng.* **2005**, 5852. [CrossRef]
222. Asran, A.S.; Henning, S.; Michler, G.H. Polyvinyl alcohol–collagen–hydroxyapatite biocomposite nanofibrous scaffold: Mimicking the key features of natural bone at the nanoscale level. *Polymer* **2010**, *51*, 868–876. [CrossRef]
223. Todo, M.; Kagawa, T. Improvement of fracture energy of HA/PLLA biocomposite material due to press processing. *J. Mater. Sci.* **2008**. [CrossRef]
224. Todo, M.; Park, S.; Arakawa, K.; Takenoshita, Y. Effect of Particle Shape on the Fracture Behavior of HA/PLLA Composite Material. *J. Jpn. Soc. Compos. Mater.* **2005**, *31*, 177–183. [CrossRef]
225. Todo, M.; Sang, D.P.; Arakawa, K.; Takenoshita, Y. Relationship between microstructure and fracture behavior of bioabsorbable HA/PLLA composites. *Compos. Part A Appl. Sci. Manuf.* **2006**, *37*, 2221–2225. [CrossRef]
226. Zhang, R.; Ma, P.X. Poly(A-hydroxyl acids)/hydroxyapatite porous composites for bone-tissue engineering. I. Preparation and morphology. *J. Biomed. Mater. Res.* **2015**, *44*, 446–455. [CrossRef]
227. Chirila, T.V.; Suzuki, S.; Bray, L.J.; Barnett, N.L.; Harkin, D.G. Evaluation of silk sericin as a biomaterial: In vitro growth of human corneal limbal epithelial cells on Bombyx mori sericin membranes. *Prog. Biomater.* **2013**, *2*, 1–10. [CrossRef]
228. Mondal, M.; Trivedy, K.; Nirmal, K.S. The silk proteins, sericin and fibroin in silkworm, *Bombyx mori* Linn.—A review. *Caspian J. Environ. Sci.* **2007**, *5*, 63–76.
229. Ferraz, M.P.; Monteiro, F.J.; Manuel, C.M. Hydroxyapatite nanoparticles: A review of preparation methodologies. *J. Appl. Biomater. Biomech.* **2004**, *2*, 74–80.
230. Helmus, M.; Scott, M.J. Enhanced Biocompatibility Coatings for Medical Implants. U.S. Patent No. EP1051210A2, 15 November 2000.
231. Zebarjad, S.M.; Sajjadi, S.A.; Sdrabadi, T.E.; Yaghmaei, A.; Naderi, B. A Study on Mechanical Properties of PMMA/Hydroxyapatite Nanocomposite. *Engineering* **2011**, *3*, 795–801.
232. Tontowi, A.E.; Raharjo, K.P.; Sihaloho, R.I.; Baroroh, D.K. Comparison of Design Method for Making Composite of (PMMA/HA/Sericin). In *Materials Science Forum*; Trans Tech Publications Ltd.: Zurich, Switzerland, 2017; pp. 85–90.
233. Tontowi, A.E.; Anggraeni, D.; Saragih, H.T.; Raharjo, K.P.N.; Utami, P. Experimental study of 3D-printable biocomposite of [HA/PMMA/Sericin] materials. *Adv. Mater. Lett.* **2017**, *8*, 857–861.
234. Sarasam, A.; Madihally, S.V. Characterization of chitosan–polycaprolactone blends for tissue engineering applications. *Biomaterials* **2005**, *26*, 5500–5508. [CrossRef] [PubMed]
235. Li, Z.; Ramay, H.R.; Hauch, K.D.; Xiao, D.; Zhang, M. Chitosan-alginate hybrid scaffolds for bone tissue engineering. *Biomaterials* **2005**, *26*, 3919–3928. [CrossRef] [PubMed]
236. Shanmugasundaram, N.; Ravichandran, P.; Reddy, P.N.; Ramamurty, N.; Rao, K.P. Collagen–chitosan polymeric scaffolds for the in vitro culture of human epidermoid carcinoma cells. *Biomaterials* **2001**, *22*, 1943–1951. [CrossRef]
237. Mi, F.L.; Tan, Y.C.; Liang, H.F.; Sung, H.W. In vivo biocompatibility and degradability of a novel injectable-chitosan-based implant. *Biomaterials* **2002**, *23*, 181–191. [CrossRef]
238. Wang, L.; Khor, E.; Wee, A.; Lim, L.Y. Chitosan-alginate PEC membrane as a wound dressing: Assessment of incisional wound healing. *J. Biomed. Mater. Res.* **2010**, *63*, 610–618. [CrossRef]
239. Cai, X.; Tong, H.; Shen, X.; Chen, W.; Yan, J.; Hu, J. Preparation and characterization of homogeneous chitosan-polylactic acid/hydroxyapatite nanocomposite for bone tissue engineering and evaluation of its mechanical properties. *Acta Biomater.* **2009**, *5*, 2693–2703. [CrossRef] [PubMed]
240. Niu, X.; Feng, Q.; Wang, M.; Guo, X.; Zheng, Q. Porous nano-HA/collagen/PLLA scaffold containing chitosan microspheres for controlled delivery of synthetic peptide derived from BMP-2. *J. Control. Release* **2009**, *134*, 111–117. [CrossRef] [PubMed]
241. Niu, X.; Fan, Y.; Liu, X.; Li, X.; Li, P.; Wang, J.; Sha, Z.; Feng, Q. Repair of bone defect in femoral condyle using microencapsulated chitosan, nanohydroxyapatite/collagen and poly(L-lactide)-based microsphere-scaffold delivery system. *Artif. Organs* **2011**, *35*, E119–E128. [CrossRef]
242. Li, X.; Ye, F.; Li, G.L.; Cui, J.; Liu, Y.X.; Yang, L.Q.; Cong, L.; Li, B. 3D Printed Hydroxyapatite/Silk Fibroin/Polycaprolactone Artificial Bone Scaffold and Bone Tissue Engineering Materials Constructed with Double-Transfected Bone Morphogenetic Protein-2 and Vascular Endothelial Growth Factor Mesenchymal Stem Cells to Repair Rabbit Radial Bone Defects. *Nanosci. Nanotechnol. Lett.* **2020**, *12*, 368–375. [CrossRef]

243. Kim, H.; Hwangbo, H.; Koo, Y.; Kim, G. Fabrication of Mechanically Reinforced Gelatin/Hydroxyapatite Bio-Composite Scaffolds by Core/Shell Nozzle Printing for Bone Tissue Engineering. *Int. J. Mol. Sci.* **2020**, *21*, 3401. [CrossRef]

244. Antonetti, C.; Ciorba, S.; Licursi, D.; Coccia, V.; Cotana, F.; Galletti, A.M.R. Production of levulinic acid and n-butyl levulinate from the waste biomasses grape pomace and *Cynara cardunculus* L. In Proceedings of the 1st International Electronic Conference on Catalysts Science, Online, 10–30 November 2020; p. 30.

245. Bouler, J.-M.; Pilet, P.; Gauthier, O.; Verron, E. Biphasic calcium phosphate ceramics for bone reconstruction: A review of biological response. *Acta Biomater.* **2017**, *53*, 1–12. [CrossRef]

246. Liu, F.; Liu, Y.; Li, X.Y.; Wang, X.H.; Li, D.N.; Chung, S.; Chen, C.; Lee, I.S. Osteogenesis of 3D printed macro-pore size biphasic calcium phosphate scaffold in rabbit calvaria. *J. Biomater. Appl.* **2019**, *33*, 1168–1177. [CrossRef]

247. Huang, W.; Zhang, X.; Wu, Q.; Wu, B. Fabrication of HA/β-TCP scaffolds based on micro-syringe extrusion system. *Rapid Prototyp. J.* **2013**, *19*, 319–326. [CrossRef]

248. Franchin, G.; Wahl, L.; Colombo, P. Direct ink writing of ceramic matrix composite structures. *J. Am. Ceram. Soc.* **2017**, *100*, 4397–4401. [CrossRef]

249. Siemens, A.G. Manufacturing of SiO_2-Coated β-TCP Structures by 3D Printing using a Preceramic Polymer as Printing Binder and Silica Source. *J. Ceram. Sci. Technol.* **2017**, *9*, 37–42.

250. Sachs, E.; Cima, M.; Williams, P.; Brancazio, D.; Cornie, J. Three dimensional printing: Rapid tooling and prototypes directly from a CAD model. *J. Eng. Ind.* **1992**, *114*, 481–488. [CrossRef]

251. Zocca, A.; Elsayed, H.; Bernardo, E.; Gomes, C.; Lopez-Heredia, M.; Knabe, C.; Colombo, P.; Günster, J.J.B. 3D-printed silicate porous bioceramics using a non-sacrificial preceramic polymer binder. *Biofabrication* **2015**, *7*, 025008. [CrossRef]

252. Musskaya, O.N.; Krut'ko, V.K.; Kulak, A.I.; Filatov, S.A.; Batyrev, E.V.; Safronova, T.V. Calcium Phosphate Compositions with Polyvinyl Alcohol for 3D Printing. *Inorg. Mater. Appl. Res.* **2020**, *11*, 192–197. [CrossRef]

253. Tang, H.-H.; Chiu, M.-L.; Yen, H.-C. Slurry-based selective laser sintering of polymer-coated ceramic powders to fabricate high strength alumina parts. *J. Eur. Ceram. Soc.* **2011**, *31*, 1383–1388. [CrossRef]

254. Ji, S.H.; Kim, D.S.; Park, M.S.; Yun, J.S.J.N. Sintering Process Optimization for 3YSZ Ceramic 3D-Printed Objects Manufactured by Stereolithography. *Nanomaterials* **2021**, *11*, 192. [CrossRef] [PubMed]

255. Bagheri, A.; Jin, J. Photopolymerization in 3D Printing. *ACS Appl. Polym. Mater.* **2019**, *1*, 593–611. [CrossRef]

256. Zhang, B.Q.; Sun, H.; Wu, L.N.; Ma, L.; Xing, F.; Kong, Q.Q.; Fan, Y.J.; Zhou, C.C.; Zhang, X.D. 3D printing of calcium phosphate bioceramic with tailored biodegradation rate for skull bone tissue reconstruction. *Bio-Des. Manuf.* **2019**, *2*, 161–171. [CrossRef]

257. Touri, M.; Moztarzadeh, F.; Osman, N.A.A.; Dehghan, M.M.; Mozafari, M. 3D–printed biphasic calcium phosphate scaffolds coated with an oxygen generating system for enhancing engineered tissue survival. *Mater. Sci. Eng. C* **2018**, *84*, 236–242. [CrossRef] [PubMed]

258. Diaz-Gomez, L.; Elizondo, M.E.; Kontoyiannis, P.D.; Koons, G.L.; Dacunha-Marinho, B.; Zhang, X.; Ajayan, P.; Jansen, J.A.; Melchiorri, A.J.; Mikos, A.G. Three-Dimensional Extrusion Printing of Porous Scaffolds Using Storable Ceramic Inks. *Tissue Eng. Part C Methods* **2020**, *26*, 292–305. [CrossRef]

259. Hench, L.L. Opening paper 2015-some comments on bioglass: Four eras of discovery and development. *Biomed. Glasses* **2015**, *1*, 1–11. [CrossRef]

260. Hench, L.L. The story of Bioglass®. *J. Mater. Sci. Mater. Med.* **2006**, *17*, 967–978. [CrossRef]

261. Jones, J.R.; Brauer, D.S.; Hupa, L.; Greenspan, D.C. Bioglass and Bioactive Glasses and Their Impact on Healthcare. *Int. J. Appl. Glass Sci.* **2016**, *7*, 423–434. [CrossRef]

262. Pleural, N.; New, N. Pleural effusion. *Postgrad. Med. J.* **2005**, *81*, 702–710.

263. Yang, Y.; Kim, K.H.; Ong, J.L. A review on calcium phosphate coatings produced using a sputtering process—an alternative to plasma spraying. *Biomaterials* **2005**, *26*, 327–337. [CrossRef]

264. Tan, Y.; Wang, X.; Wu, Q.; Yan, W. Early peri-implant osteogenesis with functionally graded nanophase hydroxyapatite/bioglass coating on Ti alloys. In *Key Engineering Materials*; Trans Tech Publications Ltd.: Zurich, Switzerland, 2007; Volume 19.

265. Pengbo, W.; Hongyan, S.; Ming, Y.; Wantao, C. The osteointergration and osteoinduction of titanium implant with nHA/BG gradient coating in rabbits. *J. Pract. Stomatol.* **2016**, *32*, 749–751.

266. Bellucci, D.; Salvatori, R.; Cannio, M.; Luginina, M.; Orrù, R.; Montinaro, S.; Anesi, A.; Chiarini, L.; Cao, G.; Cannillo, V. Bioglass and bioceramic composites processed by Spark Plasma Sintering (SPS): Biological evaluation Versus SBF test. *Biomed. Glasses* **2018**, *4*, 21–31. [CrossRef]

267. Chanchareonsook, N.; Tideman, H.; Lee, S.; Hollister, S.J.; Flanagan, C.; Jansen, J.A. Mandibular reconstruction with a bioactive-coated cementless Ti6Al4V modular endoprosthesis in Macaca fascicularis. *Int. J. Oral Maxillofac. Surg.* **2014**, *43*, 758–768. [CrossRef]

268. Xu, C.; Bai, Y.; Yang, S.; Yang, H.; Stout, D.A.; Tran, P.A.; Yang, L. A versatile three-dimensional foam fabrication strategy for soft and hard tissue engineering. *Biomed. Mater.* **2018**, *13*. [CrossRef] [PubMed]

269. Wang, D.G.; Chen, C.Z.; Jin, Q.P.; Li, H.C.; Pan, Y.K. HA/Bioglass composite films deposited by pulsed laser with different substrate temperature. *Appl. Phys. A* **2013**, *114*, 897–902. [CrossRef]

270. Qi, X.; Pei, P.; Zhu, M.; Du, X.Y.; Xin, C.; Zhao, S.C.; Li, X.L.; Zhu, Y.F. Three dimensional printing of calcium sulfate and mesoporous bioactive glass scaffolds for improving bone regeneration in vitro and in vivo. *Sci. Rep.* **2017**, *7*. [CrossRef] [PubMed]

271. Seyedmajidi, S.; Seyedmajidi, S.; Alaghehmand, H.; Hajian-Tilaki, K.; Haghanifar, S.; Zabihi, E.; Rajabnia, R.; Seyedmajidi, M. Synthesis and Characterization of Hydroxyapatite/Bioactive Glass Nanocomposite Foam and Fluorapatite/Bioactive Glass Nanocomposite Foam by Gel Casting Method as Cell Scaffold for Bone Tissue. *Eurasian J. Anal. Chem.* **2018**, *13*. [CrossRef]

272. Seyedmajidi, M.; Haghanifar, S.; Hajian-Tilaki, K.; Seyedmajidi, S. Histopathological, histomorphometrical, and radiological evaluations of hydroxyapatite/bioactive glass and fluorapatite/bioactive glass nanocomposite foams as cell scaffolds in rat tibia: An in vivo study. *Biomed. Mater.* **2018**, *13*. [CrossRef]

273. Wu, S.; Weng, Z.; Liu, X.; Yeung, K.W.K.; Chu, P.K. Functionalized TiO2 Based Nanomaterials for Biomedical Applications. *Adv. Funct. Mater.* **2014**, *24*, 5464–5481. [CrossRef]

274. Kim, H.W.; Kim, H.E.; Salih, V.; Knowles, J.C. Hydroxyapatite and titania sol-gel composite coatings on titanium for hard tissue implants; mechanical and in vitro biological performance. *J. Biomed. Mater. Res. B Appl. Biomater.* **2005**, *72*, 1–8. [CrossRef]

275. Leyens, C.; Peters, M. *Titanium and Titanium Alloys: Fundamentals and Applications*; John Wiley & Sons: Hoboken, NJ, USA, 2003.

276. Shipley, H.; McDonnell, D.; Culleton, M.; Coull, R.; Lupoi, R.; O'Donnell, G.; Trimble, D. Optimisation of process parameters to address fundamental challenges during selective laser melting of Ti-6Al-4V: A review. *Int. J. Mach. Tools Manuf.* **2018**, *128*, 1–20. [CrossRef]

277. Hermawan, H.; Ramdan, D.; Djuansjah, J.R. *Metals for Biomedical Applications*; InTech: London, UK, 2011.

278. Xia, L.; Xie, Y.; Fang, B.; Wang, X.; Lin, K. In situ modulation of crystallinity and nano-structures to enhance the stability and osseointegration of hydroxyapatite coatings on Ti-6Al-4V implants. *Chem. Eng. J.* **2018**, *347*, 711–720. [CrossRef]

279. Habibovic, P.; Barrere, F.; Van Blitterswijk, C.A.; de Groot, K.; Layrolle, P. Biomimetic hydroxyapatite coating on metal implants. *J. Am. Ceram. Soc.* **2002**, *85*, 517–522. [CrossRef]

280. Robertson, S.F.; Bandyopadhyay, A.; Bose, S. Titania nanotube interface to increase adhesion strength of hydroxyapatite sol-gel coatings on Ti-6Al-4V for orthopedic applications. *Surf. Coat. Technol.* **2019**, *372*, 140–147. [CrossRef]

281. Qi, J.; Yang, Y.; Zhou, M.; Chen, Z.; Chen, K. Effect of transition layer on the performance of hydroxyapatite/titanium nitride coating developed on Ti-6Al-4V alloy by magnetron sputtering. *Ceram. Int.* **2019**, *45*, 4863–4869. [CrossRef]

282. Guo, H.; Zhang, X.; Kang, C.; Zhang, J.; Xu, Z.; Jiang, C.; Luo, P.; Fu, Z.; Ding, M.; Lv, Y. Synthesis of magnetic Fe-doped hydroxyapatite nanocages with highly efficient and selective adsorption for Cd^{2+}. *Mater. Lett.* **2019**, *253*, 144–147. [CrossRef]

283. Unabia, R.B.; Bonebeau, S.; Candidato, R.T., Jr.; Jouin, J.; Noguera, O.; Pawłowski, L. Investigation on the structural and microstructural properties of copper-doped hydroxyapatite coatings deposited using solution precursor plasma spraying. *J. Eur. Ceram. Soc.* **2019**, *39*, 4255–4263. [CrossRef]

284. Dittler, M.L.; Unalan, I.; Grünewald, A.; Beltrán, A.M.; Grillo, C.A.; Destch, R.; Gonzalez, M.C.; Boccaccini, A.R. Bioactive glass (45S5)-based 3D scaffolds coated with magnesium and zinc-loaded hydroxyapatite nanoparticles for tissue engineering applications. *Colloids Surf. B Biointerfaces* **2019**, *182*, 110346. [CrossRef]

285. Predoi, D.; Iconaru, S.L.; Predoi, M.V.; Stan, G.E.; Buton, N. Synthesis, characterization, and antimicrobial activity of magnesium-doped hydroxyapatite suspensions. *Nanomaterials* **2019**, *9*, 1295. [CrossRef] [PubMed]

286. Yang, F.; Yang, D.; Tu, J.; Zheng, Q.; Cai, L.; Wang, L. Strontium enhances osteogenic differentiation of mesenchymal stem cells and in vivo bone formation by activating Wnt/catenin signaling. *Stem Cells* **2011**, *29*, 981–991. [CrossRef]

287. Veerla, S.C.; Kim, D.R.; Kim, J.; Sohn, H.; Yang, S.Y. Controlled nanoparticle synthesis of Ag/Fe co-doped hydroxyapatite system for cancer cell treatment. *Mater. Sci. Eng. C Mater. Biol. Appl.* **2019**, *98*, 311–323. [CrossRef]

288. Kumar, V.B.; Khajuria, D.K.; Karasik, D.; Gedanken, A. Silver and gold doped hydroxyapatite nanocomposites for enhanced bone regeneration. *Biomed. Mater.* **2019**, *14*, 055002. [CrossRef] [PubMed]

289. Nie, L.; Hou, M.J.; Wang, T.W.; Sun, M.; Hou, R.X. Nanostructured selenium-doped biphasic calcium phosphate with in situ incorporation of silver for antibacterial applications. *Sci. Rep.* **2020**, *10*. [CrossRef] [PubMed]

290. Li, J.; Liu, X.; Park, S.; Miller, A.L.; Terzic, A.; Lu, L. Strontium-substituted hydroxyapatite stimulates osteogenesis on poly(propylene fumarate) nanocomposite scaffolds. *J. Biomed. Mater. Res. Part A* **2019**, *107*, 631–642. [CrossRef] [PubMed]

291. Pan, H.B.; Li, Z.Y.; Lam, W.M.; Wong, J.C.; Darvell, B.W.; Luk, K.D.K.; Lu, W.W. Solubility of strontium-substituted apatite by solid titration. *Acta Biomater.* **2009**, *5*, 1678–1685. [CrossRef]

292. Jianqiang, X.; Yaoqi, Y.; Rong, W.; Yuhui, S.; Weibin, Z. Hydrothermal Preparation and Characterization of Ultralong Strontium-Substituted Hydroxyapatite Whiskers Using Acetamide as Homogeneous Precipitation Reagent. *Theentificworldjournal* **2014**, *2014*, 863137.

293. Yan, J.; Sun, J.F.; Chu, P.K.; Han, Y.; Zhang, Y.M. Bone integration capability of a series of strontium-containing hydroxyapatite coatings formed by micro-arc oxidation. *J. Biomed. Mater. Res. Part A* **2013**, *101A*, 2465–2480. [CrossRef] [PubMed]

294. Ribeiro, M.; Ferraz, M.P.; Monteiro, F.J.; Fernandes, M.H.; Beppu, M.M.; Mantione, D.; Sardon, H. Antibacterial silk fibroin/nanohydroxyapatite hydrogels with silver and gold nanoparticles for bone regeneration. *Nanomedicine* **2017**, *13*, 231–239. [CrossRef]

295. Gonzalez, P.; Schwarzer, E.; Scheithauer, U.; Kooijmans, N.; Moritz, T. Additive Manufacturing of Functionally Graded Ceramic Materials by Stereolithography. *JoVE* **2019**, e57943. [CrossRef] [PubMed]

296. Deckers, J.; Vleugels, J.; Kruth, J.P. Additive manufacturing of ceramics: A review. *J. Ceram. Sci. Technol.* **2014**, *5*, 245–260.

297. Travitzky, N.; Bonet, A.; Dermeik, B.; Fey, T.; Filbert-Demut, I.; Schlier, L.; Schlordt, T.; Greil, P. Additive Manufacturing of Ceramic-Based Materials. *Adv. Eng. Mater.* **2014**, *16*, 729–754. [CrossRef]

298. He, L.; Fei, F.; Wang, W.; Song, X. Support-Free Ceramic Stereolithography of Complex Overhanging Structures Based on an Elasto-viscoplastic Suspension Feedstock. *ACS Appl. Mater. Interfaces* **2019**, *11*, 18849–18857. [CrossRef]

299. Hu, K.; Wei, Y.; Lu, Z.; Wan, L.; Li, P. Design of a Shaping System for Stereolithography with High Solid Loading Ceramic Suspensions. *3D Print. Addit. Manuf.* **2018**, *5*, 311–318. [CrossRef]

300. Safonov, A.; Maltsev, E.; Chugunov, S.; Tikhonov, A.; Konev, S.; Evlashin, S.; Popov, D.; Pasko, A.; Akhatov, I.J.A.S. Design and fabrication of complex-shaped ceramic bone implants via 3d printing based on laser stereolithography. *Appl. Sci.* **2020**, *10*, 7138. [CrossRef]

301. Bae, C.-J.; Ramachandran, A.; Chung, K.; Park, S. Ceramic Stereolithography: Additive Manufacturing for 3D Complex Ceramic Structures. *J. Korean Ceram. Soc.* **2017**, *54*, 470–477. [CrossRef]

302. Chaput, C.; Chartier, T. Fabrication of ceramics by stereolithography. *Rapid Technol. E J.* **2007**, *4*. Available online: https://www.rtejournal.de/ausgabe4/1163 (accessed on 23 March 2021).

303. Yan, Q.; Dong, H.; Su, J.; Han, J.; Song, B.; Wei, Q.; Shi, Y. A Review of 3D Printing Technology for Medical Applications. *Engineering* **2018**, *4*, 729–742. [CrossRef]

304. Jazayeri, H.E.; Rodriguez-Romero, M.; Razavi, M.; Tahriri, M.; Ganjawalla, K.; Rasoulianboroujeni, M.; Malekoshoaraie, M.H.; Khoshroo, K.; Tayebi, L. The cross-disciplinary emergence of 3D printed bioceramic scaffolds in orthopedic bioengineering. *Ceram. Int.* **2018**, *44*, 1–9. [CrossRef]

305. Hollister, S.J. Porous scaffold design for tissue engineering. *Nat. Mater.* **2005**, *4*, 518–524. [CrossRef]

306. Amini, A.R.; Laurencin, C.T.; Nukavarapu, S.P. Bone tissue engineering: Recent advances and challenges. *Crit. Rev. Biomed. Eng.* **2012**, *40*, 363–408. [CrossRef]

307. Karageorgiou, V.; Kaplan, D. Porosity of 3D biomaterial scaffolds and osteogenesis. *Biomaterials* **2005**, *26*, 5474–5491. [CrossRef]

308. Kuboki, Y.; Takita, H.; Kobayashi, D.; Tsuruga, E.; Inoue, M.; Murata, M.; Nagai, N.; Dohi, Y.; Ohgushi, H. BMP-induced osteogenesis on the surface of hydroxyapatite with geometrically feasible and nonfeasible structures: Topology of osteogenesis. *J. Biomed. Mater. Res.* **2015**, *39*, 190–199. [CrossRef]

309. Svehla, M.; Morberg, P.; Zicat, B.; Bruce, W.; Sonnabend, D.; Walsh, W.R. Morphometric and mechanical evaluation of titanium implant integration: Comparison of five surface structures. *J. Biomed. Mater. Res. Part A* **2000**, *51*, 15–22. [CrossRef]

310. Lee, C.M.; Yang, S.W.; Jung, S.C.; Kim, B.H. Oxygen Plasma Treatment on 3D-Printed Chitosan/Gelatin/Hydroxyapatite Scaffolds for Bone Tissue Engineering. *J. Nanosci. Nanotechnol.* **2017**, *17*, 2747–2750. [CrossRef]

311. Sultan, S.; Mathew, A.P. 3D printed scaffolds with gradient porosity based on a cellulose nanocrystal hydrogel. *Nanoscale* **2018**, *10*, 4421–4431. [CrossRef] [PubMed]

312. Wang, L.; Kang, J.F.; Sun, C.N.; Li, D.C.; Cao, Y.; Jin, Z.M. Mapping porous microstructures to yield desired mechanical properties for application in 3D printed bone scaffolds and orthopaedic implants. *Mater. Des.* **2017**, *133*, 62–68. [CrossRef]

313. Zhang, S.; Vijayavenkataraman, S.; Lu, W.F.; Fuh, J.Y.H. A review on the use of computational methods to characterize, design, and optimize tissue engineering scaffolds, with a potential in 3D printing fabrication. *J. Biomed. Mater. Res. B* **2019**, *107*, 1329–1351. [CrossRef] [PubMed]

314. Masaeli, R.; Zandsalimi, K.; Rasoulianboroujeni, M.; Tayebi, L. Challenges in Three-Dimensional Printing of Bone Substitutes. *Tissue Eng. Part B Rev.* **2019**, *25*, 387–397. [CrossRef] [PubMed]

315. Castilho, M.; Moseke, C.; Ewald, A.; Gbureck, U.; Groll, J.; Pires, I.; Teßmar, J.R.; Vorndran, E. Direct 3D powder printing of biphasic calcium phosphate scaffolds for substitution of complex bone defects. *Biofabrication* **2014**, *6*, 015006. [CrossRef] [PubMed]

316. Ling, S.; Qin, Z.; Huang, W.; Cao, S.; Kaplan, D.L.; Buehler, M.J. Design and function of biomimetic multilayer water purification membranes. *Sci. Adv.* **2017**, *3*, e1601939. [CrossRef]

317. Keten, S.; Xu, Z.; Ihle, B.; Buehler, M.J. Nanoconfinement controls stiffness, strength and mechanical toughness of beta-sheet crystals in silk. *Nat. Mater.* **2010**, *9*, 359–367. [CrossRef]

318. Lee, J.B.; Maeng, W.Y.; Koh, Y.H.; Kim, H.E. Porous Calcium Phosphate Ceramic Scaffolds with Tailored Pore Orientations and Mechanical Properties Using Lithography-Based Ceramic 3D Printing Technique. *Materials* **2018**, *11*, 1711. [CrossRef]

319. Senatov, F.S.; Niaza, K.V.; Zadorozhnyy, M.Y.; Maksimkin, A.V.; Kaloshkin, S.D.; Estrin, Y.Z. Mechanical properties and shape memory effect of 3D-printed PLA-based porous scaffolds. *J. Mech. Behav. Biomed. Mater.* **2016**, *57*, 139–148. [CrossRef]

320. Chen, S.S.; Shi, Y.F.; Zhang, X.; Ma, J. 3D printed hydroxyapatite composite scaffolds with enhanced mechanical properties. *Ceram. Int.* **2019**, *45*, 10991–10996. [CrossRef]

321. Asghari, F.; Samiei, M.; Adibkia, K.; Akbarzadeh, A.; Davaran, S. Biodegradable and biocompatible polymers for tissue engineering application: A review. *Artif. Cell Nanomed. B* **2017**, *45*, 185–192. [CrossRef] [PubMed]

322. Saroia, J.; Wang, Y.E.; Wei, Q.H.; Zhang, K.; Lu, T.L.; Zhang, B. A review on biocompatibility nature of hydrogels with 3D printing techniques, tissue engineering application and its future prospective. *Bio-Des. Manuf.* **2018**, *1*, 265–279. [CrossRef]

323. Hsu, S.-h.; Hung, K.-C.; Chen, C.-W. Biodegradable polymer scaffolds. *J. Mater. Chem. B* **2016**, *4*, 7493–7505. [CrossRef]

324. Barszczewska-Rybarek, I.M.; Jaszcz, K.; Jurczyk, S.; Chladek, G. The novel semi-biodegradable interpenetrating polymer networks based on urethane-dimethacrylate and epoxy-polyester components as alternative biomaterials. *Acta Bioeng. Biomech.* **2015**, *17*, 13–22. [CrossRef]

325. Nair, L.S.; Laurencin, C.T. Biodegradable polymers as biomaterials. *Prog. Polym. Sci.* **2007**, *32*, 762–798. [CrossRef]

326. Shuai, C.; Wu, P.; Zhong, Y.; Feng, P.; Gao, C.; Huang, W.; Zhou, Z.; Chen, L.; Shuai, C. Polyetheretherketone/poly (glycolic acid) blend scaffolds with biodegradable properties. *J. Biomater. Sci. Polym. Ed.* **2016**, *27*, 1434–1446. [CrossRef]

327. Feng, P.; Wu, P.; Gao, C.D.; Yang, Y.W.; Guo, W.; Yang, W.J.; Shuai, C.J. A Multimaterial Scaffold with Tunable Properties: Toward Bone Tissue Repair. *Adv. Sci.* **2018**, *5*. [CrossRef] [PubMed]

328. Manavitehrani, I.; Le, T.Y.L.; Daly, S.; Wang, Y.W.; Maitz, P.K.; Schindeler, A.; Dehghani, F. Formation of porous biodegradable scaffolds based on poly(propylene carbonate) using gas foaming technology. *Mater. Sci. Eng. C-Mater. Biol. Appl.* **2019**, *96*, 824–830. [CrossRef] [PubMed]

329. Ma, Y.F.; Hu, N.; Liu, J.; Zhai, X.Y.; Wu, M.M.; Hu, C.S.; Li, L.; Lai, Y.X.; Pan, H.B.; Lu, W.W.; et al. Three-Dimensional Printing of Biodegradable Piperazine-Based Polyurethane-Urea Scaffolds with Enhanced Osteogenesis for Bone Regeneration. *ACS Appl. Mater. Interfaces* **2019**, *11*, 9415–9424. [CrossRef]

330. Odelius, K.; Hoglund, A.; Kumar, S.; Hakkarainen, M.; Ghosh, A.K.; Bhatnagar, N.; Albertsson, A.C. Porosity and Pore Size Regulate the Degradation Product Profile of Polylactide. *Biomacromolecules* **2011**, *12*, 1250–1258. [CrossRef] [PubMed]

331. Rai, V.; Dilisio, M.F.; Dietz, N.E.; Agrawal, D.K. Recent strategies in cartilage repair: A systemic review of the scaffold development and tissue engineering. *J. Biomed. Mater. Res. Part A* **2017**, *105*, 2343–2354. [CrossRef]

332. Eltom, A.; Zhong, G.Y.; Muhammad, A. Scaffold Techniques and Designs in Tissue Engineering Functions and Purposes: A Review. *Adv. Mater. Sci. Eng.* **2019**. [CrossRef]

333. Park, J.; Lee, S.J.; Lee, H.; Park, S.A.; Lee, J.Y. Three dimensional cell printing with sulfated alginate for improved bone morphogenetic protein-2 delivery and osteogenesis in bone tissue engineering. *Carbohydr. Polym.* **2018**, *196*, 217–224. [CrossRef]

334. Shao, H.; He, J.; Lin, T.; Zhang, Z.; Zhang, Y.; Liu, S. 3D gel-printing of hydroxyapatite scaffold for bone tissue engineering. *Ceram. Int.* **2019**, *45*, 1163–1170. [CrossRef]

335. Hutmacher, D.W. Scaffold design and fabrication technologies for engineering tissues–state of the art and future perspectives. *J. Biomater. Sci. Polym. Ed.* **2001**, *12*, 107–124. [CrossRef] [PubMed]

336. Golubevas, R.; Stankeviciute, Z.; Zarkov, A.; Golubevas, R.; Hansson, L.; Raudonis, R.; Kareiva, A.; Garskaite, E. Acrylate–gelatin–carbonated hydroxyapatite (cHAP) composites for dental bone-tissue applications. *Mater. Adv.* **2020**, *1*, 1675–1684. [CrossRef]

337. Szczes, A.; Holysz, L.; Chibowski, E. Synthesis of hydroxyapatite for biomedical applications. *Adv. Colloid Interfaces* **2017**, *249*, 321–330. [CrossRef]

338. Yuan, H.F.; Zheng, X.Y.; Liu, W.; Zhang, H.; Shao, J.J.; Yao, J.X.; Mao, C.Y.; Hui, J.F.; Fan, D.D. A novel bovine serum albumin and sodium alginate hydrogel scaffold doped with hydroxyapatite nanowires for cartilage defects repair. *Colloid Surf. B* **2020**, *192*. [CrossRef] [PubMed]

339. Mondal, S.; Pal, U. 3D hydroxyapatite scaffold for bone regeneration and local drug delivery applications. *J. Drug Deliv. Sci. Technol.* **2019**, *53*. [CrossRef]

340. Chaudhari, A.A.; Vig, K.; Baganizi, D.R.; Sahu, R.; Dixit, S.; Dennis, V.; Singh, S.R.; Pillai, S.R. Future prospects for scaffolding methods and biomaterials in skin tissue engineering: A review. *Int. J. Mol. Sci.* **2016**, *17*, 1974. [CrossRef]

341. Ramakrishna, S.; Jose, R.; Archana, P.S.; Nair, A.S.; Balamurugan, R.; Venugopal, J.; Teo, W.E. Science and engineering of electrospun nanofibers for advances in clean energy, water filtration, and regenerative medicine. *J. Mater. Sci.* **2010**, *45*, 6283–6312. [CrossRef]

342. Pei, X.; Ma, L.; Zhang, B.Q.; Sun, J.X.; Sun, Y.; Fan, Y.J.; Gou, Z.R.; Zhou, C.C.; Zhang, X.D. Creating hierarchical porosity hydroxyapatite scaffolds with osteoinduction by three-dimensional printing and microwave sintering. *Biofabrication* **2017**, *9*. [CrossRef]

343. Song, X.L.; Tetik, H.; Jirakittsonthon, T.; Parandoush, P.; Yang, G.; Lee, D.; Ryu, S.; Lei, S.T.; Weiss, M.L.; Lin, D. Biomimetic 3D Printing of Hierarchical and Interconnected Porous Hydroxyapatite Structures with High Mechanical Strength for Bone Cell Culture. *Adv. Eng. Mater.* **2019**, *21*. [CrossRef]

344. Bas, O.; De-Juan-Pardo, E.M.; Meinert, C.; D'Angella, D.; Baldwin, J.G.; Bray, L.J.; Wellard, R.M.; Kollmannsberger, S.; Rank, E.; Werner, C.; et al. Biofabricated soft network composites for cartilage tissue engineering. *Biofabrication* **2017**, *9*. [CrossRef] [PubMed]

345. Wang, J.Q.; Zhang, F.J.; Tsang, W.P.; Wan, C.; Wu, C. Fabrication of injectable high strength hydrogel based on 4-arm star PEG for cartilage tissue engineering. *Biomaterials* **2017**, *120*, 11–21. [CrossRef]

346. Rajzer, I.; Kurowska, A.; Jablonski, A.; Jatteau, S.; Sliwka, M.; Ziabka, M.; Menaszek, E. Layered gelatin/PLLA scaffolds fabricated by electrospinning and 3D printing—For nasal cartilages and subchondral bone reconstruction. *Mater. Des.* **2018**, *155*, 297–306. [CrossRef]

347. Hsieh, Y.-H.; Shen, B.-Y.; Wang, Y.-H.; Lin, B.; Lee, H.-M.; Hsieh, M.-F. Healing of osteochondral defects implanted with biomimetic scaffolds of poly (ε-caprolactone)/hydroxyapatite and glycidyl-methacrylate-modified hyaluronic acid in a minipig. *Int. J. Mol. Sci.* **2018**, *19*, 1125. [CrossRef] [PubMed]

348. Oberoi, G.; Nitsch, S.; Edelmayer, M.; Janjić, K.; Müller, A.S.; Agis, H. 3D Printing—encompassing the facets of dentistry. *Front. Bioeng. Biotechnol.* **2018**, *6*, 172. [CrossRef] [PubMed]

349. Ucar, Y.; Meric, I.A.; Ekren, O. Layered Manufacturing of Dental Ceramics: Fracture Mechanics, Microstructure, and Elemental Composition of Lithography-Sintered Ceramic. *J. Prosthodont.* **2019**, *28*, E310–E318. [CrossRef] [PubMed]

350. Shah, P.; Chong, B.S. 3D imaging, 3D printing and 3D virtual planning in endodontics. *Clin. Oral Investig.* **2018**, *22*, 641–654. [CrossRef] [PubMed]

351. Lin, L.W.; Fang, Y.F.; Liao, Y.X.; Chen, G.; Gao, C.X.; Zhu, P.Z. 3D Printing and Digital Processing Techniques in Dentistry: A Review of Literature. *Adv. Eng. Mater.* **2019**, *21*. [CrossRef]

352. Venkatasubbu, G.D.; Ramasamy, S.; Ramakrishnan, V.; Kumar, J. Hydroxyapatite-alginate nanocomposite as drug delivery matrix for sustained release of ciprofloxacin. *J. Biomed. Nanotechnol.* **2011**, *7*, 759–767. [CrossRef]

353. Bi, Y.-G.; Lin, Z.-T.; Deng, S.-T. Fabrication and characterization of hydroxyapatite/sodium alginate/chitosan composite microspheres for drug delivery and bone tissue engineering. *Mater. Sci. Eng. C* **2019**, *100*, 576–583. [CrossRef]

354. Zhou, Q.J.; Wang, T.W.; Wang, C.; Wang, Z.; Yang, Y.A.; Li, P.; Cai, R.H.; Sun, M.; Yuan, H.Y.; Nie, L. Synthesis and characterization of silver nanoparticles-doped hydroxyapatite/alginate microparticles with promising cytocompatibility and antibacterial properties. *Colloid Surf. A* **2020**, *585*. [CrossRef]

355. Nie, L.; Deng, Y.; Zhang, Y.; Zhou, Q.; Shi, Q.; Zhong, S.; Sun, Y.; Yang, Z.; Sun, M.; Politis, C.; et al. Silver-doped biphasic calcium phosphate/alginate microclusters with antibacterial property and controlled doxorubicin delivery. *J. Appl. Polym. Sci.* **2021**, *138*, 50433. [CrossRef]

356. Rodzeń, K.; Sharma, P.K.; McIlhagger, A.; Mokhtari, M.; Dave, F.; Tormey, D.; Sherlock, R.; Meenan, B.J.; Boyd, A.J.P. The Direct 3D Printing of Functional PEEK/Hydroxyapatite Composites via a Fused Filament Fabrication Approach. *Polymers* **2021**, *13*, 545. [CrossRef]

357. Robles-Aguila, M.J.; Reyes-Avendano, J.A.; Mendoza, M.E. Structural analysis of metal-doped (Mn, Fe, Co, Ni, Cu, Zn) calcium hydroxyapatite synthetized by a sol-gel microwave-assisted method. *Ceram. Int.* **2017**, *43*, 12705–12709. [CrossRef]

358. Popescu, A.C.; Florian, P.E.; Stan, G.E.; Popescu-Pelin, G.; Zgura, I.; Enculescu, M.; Oktar, F.N.; Trusca, R.; Sima, L.E.; Roseanu, A.; et al. Physical-chemical characterization and biological assessment of simple and lithium-doped biological-derived hydroxyapatite thin films for a new generation of metallic implants. *Appl. Surf. Sci.* **2018**, *439*, 724–735. [CrossRef]

359. Yazici, M.; Gulec, A.E.; Gurbuz, M.; Gencer, Y.; Tarakci, M. Biodegradability and antibacterial properties of MAO coatings formed on Mg-Sr-Ca alloys in an electrolyte containing Ag doped hydroxyapatite. *Thin Solid Films* **2017**, *644*, 92–98. [CrossRef]

360. Tappa, K.; Jammalamadaka, U. Novel Biomaterials Used in Medical 3D Printing Techniques. *J. Funct. Biomater.* **2018**, *9*, 17. [CrossRef] [PubMed]